Universitatea Politehnica Timişoara

TENSOR PRODUCT-BASED MODEL TRANSFORMATION USED IN CONTROL SYSTEMS MODELING AND DESIGN

PhD THESIS

Eng. Elena-Lorena CONSTANTIN
(căs. HEDREA)

PhD Supervisor: Prof.dr.eng. Radu-Emil PRECUP,
Politechnica University Timisoara
Scientific Reviewers: Prof.dr.eng. Dan SELISTEANU,
University of Craiova
Prof.dr.eng. Ciprian LUPU,
University Politechnica of Bucharest
Prof.dr.eng. Stefan PREITL,
Politechnica University Timisoara
PhD Committee Chair: Prof.dr.eng. Octavian PROSTEAN,
Politechnica University Timisoara

Date of the PhD Thesis Defense: 1 September 2022

Timişoara, 2022

Foreword

This thesis has been elaborated during my activity in the Department of Automation and Applied Informatics of the Politehnica University Timişoara, Romania. The work started during the academic year 2014-2015 in the framework of the B.Sc. studies, continued with the M.Sc. studies (2015-2017) and with the PhD studies (since October 2017).

I address my special thanks to the PhD supervisor, Prof.dr.eng. Radu-Emil PRECUP for all the support and guiding provided during the elaboration and the development of this thesis and for the excellent collaboration started since the begining of the B.Sc. studies.

I also thank the members of the guidance committee consisting of Lect.dr.eng Claudia-Adina BOJAN-DRAGOS, Lect.dr.eng. Alexandra-Iulia SZEDLAK-STINEAN and Assist.dr.eng. Raul-Cristian ROMAN from Politechnica University Timisoara, and also Prof.dr.eng. Emil M. PETRIU from University of Ottawa, Canada for the close collaboration. Our work has been valorified by commun publications. I hope that this collaboration will continue in the future.

I address my thanks to the members of the PhD committee, Prof.dr.eng. Dan SELISTEANU from University of Craiova, Prof.dr.eng. Ciprian LUPU from University Politechnica of Bucharest, Prof.dr.eng. Octavian PROSTEAN and Prof.dr.eng. Stefan PREITL from Politechnica University Timisoara for the reports and for all the usefull observations for the improvement of the thesis and for participating at the PhD thesis defense.

I also address thanks to all my colleagues from the Automation and Applied Informatics Department of the Politehnica University Timisoara.

Not least I thank my family for all their support.

Timişoara, June 2022 Elena-Lorena Constantin (căs. Hedrea)

Contents

Notations, abbreviations, acronyms **4**
List of tables **5**
List of figures **6**
1. Introduction **10**
1.1. Research background 10
1.2. General presentation of the thesis 11
2. Tensor Product (TP)-based Model Transformation **12**
2.1. Introduction to TP-based Model Transformation technique 12
2.2. Bibliographic study on TP-based Model Transformation technique 13
3. TP-based Model Transformation technique used in system modeling ... **17**
3.1. The TP-based Model Transformation modeling algorithm 17
3.2. The derivation of the TP model for Vertical Three Tank System 222
3.3. The derivation of the TP model for a partial state feedback controlled Magnetic Levitation System 29
3.4. The derivation of the TP model for Pendulum Cart System 38
3.5. Chapter conclusions 45
4. TP-based Model Transformation technique used in control system design **50**
4.1. The TP-based Model Transformation control algorithm 50
4.2. The TP-based Model Transformation used for level control of Vertical Three Tank System 52
4.3. The TP-based Model Transformation used for position control of a partial state feedback controlled Magnetic Levitation System 69
4.4. The TP-based Model Transformation used for position control of Pendulum Cart System 80
4.5. Chapter conclusions 90
5. Conclusions and personal contributions **94**
5.1. Personal contributions 94
5.2. Dissemination of the results 96
5.3. Future research 103
Bibliography **104**
Appendices **113**
Appendix 1. The state-space system matrices of three linearized processes 113
Appendix 2. The LTI system matrices of three processes 114
Appendix 3. The LTI state feedback gain matrices of three processes 115
Appendix 4. The state feedback gain matrices of three processes 116

Notations, abbreviations, acronyms

Abbreviation	**Meaning**
AIC	- Akaike Information Criterion
BIC	- Bayesian Information Criterion
CNO	- Close to Normal
CS	- Control Structure
CCS	- Cascade Control Structure
EACS	- Electromagnetic Actuated Clutch System
HOSVD	- Higher Order Singular Value Decomposition
LMIs	- Linear Matrix Inequalities
LPV	- Linear Parameter Varying
LTI	- Linear Time Invariant
qLPV	- quasi-Linear Parameter Varying
MLS	- Magnetic Levitation System
MO-m	- Modulus Optimum method
MSE	- Mean Square Error
MSU	- Mean Square Control Effort
MVS	- Minimal Volume Simplex
NN	- Non-Negative
NO	- Normal
PCS	- Pendulum Cart System
PDC	- Parallel Distributed Compensation
PRBS	- Pseudo Random Binary Signal
psfcMLS	- partial state feedback controlled Magnetic Levitation System
PWM	- Pulse-Width Modulation
RMSE	- Root Mean Square Error
SFCS	- State Feedback Control Structure
SN	- Sum Normalized
stMLS	- stabilized linearized model for MLS
SVD	- Singular Value Decomposition
TORA	- Translational Oscillations with an Eccentric Rotational Proof Mass Actuator
TC	- Tower Crane
TP	- Tensor Product
TPCS	- TP-based Control Structure
TSK	- Takagi-Sugeno-Kang
V3TS	- Vertical Three Tank System
VAF	- Value of Accounted For

List of tables

Tabel No.	Meaning
Table 3.2.1.	Values of performance indices for V3TS.
Table 3.3.1.	Values of performance indices for MLS.
Table 3.4.1.	Values of performance indices for PCS.
Table 4.2.1.	Values of parameters of the third order t.f.s. computed for TPCS.
Table 4.2.2.	Values of parameters of the PID controllers designed for TPCS.
Table 4.2.3.	Values of parameters of the third order t.f.s. computed for SFCSs.
Table 4.2.4.	Values of parameters of the PID controllers designed for SFCSs.
Table 4.2.5.	Values of control system performance indices for V3TS in the simulation scenario.
Table 4.2.6.	Values of control system performance indices for V3TS in the experimental scenario.
Table 4.3.1.	Values of parameters of the second order t.f.s. computed for SFCSs in the simulation scenario.
Table 4.3.2.	Values of parameters of the second order t.f.s. computed for SFCSs in the experimental scenario.
Table 4.3.3.	Values of parameters of the PI controllers designed for psfcMLS in the simulation scenario.
Table 4.3.4.	Values of parameters of the PI controllers designed for psfcMLS in the experimental scenario.
Table 4.3.5.	Values of control system performance indices for psfcMLS in the simulation scenario.
Table 4.3.6.	Values of control system performance indices for psfcMLS in the experimental scenario.
Table 4.4.1.	Values of parameters of the second order t.f.s. computed for SFCSs.
Table 4.4.2.	Values of parameters of the PI controllers designed for PCS.
Table 4.4.3.	Values of control system performance indices for PCS in the simulation scenario.
Table 4.4.4.	Values of control system performance indices for PCS in the experimental scenario.

List of figures

Fig. No.	Meaning
Fig.3.1.	The TP-based model transformation diagram [Hed18a].
Fig.3.2.	The transformation space for two parameters [Hed18a], [Hed19e].
Fig.3.3.	The discretization grid for two parameters [Hed18a], [Hed19e].
Fig.3.4.	Diagram of principle of V3TS [Int07].
Fig.3.5.	Weighting functions obtained for the first parameter.
Fig.3.6.	Testing block diagram for V3TS.
Fig.3.7.	Control signal versus time used in the testing scenario.
Fig.3.8.	First tank fluid level vs. time for V3TS laboratory equipment, nonlinear model, TP model, 1st linear model, 2nd linear model, 3rd linear model and 4th linear model in the testing scenario.
Fig.3.9.	Second tank fluid level vs. time for V3TS laboratory equipment, nonlinear model, TP model, 1st linear model, 2nd linear model, 3rd linear model and 4th linear model in the testing scenario.
Fig.3.10.	Third tank fluid level vs. time for V3TS laboratory equipment, nonlinear model, TP model, 1st linear model, 2nd linear model, 3rd linear model and 4th linear model in the testing scenario.
Fig.3.11.	Experimental setup for MLS [Int08].
Fig.3.12.	Block diagram of psfcMLS.
Fig.3.13.	W.f.s obtained by TP-based model transformation of psfcMLS [Hed17a], [Hed19e].
Fig.3.14.	Testing block diagram for psfcMLS.
Fig.3.15.	PRBS control signal versus time used in the first testing scenario.
Fig.3.16.	Sphere position vs. time for psfcMLS, nonlinear model, TP model, 1st linear model, 2nd linear model, 3rd linear model and 4th linear model in the first testing scenario.
Fig.3.17.	Sine control signal versus time used in the second testing scenario.
Fig.3.18.	Sphere position vs. time for psfcMLS, nonlinear model, TP model, 1st linear model, 2nd linear model, 3rd linear model and 4th linear model in the second testing scenario.
Fig.3.19.	Chirp control signal versus time used in the third testing scenario.
Fig.3.20.	Sphere position vs. time for psfcMLS, nonlinear model, TP model, 1st linear model, 2nd linear model, 3rd linear model and 4th linear model in the third testing scenario.
Fig.3.21.	PWM control signal versus time used in the fourth testing scenario.
Fig.3.22.	Sphere position vs. time for psfcMLS, nonlinear model, TP model, 1st linear model, 2nd linear model, 3rd linear model and 4th linear model in the fourth testing scenario.
Fig.3.23.	Block diagram of PCS [Hed21a].
Fig.3.24.	Two control problems of PCS [Fee98].
Fig.3.25.	Weighting functions for pendulum angle.
Fig.3.26.	Testing block diagram for PCS.
Fig.3.27.	Sine control signal versus time used in the first testing scenario.

Fig.3.28. Cart position vs. time for PCS, nonlinear model, TP model, 1st linear model, 2nd linear model, 3rd linear model and 4th linear model in the first testing scenario.
Fig.3.29. Random control signal versus time used in the second testing scenario.
Fig.3.30. Cart position vs. time for PCS, nonlinear model, TP model, 1st linear model, 2nd linear model, 3rd linear model and 4th linear model in the second testing scenario.
Fig.4.1. The TP-based model transformation control algorithm diagram.
Fig.4.2. Block diagram of the TPCS designed for V3TS [Hed19a].
Fig.4.3. General block diagram of the four SFCSs designed for V3TS [Hed17b], [Hed19a].
Fig.4.4. First tank fluid levels (y1) versus time in case of TPCS and the four SFCSs with staircase reference input in the simulation scenario.
Fig.4.5. Second tank fluid levels (y2) versus time in case of TPCS and the four SFCSs with staircase reference input in the simulation scenario.
Fig.4.6. Third tank fluid levels (y3) versus time in case of TPCS and the four SFCSs with staircase reference input in the simulation scenario.
Fig.4.7. Control signal versus time in case of TPCS and the four SFCSs with staircase reference input in the simulation scenario.
Fig.4.8. First tank fluid levels (y1) versus time in case of TPCS and the four SFCSs with staircase reference input in the experimental scenario.
Fig.4.9. Second tank fluid levels (y2) versus time in case of TPCS and the four SFCSs with staircase reference input in the experimental scenario.
Fig.4.10. Third tank fluid levels (y3) versus time in case of TPCS and the four SFCSs with staircase reference input in the experimental scenario.
Fig.4.11. Control signal versus time in case of TPCS and the four SFCSs with staircase reference input in the experimental scenario.
Fig.4.12. Block diagram of the SISO PID-TPCSs designed for V3TS [Hed19a].
Fig.4.13. Block diagram of the SISO PID-SFCSs designed for V3TS [Hed19a].
Fig.4.14. First tank fluid levels (y1) versus time in case of PID-TPCS and the PID-SFCSs designed for the liquid level control of the first tank in the simulaton scenario.
Fig.4.15. Second tank fluid levels (y2) versus time of PID-TPCS and the PID-SFCSs designed for the liquid level control of the second tank in the simulaton scenario.
Fig.4.16. Third tank fluid levels (y3) versus time of PID-TPCS and the PID-SFCSs designed for the liquid level control of the third tank in the simulaton scenario.
Fig.4.17. Control signal versus time in case of PID-TPCS and the PID-SFCSs designed for the level control of the first tank in the simulaton scenario.
Fig.4.18. Control signal versus time in case of PID-TPCS and the PID-SFCSs designed for the level control of the second tank in the simulaton scenario.
Fig.4.19. Control signal versus time in case of PID-TPCS and the PID-SFCSs designed for the level control of the third tank in the simulaton scenario.

Fig.4.20. First tank fluid levels (y1) versus time in case of PID-TPCS and the PID-SFCSs designed for the liquid level control of the first tank in the experimental scenario.
Fig.4.21. Second tank fluid levels (y2) versus time of PID-TPCS and the PID-SFCSs designed for the liquid level control of the second tank in the experimental scenario.
Fig.4.22. Third tank fluid levels (y3) versus time of PID-TPCS and the PID-SFCSs designed for the liquid level control of the third tank in the experimental scenario.
Fig.4.23. Control signal versus time in case of PID-TPCS and the PID-SFCSs designed for the level control of the first tank in the experimental scenario.
Fig.4.24. Control signal versus time in case of PID-TPCS and the PID-SFCSs designed for the level control of the second tank in the experimental scenario.
Fig.4.25. Control signal versus time in case of PID-TPCS and the PID-SFCSs designed for the level control of the third tank in the experimental scenario.
Fig.4.26. Block diagram of the TPCS designed for psfcMLS [Hed17a].
Fig.4.27. General block diagram of the four SFCSs designed for psfcMLS.
Fig.4.28. Sphere position versus time in case of TPCS and the four SFCSs with staircase reference input in the simulation scenario.
Fig.4.29. Control signal versus time in case of TPCS and the four SFCSs with staircase reference input in the simulation scenario.
Fig.4.30. Sphere position versus time in case of TPCS and the four SFCSs with staircase reference input in the experimental scenario.
Fig.4.31. Control signal versus time in case of TPCS and the four SFCSs with staircase reference input in the experimental scenario.
Fig.4.32. Block diagram of the SISO PI-TPCSs designed for psfcMLS.
Fig.4.33. Block diagram of the SISO PI-SFCSs designed for psfcMLS.
Fig.4.34. Sphere position versus time in case of PI-TPCS and the PI-SFCSs designed for the sphere position control of psfcMLS in the simulation scenario.
Fig.4.35. Control signal versus time in case of PI-TPCS and the PI-SFCSs designed for the sphere position control of psfcMLS in the simulation scenario.
Fig.4.36. Sphere position versus time in case of PI-TPCS and the PI-SFCSs designed for the sphere position control of psfcMLS in the experimental scenario.
Fig.4.37. Control signal versus time in case of PI-TPCS and the PI-SFCSs designed for the sphere position control of psfcMLS in the experimental scenario.
Fig.4.38. Block diagram of the TPCS designed for PCS [Hed21a].
Fig.4.39. General block diagram of the four SFCSs designed for PCS.
Fig.4.40. Cart position versus time in case of TPCS and the four SFCSs with staircase reference input in the simulation scenario.
Fig.4.41. Control signal versus time in case of TPCS and the four SFCSs with staircase reference input in the experimental scenario.
Fig.4.42. Cart position versus time in case of TPCS and the four SFCSs with staircase reference input in the experimental scenario.

Fig.4.43. Control signal versus time in case of TPCS and the four SFCSs with staircase reference input in the simulation scenario.
Fig.4.44. Block diagram of the SISO PI-TPCSs designed for PCS.
Fig.4.45. Block diagram of the SISO PI-SFCSs designed for PCS.
Fig.4.46. Cart position versus time in case of PI-TPCS and the PI-SFCSs designed for the cart position control of PCS in the simulation scenario.
Fig.4.47. Control signal versus time in case of PI-TPCS and the PI-SFCSs designed the cart position control of PCS in the simulation scenario.
Fig.4.48. Cart position versus time in case of PI-TPCS and the PI-SFCSs designed for the cart position control of PCS in the experimental scenario.
Fig.4.49. Control signal versus time in case of PI-TPCS and the PI-SFCSs designed the cart position control of PCS in the experimental scenario.

1. Introduction

1.1. Research background

The Singular Value Decomposition (SVD) theory has been developed lately with the work of many mathematicians as Beltrami, Jordan, Sylvester, Schmidt, Weyl, etc. One of the most recent results in this field refers to the generation of tensors using Higher Order Singular Value Decomposition (HOSVD) [Apk95]. The main feature of HOSVD consists in decomposing a N-dimensional tensor into an orthonormal system by the special ordering of higher order singular values. Based on this feature HOSVD is capable of extracting the unique structure of the decomposed tensor [Apk95]. Therefore, on one hand, there are many techniques of optimization and design of control structures for polytopic forms of Linear Parameter Varying (LPV) models and, on the other hand, there are many identification techniques. However, these two aspects can be connected very difficult because of the uniform representation problem. This is why the Tensor Product (TP)-based Model Transformation technique is a good solution in solving this problem.

The TP-based Model Transformation technique transforms LPV models into polytopic forms on which the Linear Matrix Inequalities (LMIs) techniques can be applied immediately. The result of this transformation consists in TP models which have the well defined structure of a given LPV model.

The two main objectives of this thesis were formulated in order to validate the TP-based Model Transformation technique by obtaining TP models for various processes, other that the ones already presented in the literature, and also to improve the control performances of the TP-based control structures by combining the TP-based Model Transformation technique with other control techniques in the design of cascade control structures.

The first objective of the thesis consists in the validation of the modeling algorithm of the TP-based Model Transformation technique on many laboratory equipments. The corresponding derived TP models were validated using many testing scenarios and they were compared with other models of the same processes in order to highlight their performance.

The second objective of the thesis consists in the validation of the control algorithm of the TP-based Model Transformation technique using LMIs and Parallel Distributed Compensation (PDC) framework. Therefore, many conventional and cascade control structures were design for the control of various laboratory equipments. The proposed control structures were tested and compared with other similar ones and their performance was highlighted.

Finally, the main conclusion consists in the fact that the TP-based Model Transformation technique proved its utility by being applied on many processes as laboratory equipments, industrial processes, biomedical processes, etc.

1.2. General presentation of the thesis

The thesis is structured in five chapters and four appendices. A short overview of each chapter is presented as follows.

The scientific background along with a short general presentation of the thesis are presented in **Chapter 1**.

Chapter 2 consists in a short general presentation of the main idea of TP-based Model Transformation technique and a bibliographic study which highlights the main theoretical and practical contributions obtained so far.

C**hapter 3** is organized in five sub-chapters. The modeling algorithm of the TP-based Model Transformation technique is widely presented in Sub-chapter 3.1. The next first three sub-chapters are dedicated to the presentation of the derivation of TP models for: the vertical three tank systems, the partial state feedback controlled magnetic levitation systems, and the inverted pendulum systems. Each TP model is validated using many testing scenarios and its performance is highlighted. A comparative analysis with other models is also made. Finally, the conclusions are given in Sub-chapter 3.5.

Chapter 4 is organized in five sub-chapters. Sub-chapter 4.1 presents the control algorithm of the TP-based Model Transformation technique. The next three sub-chapters present the design of conventional and cascade control structures for the following laboratory equipments: the vertical three tank systems, the partial state feedback controlled magnetic levitation systems and the inverted pendulum system. A comparative analysis is conducted in each sub-chapter. Sub-chapter 4.5. presents the conclusions.

Chapter 5 highlights the main conclusions and the personal contributions and presents further research directions.

2. Tensor Product (TP)-based Model Transformation

2.1. Introduction to TP-based Model Transformation technique

The TP-based Model Transformation technique was first introduced by Peter Baranyi in the paper [Bar03a]. The main purpose of this approach is to transform a given LPV or quasi-Linear Parameter Varying (qLPV) state-space model into a TP model made of Linear Time Invariant (LTI) systems using the HOSVD. Therefore, **the input(s)** of the transformation is/are the **LPV or qLPV models** and the **output**s consist in the **LTI matrices**, which form **the core tensor of the TP model**. The computation time of the TP-based Model Transformation depends on the computation time of the HOSVD.

The transformation steps are briefly presented as follows, they represent **the modeling approach**, and will be widely discussed in Chapter 3 of this thesis.

Step 1. Defining the parameter vector. Starting with the physical restrictions applied to the process (or plant) operation, the vector of the variable parameters is defined.

Step 2. Defining the discretization grid. The discretization grid is found by discretizing the parameter vector using a certain number of discretization points.

Step 3. Computation of the discretized tensor. The discretized system matrices, which form the discretized tensor are computed.

Step 4. HOSVD of the discretized tensor. The HOSVD is applied on the discretized tensor obtained in the previous step.

Step 5. Computation of the weighting functions. The values of the weighting functions are obtained after applying the HOSVD on the discretized tensor and are stored in weighting vectors. The main types of weighting vectors are presented as follows.

The weighting vector is Sum Normalized (**SN**) if the sum of all weighting functions is 1.

The weighting vector is Non Negative (**NN**) if the values of all weighting functions are non-negative.

The weighting vector is Normal (**NO**) if it is SN and NN and the biggest value of all weighting functions is 1.

The weighting vector is Close to Normal (**CNO**) if the biggest value of all weighting functions is close to 1.

Step 6. Computing the LTI systems. Finally, the LTI system matrices, which form the core tensor of the TP model, are computed.

Based on the LTI system matrices resulted from the TP-based Model Transformation, the PDC technique along with LMIs are involved in the TP controller design and tuning. Therefore, the input of the TP controller design approach is the core tensor made by the LTI system matrices and the output are the LTI feedback gains which are stored in the tensor of the TP controller. The controller design approach steps are briefly presented as follows and they will be widely discussed in Chapter 4 of this thesis.

Step 1. Defining the four LMIs. Four LMIs are defined. The first two LMIs are formulated to ensure the asymptotic stability of the control system and the other two are used to constrain the control signal (or control input).

Step 2. Solving the stability LMIs. The first two LMIs defined in step 1 are solved using a dedicated LMI software or toolbox.

Step 3. Computing the LTI feedback gains. Based on the solutions of the previous LMIs, the LTI feedback gains are computed and stored in the TP controller tensor.

Step 4. Solving the constraints LMIs. The last two LMIs, which consist in constraints applied to the control signal, are solved based on the solutions obtained in step 2.

Step 5. Application of PDC technique. Finally, the PDC technique is applied to derive the control law based on the feedback gain tensor.

2.2. Bibliographic study on TP-based Model Transformation technique

Over the last few years the TP-based Model Transformation technique was successfully applied to many processes. An analysis of the state-of-the art is presented as follows considering several classification criteria.

The first classification criterion consists in dividing the application of the TP-based model transformation technique to **process modeling (I)** and **process control (II)**.

(I) TP-based Model Transformation technique applied to process modeling. The modeling approach is applied in the **conventional** way by following the six steps presented in the previous sub-chapter.

The **conventional** application to the TP-based Model Transformation modeling algorithm was used in the following papers:

- [Tik04] for a mass-spring system;
- [Bar06b], [Nag07c] and [Sze07] for a Translational Oscillator with an Eccentric Rotational Proof Mass Actuator (TORA) system;
- [Kun07] for a DC motor;
- [Nag07a], [Nag07b], [Zha18], [Bar22a], [Kuc21] and [Hed21a] for a pendulum-cart system;
- [Gro10] for a pneumatic system;
- [Tak13], [Eig16a], [Kov16] and [Eig17a] for the type 1 and type 2 diabetes.
- [Gal13], [Szo14a], [Szo18] and [Gal15a] for cognitive processes;

- [Bar14], [Szo14b], [Bar15], [Bar16] and [Tak15] for a 3 Degrees of Freedom (3DOF) aeroelastic wing system;
- [Che14] for an industrial robot with flexible joints.
- [He16] for a morphing aircraft;
- [Hed18a] for a vertical three tank system;
- [Wan18] for a nonlinear discreet-time system;
- [Hed19b] and [Hed19e] for a magnetic levitation system;
- [Nem19] and [Nem21] for an induction machine;
- [Var21] for a white noise model and in [Gon20] for a frequency modulated signal;
- [Hed21b] for a tower crane system;
- [Csa21] for black box models.
- [Hed21c] for servo systems

The main advantage of the TP-based Model Transformation modeling approach consists in the fact that it transforms LPV models into polytopic forms (LTIs) on which the Linear Matrix Inequalities (LMIs) techniques can be applied immediately. That is the reason why this technique was successfully applied to many processes. However some disadvantages emerged.

The main disadvantage of the TP-based Model Transformation modeling approach consists in the large dimension of the core tensor of the derived TP model which generates:

a) large computation volume;
b) large execution time;
c) large amount of memory.

Therefore, solving this disadvantage has become an important research topic which was treated in many of the recent papers. The results of the improved TP-based Model Transformation modeling algorithm are presented in [Pet06], [Liu17a] and [Kut17b] where the volume of computations was significantly decreased. More than that, the dimension of the core tensor was decreased by varying the dimensions of the process inputs and outputs in the generalized TP-Based Model Transformation modeling algorithm proposed by Baranyi in [Bar18] and [Bar22b].

(II) TP-based Model Transformation technique applied to process control. The controller design approach was either applied in the **initial form proposed by Baranyi in 2003** or it was **improved** by adding additional steps or features in order to overcome the eventual disadvantages of the classical form or to improve the derived TP controller performance.

The initial form of the TP controller design approach consists of proceeding the steps presented in the previous sub-chapter in the derivation of the TP controller. The resulted TP controller was next used either alone in conventional control structures (a) or in combination with other control techniques in cascade control structures (b). Therefore, two other subcriteria result as follows:

a) The TP-based conventional control structures were proposed in:

- [Bar03a], [Bar03b], [Bar04a], [Bar04b], [Bok05], [Bar05b], [Bar06a], [Bar06b], [Bar06d], [Tak10c], [Szo15] and [Tak21], for an aeroelastic system;
- [Bar05a] and [Sun18], for a 3DOF helicopter;
- [Pet04] and [Pet07], for a TORA system;
- [Kol06], [Nag08], [Sza09], [Ile11], [Gro15], [Kuc19] and [Hed21a] for a pendulum-cart system.

- [Gro12] and [Gal15b], for impedance model with feedback delay;
- [Eig16b], for type 1 diabetes and in [Eig17b] for tumor growth;
- [Pre10a] and [Hed17b], for a three tank system and vertical three tank system respectively;
- [Pre10b], for an electromagnetic actuated clutch system;
- [Pre12], for an automatic transmission system;
- [Tak10b], for a DC motor;
- [Hed17a], for a magnetic levitation system;
- [Tak16], for a medical robot;
- [Tak18], for an aircraft;
- [Boo20], for a Lotka-Volterra fractional order model;
- [Cha20], for a mass-spring dumper system and for the Lorentz system.

b) The TP-based cascade control structures were presented in:

- [Pre08], [Pre15], [Hed18c] and [Hed19c] using a combination with fuzzy control technique;
- [Pet08] and [Hed18b] using a combination with gain scheduling control technique;
- [Mat11] using a combination with neural networks;
- [Tak10a], [Hua15], [Kor06], [Che17], [Zha14] and [Hed19d] using a combination with sliding mode technique;
- [Ile14] and [Han17] using a combination with the model predictive control technique;
- [Liu17b] using a combination with adaptive control techniques;
- [Hed19a] using a combination with Proportional Integral Derivative (PID) controller.

The main advantage of the TP controller design approach is that both the LMIs and PDC technique are combined in order to compute the feedback gain tensor. This advantage led to the successfully application of the TP-based control technique to a wide range of processes. However, as in case of the TP modeling approach, the large dimension of the feedback gain tensor represents **a big disadvantage** especially for higher order systems as it can negatively influence the control performance. Therefore, in order to solve this issue, two possible solutions were proposed:

- in [Yu19], the iterative TP-based Model Transformation technique is proposed which significantly reduces the feedback tensor dimension;
- in [Kut17a], the Minimal Volume Simplex (MVS) method is used in order to determine only on feedback gain on each dimension of the transformation space.

Another disadvantage of the TP controller design approach presented above consists in the fact that in the parameter tuning, which is based on LMIs, the stability and control specifications are guaranteed only for the derived TP model and not for the initial process. Therefore, other LMIs were added as follows in the controller design approach in order to fulfill the stability requirements:

- in [Wu13], the Chebyshev LMI is introduced in order to ensure the stability of the original process;
- in [Kut16], additional LMIs are used in order to exclude in instability regimes;

- in [Sza10], auxiliary variables are introduced in order to highlight if the performances of the TP controller can or can not be improved.

The second classification criterion consists in the type of the initial model which is used by the TP-based Model Transformation technique, namely: **LPV model (I)** and **qLPV model (II)**.

(I) LPV models. Only the varying parameters are taken into consideration when defining the transformation space used in the first step of the modeling algorithm. The LPV models are derived in:

- [Tik04], for a mass-spring system;
- [Hua12], for a supersonic vehicle;
- [Pre12], for an automatic transmission system;
- [Bar18], in the generalized TP-based model transformation technique;
- [Ile21], for a tower crane system.

(II) qLPV models. Some of the varying parameters are also state variables of the process. The qLPV models are derived in:

- [Bar06b], for the TORA system;
- [Hed19b] and [Hed19e], for a magnetic levitation system;
- [Nag07a], [Nag07b], [Bar22a], [Kuc21] and [Hed21a], for a pendulum-cart system;
- [Ile14] and [Hed21b], for a tower crane system;
- [Szo14b], [Szo14c] and [Bar15], for an aeroelastic system.

3. TP-based Model Transformation technique used in system modeling

3.1. The TP-based Model Transformation modeling algorithm

The Tensor Product (TP)-based Model Transformation technique is a numerical, non-heuristic method that is capable of transforming a dynamic system model, into parameter-varying weighted combination of parameter independent (constant) system models under the form of Linear Time Invariant (LTI) systems. It has the advantage of allowing LMI and Parallel Distributed Compensation (PDC) frameworks to be applied immediately to the resulting affine models. This leads to tractable and improved control system performance.

The parameters introduced in the modeling algorithm are of two categories, (i) and (ii):

(i) the extremities of the varying domains of the transformation space, which are imposed according to the contratints applied to the process operation,

(ii) the number of varying parameters, the number of discretization points and the number of singular values, which are chosen by the designer, and are directly correlated to the complexity of computations and the number of LTI systems of the TP model that will be derived by the algorithm.

The six steps of the TP-based Model Transformation modeling algorithm are illustrated in Fig.3.1 and are presented in detail in the following paragraphs.

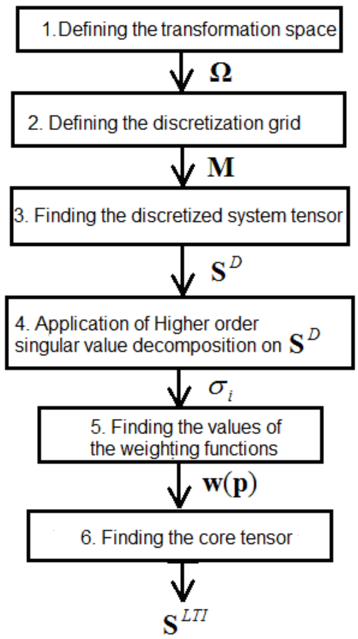

Fig.3.1. The TP-based model transformation diagram [Hed18a].

1. Defining the transformation space.

The transformation space denoted by $\mathbf{\Omega}$ is made of the intersection of the varying domains of the model parameters. Therefore,

$\mathbf{\Omega} = [a_1, b_1] \times [a_2, b_2] \times ... \times [a_n, b_n] \subset \Re^n$, where the extremities of the intervals $[a_i, b_i]$, with $p_i, p_i \in [a_i, b_i]$ and $i = 1...n$, are chosen depending on the restrictions applied to the operation of the process. The parameter vector is denoted by $\mathbf{p} = [p_1 \;\; p_2 \, ... \, p_n]^T \in \mathbf{\Omega}$, where n indicates the number of parameters and the superscript T denotes the matrix transposition. For example, in case of two varying parameters $p_1 \in [a_1, b_1]$ and $p_2 \in [a_2, b_2]$ the transformation space $\mathbf{\Omega} = [a_1, b_1] \times [a_2, b_2]$ is illustrated in Fig.3.2.

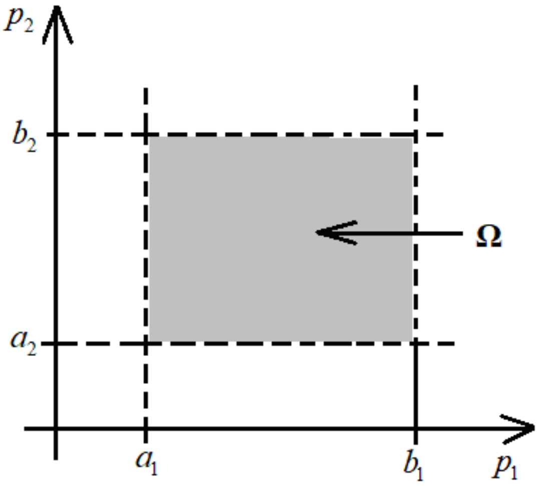

Fig.3.2. The transformation space for two parameters [Hed18a], [Hed19e].

2. Defining the discretization grid.

In the second step of the TP-based Model Transformation, every interval $[a_i, b_i]$, $i = 1...n$, of the transformation space $\mathbf{\Omega}$ is discretized using a number of discretization points denoted by $M_i, M_i \in \mathbf{N}, M_i \geq 2$ including the ends of each interval. The discretization points have the following expression [Bar13]:

$$g_{i,m_i} = a_i + (b_i - a_i)(m_i - 1)/(M_i - 1), \\ a_i \leq g_{i,m_i} \leq b_i, \, m_i = 1...M_i, \, i = 1...n, \tag{3.1}$$

where a discretization point $\mathbf{g}_{m_1, m_2, ..., m_n}$, $\mathbf{g}_{m_1, m_2, ..., m_n} \in \mathbf{\Omega}$ is:

$$\mathbf{g}_{m_1, m_2, ..., m_n} = [g_{1,m_1} \quad g_{2,m_2} \quad ... \quad g_{n,m_n}]^T. \tag{3.2}$$

Thus, the discretization grid becomes:

$$\mathbf{M} = \{\mathbf{g}_{m_1, m_2, ..., m_n} \in \mathbf{\Omega}\}, \; m_i = 1...M_i, i = 1...n, \\ |\mathbf{M}| = M_1 \cdot M_2 \cdot ... \cdot M_n. \tag{3.3}$$

In the particular case of two varying parameters, for $M_1 = 8$ and $M_2 = 6$ the discretization grid $\mathbf{M}$ with $|\mathbf{M}| = M_1 \cdot M_2 = 8 \cdot 6$ points is illustrated in Fig.3.3.

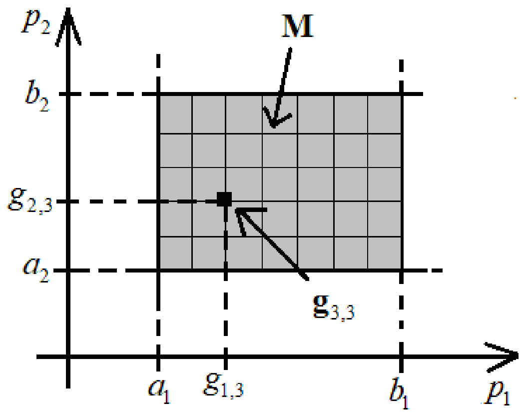

Fig.3.3. The discretization grid for two parameters [Hed18a], [Hed19e].

3. Finding the discretized system tensor.

In the third step of the TP-based Model Transformation, the discretized system tensor is defined starting with the continuous state-space model representation of the LPV process:

$$\begin{aligned}&\dot{\mathbf{x}}(t)=\mathbf{A}(\mathbf{p})\mathbf{x}(t)+\mathbf{B}(\mathbf{p})\mathbf{u}(t),\ \mathbf{x}(0)=\mathbf{x}_0,\\&\mathbf{y}(t)=\mathbf{C}(\mathbf{p})\mathbf{x}(t)+\mathbf{D}(\mathbf{p})\mathbf{u}(t),\end{aligned}\tag{3.4}$$

where $\mathbf{x}(t)$, $\mathbf{x}(t)\in\Re^q$ is the state vector, $t\in\Re, t\geq 0$ is the time variable, $\mathbf{x}_0\in\Re^q$ is the initial state vector, q is the number of states, $\mathbf{u}(t)\in\Re^m$ is the input vector, m is the number of inputs, $\mathbf{y}(t)\in\Re^l$ is the output process vector, l is the number of outputs, and $\mathbf{A}(\mathbf{p})\in\Re^{q\times q}$, $\mathbf{B}(\mathbf{p})\in\Re^{q\times m}$, $\mathbf{C}(\mathbf{p})\in\Re^{l\times q}$, $\mathbf{D}(\mathbf{p})\in\Re^{l\times m}$ are the system matrices.

Thus, the following system matrix is defined [Bar13]:

$$\begin{aligned}&\mathbf{S}(\mathbf{p})=\begin{bmatrix}\mathbf{A}(\mathbf{p}) & \mathbf{B}(\mathbf{p})\\ \mathbf{C}(\mathbf{p}) & \mathbf{D}(\mathbf{p})\end{bmatrix}\in\Re^{(l+q)\times(m+q)},\\&\mathbf{S}(\mathbf{p})=[s_{ij}(\mathbf{p})]_{i=1\dots(l+q),\,j=1\dots(m+q)}.\end{aligned}\tag{3.5}$$

For each discretization point $\mathbf{g}_{m_1,m_2,\dots,m_n}\in\mathbf{M}$, the discretized system matrix is defined as:

$$\begin{aligned}&\mathbf{S}^D_{m_1,m_2,\dots,m_n}=\mathbf{S}(\mathbf{g}_{m_1,m_2,\dots,m_n})\in\Re^{(l+q)\times(m+q)}\\&\mathbf{S}^D_{m_1,m_2,\dots,m_n}=[s_{ij}(\mathbf{g}_{m_1,m_2,\dots,m_n})]_{i=1\dots(l+q),\,j=1\dots(m+q)}\end{aligned}\tag{3.6}$$

The main idea resulting from (3.6) is that the discretized system matrix $\mathbf{S}^D_{m_1,m_2,\dots,m_n}$ is in fact the system matrix $\mathbf{S}(\mathbf{p})$ in (3.5) computed for the parameter vector equal to the discretization point $\mathbf{p}=\mathbf{g}_{m_1,m_2,\dots,m_n}=[g_{1,m_1}\quad g_{2,m_2}\quad\dots\quad g_{n,m_n}]^T\in\mathbf{M}$. Finally, the discretized tensor $\mathbf{S}^D$, whose cells are the discretized system matrices $\mathbf{S}^D_{m_1,m_2,\dots,m_n}$, is defined as:

$$\begin{aligned}&\mathbf{S}^D=[\mathbf{S}^D_{m_1,m_2,\dots,m_n}]_{m_1=1\dots M_1,\,m_2=1\dots M_2,\dots,m_n=1\dots M_n}\\&\mathbf{S}^D\in\Re^{M_1\times M_2\times\dots\times M_n\times(l+q)\times(m+q)}.\end{aligned}\tag{3.7}$$

The discretized tensor computed for a system with two varying parameters has the particular expression:

$$\mathbf{S}^D = [\mathbf{S}^D_{m_1,m_2}]_{m_1=1...8, m_2=1...6}$$
$$= \begin{bmatrix} \mathbf{S}^D_{1,1} & \mathbf{S}^D_{1,2} & \ldots & \mathbf{S}^D_{1,6} \\ \mathbf{S}^D_{2,1} & \mathbf{S}^D_{2,2} & \ldots & \mathbf{S}^D_{2,6} \\ \ldots & \ldots & \ldots & \ldots \\ \mathbf{S}^D_{8,1} & \mathbf{S}^D_{8,2} & \ldots & \mathbf{S}^D_{8,6} \end{bmatrix} \in \Re^{8\times 6\times(l+q)\times(m+q)}. \tag{3.8}$$

4. Application of the HOSVD on the tensor $\mathbf{S}^D$.

The discretized tensor $\mathbf{S}^D \in \mathbf{R}^{M_1\times M_2\times..\times M_n\times(l+q)\times(m+q)}$ in (3.8) can be written as [Hed19e]:

$$\mathbf{S}^D = \mathbf{S} \underset{n=1}{\overset{N}{\otimes}} \mathbf{U}_n, \tag{3.9}$$

where:

- $\mathbf{U}_n = [\mathbf{u}_{n,1}\ \mathbf{u}_{n,2}\ \ldots\ \mathbf{u}_{n,I_n}],\ n = 1...N$ is an orthonormal matrix meaning that it is an orthogonal matrix made of unitary vectors, $\mathbf{U}_n \in \Re^{M_n\times I_n}$, $\mathbf{u}_{n,I_n} \in \Re^{M_n\times 1}$ and I_n indicates the number of singular values;
- $\mathbf{S}$ is a real tensor, $\mathbf{S} \in \mathbf{R}^{M_1\times M_2\times..\times M_n\times(l+q)\times(m+q)}$;
- $\otimes$ indicates the *n*-mode product of a tensor defined as:

$$\mathbf{S} \underset{n=1}{\overset{N}{\otimes}} \mathbf{U}_n = \mathbf{S} \times_1 \mathbf{U}_1 \times_2 \mathbf{U}_2 \times_3 \ldots\ldots \times_N \mathbf{U}_N, \tag{3.10}$$

which means the tensor $\mathbf{S}$ is multiplied along its *n*-th dimension with $\mathbf{U}_n$ for $n = 1...N$.

The *n*-mode product of a tensor in (3.10), namely $\mathbf{S}^D = \mathbf{S} \times_n \mathbf{U}$, $n = 1...N$, is a matrix product obtained by first finding the *n*-mode matrix of tensor $\mathbf{S}$, $\mathbf{S}_{(n)}$, then by computing the matrix product $\mathbf{S}^D_{(n)} = \mathbf{U} \cdot \mathbf{S}_{(n)}$ and finally by finding the discretized tensor $\mathbf{S}^D$ in $\mathbf{S}_{(n)}$ [Hed19e].

The *n*-mode matrix $\mathbf{S}^D_{(n)} \in \Re^{M_n\times(M_{n+1}M_{n+2}...(m+q)M_1M_2...(l+q))}$ is defined as:

$$\mathbf{S}^D_{(n)} = [\mathbf{s}^D_r], \tag{3.11}$$

where $\mathbf{s}^D_r \in \Re^{M_n}$ denote the column vectors of the M_n dimension of tensor $\mathbf{S}^D$ and $r = 1...R$, with $R = M_{n+1}M_{n+2}...(m+q)M_1M_2...(l+q)$.

The Higher Order Singular Value Decomposition (HOSVD) applied on the tensor $\mathbf{S}^D$ implies *n* singular value decompositions (SVD) made for all the *n*-mode matrices $\mathbf{S}^D_{(n)}$. The SVD of the *n*-mode matrix $\mathbf{S}^D_{(n)}$ makes use of with the following theorem with the proof given in [Lat00].

Theorem 1. Whatever the matrix $\mathbf{S}^D_{(n)}$ there are the orthogonal matrices $\mathbf{U}_n, \mathbf{V}_n$ such that

$$\mathbf{U}^T_n \mathbf{S}^D_{(n)} \mathbf{V}_n = \mathbf{\Sigma}_n,$$
$$\mathbf{\Sigma}_n = \begin{bmatrix} \mathbf{\Sigma}_1 & 0 \\ 0 & 0 \end{bmatrix}, \tag{3.12}$$
$$\mathbf{\Sigma}_1 = \mathbf{diag}(\sigma_1, \sigma_2, ..., \sigma_{I_n}),$$

where $\sigma_1 \geq \sigma_2 \geq .... \geq \sigma_{I_n}$ are the singular values.

The SVD of the n-mode matrix $\mathbf{S}_{(n)}^D$ is then computed as:

$$\mathbf{S}_{(n)}^D = \mathbf{U}_n \mathbf{\Sigma}_n \mathbf{V}_n^T, \tag{3.13}$$

where $\mathbf{\Sigma}_n$ is defined in (3.12) and $\mathbf{U}_n$ and $\mathbf{V}_n$ are the left and the right singular matrices and they are unique. The singular values of the matrix $\mathbf{S}_{(n)}^D$ are the unique positive square roots of the eigenvalues of the matrix $\mathbf{X} = \mathbf{S}_{(n)}^{D^T} \mathbf{S}_{(n)}^D$.

The SVD algorithm is presented as follows using the steps a), b) and c) [Lat00]:

a) Computation of $\mathbf{X} = \mathbf{S}_{(n)}^{D^T} \mathbf{S}_{(n)}^D$.

b) Computation of the eigenvalues λ_r of the matrix $\mathbf{X}(\lambda_r), r = 2..., N$.

c) Computation of the singular values of the matrix $\mathbf{S}_{(n)}^D$ (using only the positive eigenvalues):

$$\sigma_r = \sqrt{\lambda_r}, r = 1...I_n. \tag{3.14}$$

After finding the singular values of $\mathbf{S}_{(n)}^D$, the matrices $\mathbf{U}_n$ and $\mathbf{V}_n$ are computed after solving the system (3.14). The column vectors $\mathbf{u}_{n,I_n}$ in the matrix $\mathbf{U}_n$ are called weighting vectors and they are later used for finding the values of the weighting functions (w.f.s).

5. Finding the values of the weighting functions.

The values of the column vectors $\mathbf{u}_{n,I_n}$ of $\mathbf{U}_n$ define the values of the w.f. $\mathbf{w}_n(\mathbf{p}_{m_1,m_2,..m_n})$ for $\mathbf{p}_{m_1,m_2,..m_n} = (g_{1,m_1},....g_{n,m_n})$ [Hed19e]:

$$\mathbf{w}_n(\mathbf{p}_{m_1,m_2,..m_n}) = \mathbf{u}_{n,I_n}. \tag{3.15}$$

6. Finding the core tensor.

The core tensor $\mathbf{S}_f$ is computed by bringing to the left of the tensor $\mathbf{S}^D$ the singular matrices $\mathbf{U}_n$ [Bar13]:

$$\mathbf{S}_f = \mathbf{S}^D \bigotimes_{n=1}^{N} \mathbf{U}_N^T = \mathbf{S}^D \times_1 \mathbf{U}_1^T \times_2 \mathbf{U}_2^T \times_3 .....\times_N \mathbf{U}_N^T. \tag{3.16}$$

For any parameter vector $\mathbf{p} \in \mathbf{\Omega}$, the core tensor $\mathbf{S}_f$ is expressed as a convex combination of the LTI system matrices $\mathbf{S}_{m_1,m_2,...m_n}^{LTI} \in \Re^{(l+q)\times(m+q)}$ called also vertex systems:

$$\mathbf{S}_f = \sum_{m_1=1}^{M_1} \sum_{m_2=1}^{M_2} \cdots \sum_{m_n=1}^{M_n} \prod_{n=1}^{N} \mathbf{w}_n(\mathbf{p}_{m_1,m_2,..m_n}) \mathbf{S}_{m_1,m_2,...m_n}^{LTI}. \tag{3.17}$$

Using the compact notation specified in (3.9), the following expression is obtained [Bar04b]:

$$\mathbf{S}(\mathbf{p}(t)) = \mathbf{S}_f \otimes \mathbf{w}_n(\mathbf{p}_{m_1,m_2,..m_n}). \tag{3.18}$$

3.2. The derivation of the TP model for Vertical Three Tank System

The Vertical Three Tank System (V3TS) is a laboratory equipment designed for experiments which has the diagram of principle presented in Fig.3.4. The system is made of four thanks: three of them (T1, T2 and T3) placed vertically and the fourth one (T4) which is placed under the third tank. The system also contains a variable speed pump driven by a DC motor and three electrical servo valves. Three piezo-resistive pressure sensors PS1, PS2 and PS3are used to measure the water levels y_1, y_2 and y_3.

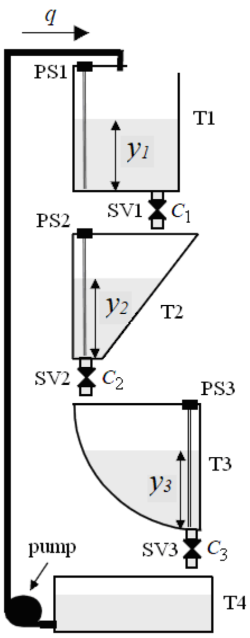

Fig.3.4. Diagram of principle of V3TS [Int07].

The state-space equations of the process are [Int07]

$$\begin{aligned}
\dot{y}_1 &= q/\beta_1(y_1) - C_1 y_1^{\alpha_1}/\beta_1(y_1),\\
\dot{y}_2 &= C_1 y_1^{\alpha_1}/\beta_2(y_2) - C_2 y_2^{\alpha_2}/\beta_2(y_2),\\
\dot{y}_3 &= C_2 y_2^{\alpha_2}/\beta_3(y_3) - C_3 y_3^{\alpha_3}/\beta_3(y_3),
\end{aligned} \tag{3.19}$$

where $q = 0.435 \cdot 10^{-4}$ (m^3/s) is the inflow rate, u is the control signal, i.e. the Pulse Width Modulation (PWM) duty cycle of DC motor for the speed pump control, $k_P = 1.6 \cdot 10^{-4}$ (m^3/s) is the pump gain, y_i (m), $i \in \{1,2,3\}$, is the fluid level of i^{th} tank with the maximum values $y_{1\max} = y_{2\max} = y_{3\max} = 0.35$ (m), α_i is the flow coefficient for i^{th} tank with $\alpha_1 = \alpha_2 = \alpha_3 = 0.5$ (l/min), C_i is the resistance of the output orifice of i^{th} tank with $C_1 = C_2 = C_3 = 11.08 \cdot 10^{-5}$ (kg/m^2), $\beta_i(y_i)$ is the cross sectional area of i^{th} tank computed at the level y_i:

$$\begin{aligned}
\beta_1(y_1) &= a\,w,\\
\beta_2(y_2) &= c\,w + (y_2/y_{2\max})\,b\,w,\\
\beta_3(y_3) &= w\sqrt{R^2 - (R - y_3)^2},
\end{aligned} \tag{3.20}$$

and $a = 0.25$ (m), $b = 0.345$ (m), $c = 0.1$ (m), $w = 0.035$ (m), $R = 0.364$ (m) represent the geometrical parameters of the three tanks. The three electrical servo valves are closed. However, the manual valves are open.

In order to simplify the further development of control structures for the liquid level control of V3TS, which will be presented in Chapter 4, the nonlinear model is linearized around two operating points (o.p.s) $P^{(j)} = (y_1^{(j)}, y_2^{(j)}, y_3^{(j)}, u^{(j)})^T$ where $j = \overline{1,2}$ is the index of the o.p.s. The o.p.s are chosen to cover the usual operating regimes and to avoid the extremities of the input-output map, which create problems in the computation of the process gains. Therefore, the two o.p.s are $P^{(1)}(0.1, 0.1, 0.1, 0.4)$ and $P^{(2)}(0.21, 0.21, 0.21, 0.4)$ [Boj18b], [Boj19].

Using the two o.p.s, the following state-space linearized mathematical model is obtained for V3TS:

$$\begin{cases} \Delta\dot{\mathbf{x}}^{(j)} = \mathbf{A}^{(j)}\,\Delta\mathbf{x}^{(j)} + \mathbf{b}^{(j)}\Delta u^{(j)} \\ \Delta y^{(j)} = \mathbf{C}\Delta\mathbf{x}^{(j)} \end{cases},$$
$$\Delta\mathbf{x}^{(j)} = \begin{bmatrix}\Delta y_1^{(j)} & \Delta y_2^{(j)} & \Delta y_3^{(j)}\end{bmatrix}^T, \tag{3.21}$$
$$\mathbf{A}^{(j)} = \begin{bmatrix} a_{11}^{(j)} & 0 & 0 \\ a_{21}^{(j)} & a_{22}^{(j)} & 0 \\ 0 & a_{32}^{(j)} & a_{33}^{(j)} \end{bmatrix}, \mathbf{b}^{(j)} = \begin{bmatrix} b_{11}^{(j)} \\ 0 \\ 0 \end{bmatrix}, \ \mathbf{C} = \begin{bmatrix} 1 & 0 & 0 \\ 0 & 1 & 0 \\ 0 & 0 & 1 \end{bmatrix}, \ j = \overline{1,2},$$

with the matrix parameters

$$\begin{aligned} a_{11}^{(j)} &= -C_1\alpha_1/(a\,w\,\mathrm{y}_{10}^{1-\alpha_1}), \\ a_{21}^{(j)} &= C_1\alpha_1/(a\,w\,\mathrm{y}_{10}^{1-\alpha_1}), \\ a_{22}^{(j)} &= -C_2\alpha_2/[w(c + b\,y_{20}/y_{2\max})y_{20}^{1-\alpha_2}], \\ a_{32}^{(j)} &= C_2\alpha_2/[w(c + b\,y_{20}/y_{2\max})H_{20}^{1-\alpha_2}], \\ a_{33}^{(j)} &= -C_3\alpha_3/[w\sqrt{R^2 - (R - y_3)^2}\,y_{30}^{1-\alpha_3}], \\ b_{11}^{(j)} &= q/(a\,w),\ j = \overline{1,2}, \end{aligned} \tag{3.22}$$

where $\mathbf{x} = [x_1 \quad x_2 \quad x_3]^T = [y_1 \quad y_2 \quad y_3]^T \in \Re^3$ is the process state vector, $x_1 = y_1$ (m), $x_2 = y_2$ (m) and $x_3 = y_3$ (m) are the state variables, $\Delta y_1^{(j)} = y_1^{(j)} - y_{10}^{(j)}$, $\Delta y_2^{(j)} = y_2^{(j)} - y_{20}^{(j)}$, $\Delta y_3^{(j)} = y_3^{(j)} - y_{30}^{(j)}$, $\Delta u^{(j)} = u^{(j)} - u_0^{(j)}$ are the differences of the variables $y_1^{(j)}$, $y_2^{(j)}$, $y_3^{(j)}$, and $u^{(j)}$ with respect to the values at the operating points, $y_{10}^{(j)}$, $y_{20}^{(j)}$, $y_{30}^{(j)}$ and $u_0^{(j)}$, respectively.

After replacing the values of the two o.p.s in (3.21), two linearized models are obtained for V3TS with the corresponding matrices given in Equation (1) in Appendix 1.

Next, the derivation of the TP model for V3TS is presented. It starts with the qLPV model of V3TS:

$$\begin{aligned} \dot{\mathbf{x}} &= \mathbf{A}(\mathbf{p})\mathbf{x} + \mathbf{b}(\mathbf{p})u, \\ \mathbf{y} &= \mathbf{C}\,\mathbf{x}, \end{aligned} \tag{3.23}$$

where $\mathbf{p} = p_1 = y_1 \in \Re^1$ is the bounded parameter vector, which contains the first state variable, that is the reason why it is actually a scalar, $\mathbf{y}$ is the controlled output variable, i.e. the tank fluid level, $\mathbf{A}(\mathbf{p}), \mathbf{b}(\mathbf{p}), \mathbf{C}$ result from [Int07]:

$$\mathbf{A}(\mathbf{p}) = \begin{bmatrix} a_{11}(\mathbf{p}) & 0 & 0 \\ a_{21}(\mathbf{p}) & a_{22} & 0 \\ 0 & a_{32} & a_{33} \end{bmatrix} \in \Re^{3x3}, \qquad (3.24)$$
$$\mathbf{b} = \begin{bmatrix} b_{11} \\ 0 \\ 0 \end{bmatrix} \in \Re^{3x1}, \ \mathbf{C} = \begin{bmatrix} 1 & 0 & 0 \\ 0 & 1 & 0 \\ 0 & 0 & 1 \end{bmatrix} \in \Re^{3x3},$$

and the elements of the matrices result from (3.21).

Introducing in (3.23) the system matrix

$$\mathbf{S}(\mathbf{p}) = [\mathbf{A}(\mathbf{p}) \quad \mathbf{b}] \in \Re^{3\times 4}, \qquad (3.25)$$

the model is transformed in the LPV state-space form [Bar04b]

$$\dot{\mathbf{x}} = \mathbf{S}(\mathbf{p})[\mathbf{x}^T \quad u]^T, \qquad (3.26)$$
$$\mathbf{y} = \mathbf{C}\mathbf{x}.$$

The idea of the TP-based Model Transformation is to obtain LTI models from the qLPV model (3.23) as follows [Hed18a]:

$$\dot{\mathbf{x}} = \mathbf{S}(\mathbf{p}(t)) \bigotimes_{n=1}^{N} \mathbf{w}_n(\mathbf{p}_n)[\mathbf{x}^T \ u]^T = \sum_{m_1=1}^{M_1} w_{1,m_1}(p_1)\mathbf{S}_{m_1}[\mathbf{x}^T \ u]^T, \qquad (3.27)$$
$$\mathbf{y} = \mathbf{C}\mathbf{x},$$

where the values of the continuous w.f.s are given by the row matrix $\mathbf{w}_n(\mathbf{p}_n)$, $\mathbf{S}$ is the system tensor of dimension N, the initial state vector $\mathbf{x}_0 \in \Re^q$ is not specified for the sake of simplicity, and q=3. The LTI system matrices are $\mathbf{S}_{m_1} = [\mathbf{A}_{m_1} \quad \mathbf{b}_{m_1}]$, with $M_1 = 2$ - the number of singular values, which is chosen by the designer such that to ensure a small number of models in the TP. The resulted TP model is expressed as:

$$\dot{\mathbf{x}} = \sum_{m_1=1}^{2} w_{1,m_1}(p_1)(\mathbf{A}_{m_1}\mathbf{x} + \mathbf{b}_{m_1}u), \qquad (3.28)$$
$$\mathbf{y} = \mathbf{C}\mathbf{x}.$$

Using the TP Tool [Nag07c] the LTI system matrices are obtained for V3TS [Hed18a] and are given in equation (1) in Appendix 2. The w.f.s are of canonic type [Hed18a] and are illustrated in Fig.3.5.

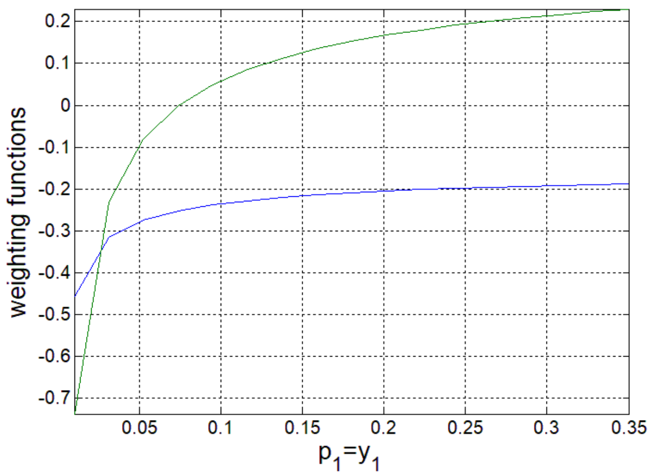

Fig.3.5. Weighting functions obtained for the first parameter.

One testing scenario was conducted in order to test the derived TP model for V3TS given in (3.28). In order to compare the performance of the TP model with other models derived for V3TS, four linear models are also tested in the same scenario as the TP model using the testing block diagram illustrated in Fig.3.6. The first linear model is represented by the first linearized model presented in (3.21) corresponding to the first o.p. with the numerical values given in Equation (1) in Appendix 1, the second linear model is represented by the second linearized model presented in (3.21) corresponding to the second o.p. with the numerical values given in Equation (1) in Appendix 1, the third linear model is represented by the LTI model resulting from the TP model, characterized by the LTI system matrix $\mathbf{S}_1$ given in Equation (1) in Appendix 2 and the fourth linear model is represented by the LTI model resulting from the TP model, characterized by the LTI system matrix $\mathbf{S}_2$ given in Equation (1) in Appendix 2.

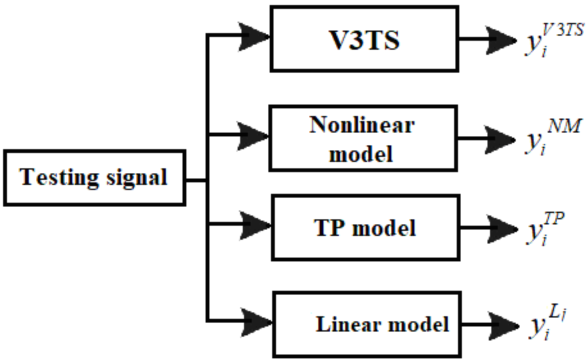

Fig.3.6. Testing block diagram for V3TS.

A Pseudo Random Binary Signal (PRBS) signal with a 0.2 amplitude, which is illustrated in Fig.3.7, was applied to the V3TS laboratory equipment, to the nonlinear model given in (3.19), to the TP model given in (3.26) and to the four linear models of V3TS on the time horizon of 1000 s. The initial state vector matching the experiments is $\mathbf{x}_0 = [0 \quad 0 \quad 0]^T$.

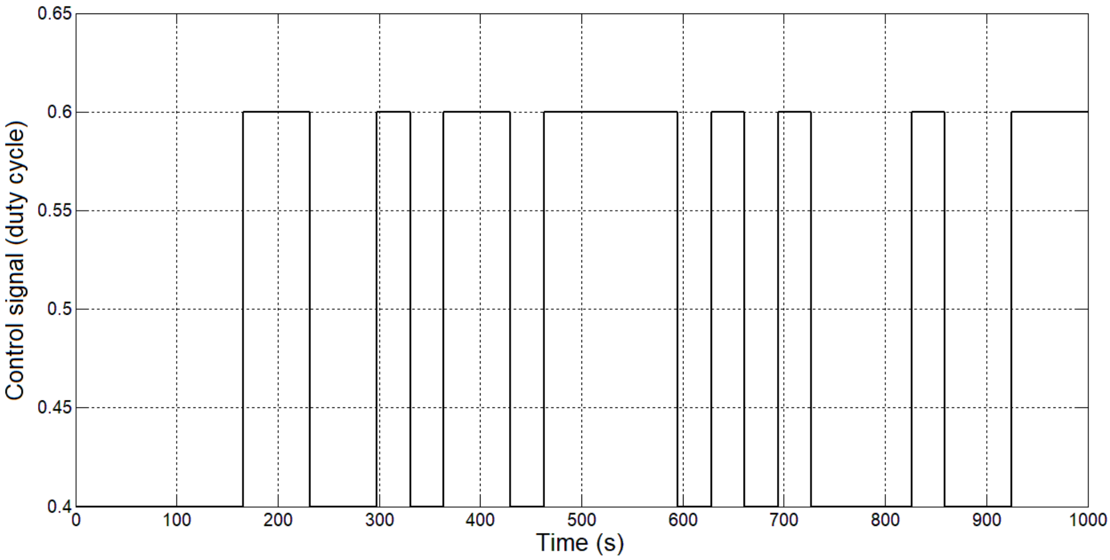

Fig.3.7. Control signal versus time used in the testing scenario.

The corresponding outputs of the V3TS laboratory equipment, of the nonlinear model, of the TP model and of the four linear models illustrated in Figs.3.8-3.10, were collected and compared.

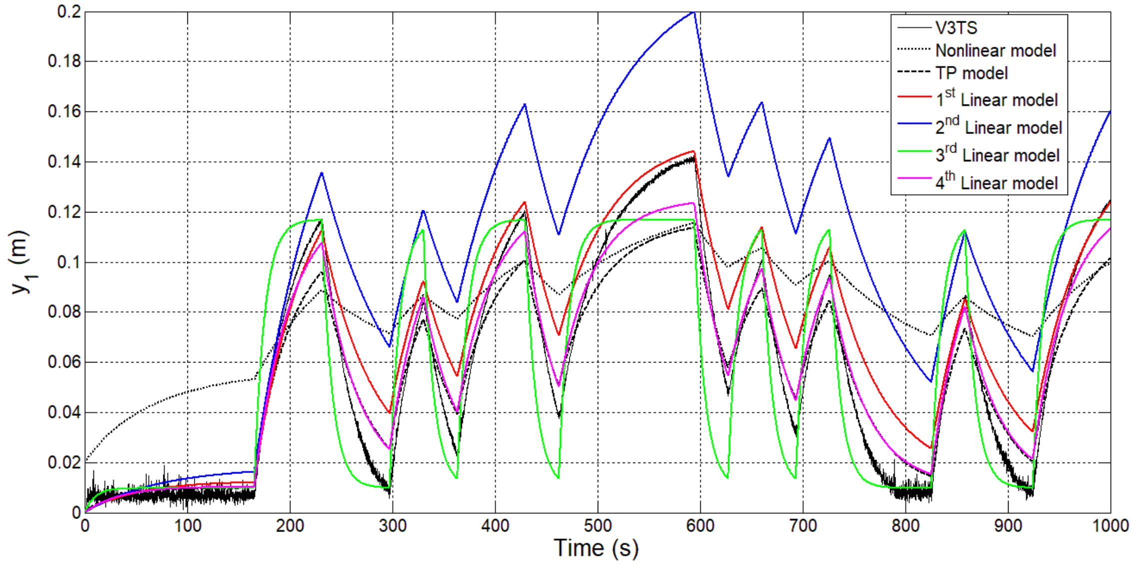

Fig.3.8. First tank fluid level vs. time for V3TS laboratory equipment, nonlinear model, TP model, 1st linear model, 2nd linear model, 3rd linear model and 4th linear model in the testing scenario.

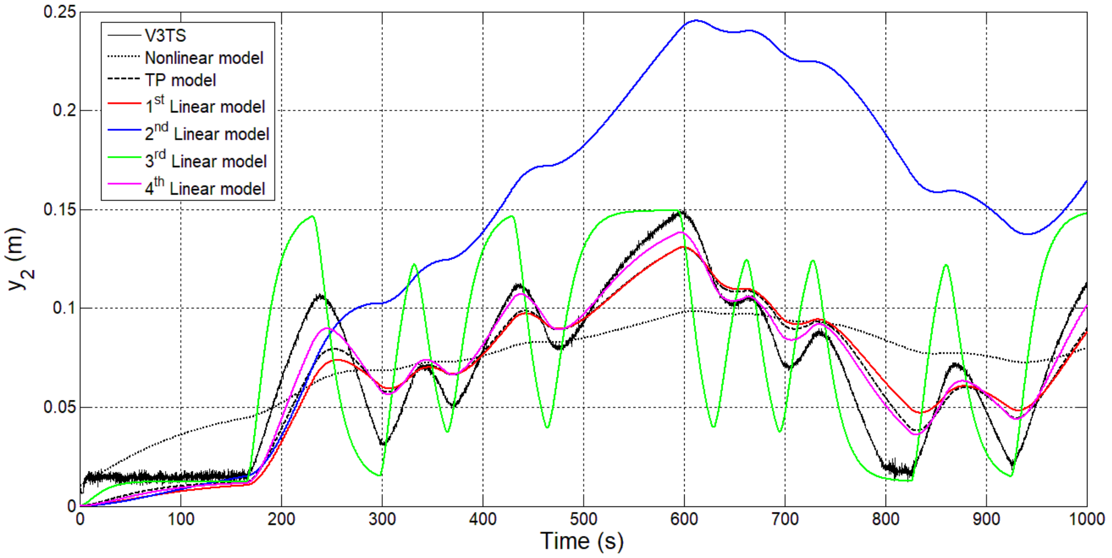

Fig.3.9. Second tank fluid level vs. time for V3TS laboratory equipment, nonlinear model, TP model, 1st linear model, 2nd linear model, 3rd linear model and 4th linear model in the testing scenario.

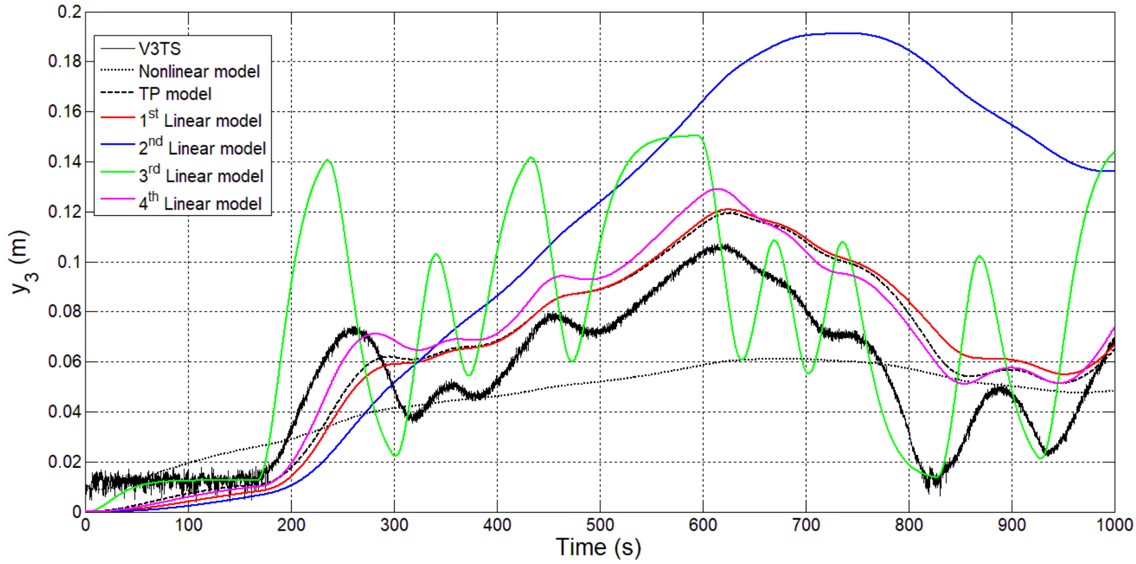

Fig.3.10. Third tank fluid level vs. time for V3TS laboratory equipment, nonlinear model, TP model, 1st linear model, 2nd linear model, 3rd linear model and 4th linear model in the testing scenario.

Four performance indices, namely Root Mean Square Error (RMSE), Value of Accounted For (VAF), Akaike Information Criterion (AIC) and Bayesian Information Criterion (BIC), are measured in order to better highlight the performance of the TP model derived for the V3TS in the testing scenario.

The RMSEs are computed as

$$RMSE = \sqrt{\frac{1}{M}\sum_{k=1}^{M} e_i^{\psi\,2}(k)}, \tag{3.29}$$

where $e_i^{\psi}(k)$ represent the modeling errors, which in case of V3TS are computed as

$$e_i^{\psi} = y_i^{V3TS} - y_i^{\psi}, i = 1...3. \tag{3.30}$$

The superscript $\psi = NM$ indicates the nonlinear model, $\psi = TP$ indicates the TP model, $\psi = L_1$ indicates the first linear model, $\psi = L_2$ indicates the second linear model, $\psi = L_3$ indicates the third linear model, $\psi = L_4$ indicates the fourth linear model, y_i^{V3TS} are the outputs of the V3TS system (i.e. the real-world process), y_i^{ψ} are the outputs of the models, i represents the number of tank, $M = 10000$ is the number of samples and the sampling period $T_s = 0.1$ s.

The VAF values were computed in terms of [Sub12]

$$\begin{aligned} VAF_i^{\psi} &= 100 \cdot [1 - \sigma^2(e_i^{\psi}) / \sigma^2(y_i^{\psi})], \\ \sigma^2(e_i^{\psi}) &= \left[\sum_{k=1}^{M} (e_i^{\psi}(k) - \bar{e}_i^{\psi})^2\right] \Big/ [M-1], \\ \sigma^2(y_i^{\psi}) &= \left[\sum_{k=1}^{M} (y_i^{\psi}(k) - \bar{y}_i^{\psi})^2\right] \Big/ [M-1], \end{aligned} \tag{3.31}$$

where e_i^{ψ} results from (3.28), $\sigma^2(e_i^{\psi})$ represent the variances computed for the modeling errors, and $\sigma^2(y_i^{\psi})$ represent the general form of the variances computed for the outputs of the models, respectively, $\bar{e}_i^{\psi}$ are the means of the modeling errors and $\bar{y}_i^{\psi}$ are the means of the outputs.

The AIC introduced in [Aka73] and the BIC introduced in [Sch78] were also computed for both models in terms of

$$AIC_i^{\psi} = \ln\left(\frac{1}{M}\sum_{k=1}^{M} e_i^{\psi^2}(k)\right) + \frac{k^{\psi}}{2},$$
$$BIC_i^{\psi} = AIC_i^{\psi} + [\ln(M)/M], \qquad (3.32)$$

where *ln()* is the natural logarithm and k^{ψ} represents the number of paramaters of each model. In case of V3TS $k^{TP} = 48$ is the number of parameters of the TP model, $k^{NM} = 16$ is the number of parameters of the nonlinear model, $k^{L_1} = k^{L_2} = 16$ is the number of parameters of the first and second linear model, and $k^{L_3} = k^{L_4} = 6$ is the number of parameters of the third and fourth linear model. The values of the performance indices are given in Table 3.2.1.

Table 3.2.1.
Values of performance indices for V3TS.

Model	***Criterion***			
	RMSE (m)	**VAF (%)**	**AIC**	**BIC**
TP model/ 1st tank	0.0118	86.8403	15.1173	15.1182
TP model/ 2nd tank	0.0148	82.9007	15.5675	15.5684
TP model/ 3rd tank	0.0203	76.8452	16.2054	16.2063
Nonlinear model/ 1st tank	0.0356	73.1740	1.3314	1.3323
Nonlinear model/ 2nd tank	0.0277	55.3223	0.8287	0.8296
Nonlinear model/ 3rd tank	0.0222	92.4840	0.3862	0.3871
1st Linear model/1st tank	0.0174	91.1566	0.0937	0.0983
1st Linear model/2nd tank	0.0174	77.0904	0.1069	0.1078
1st Linear model/3rd tank	0.0226	71.9618	0.4246	0.4255
2nd Linear model/1st tank	0.0486	79.5526	1.9520	1.9503
2nd Linear model/2nd tank	0.0904	44.4969	3.1931	3.1940
2nd Linear model/3rd tank	0.0773	30.5677	2.8808	2.8817
3rd Linear model/1st tank	0.0213	77.7836	4.6972	4.6981
3rd Linear model/2nd tank	0.0311	63.8652	3.9405	3.9415
3rd Linear model/3rd tank	0.0373	54.2338	3.5777	3.5786
4th Linear model/1st tank	0.0085	94.8032	6.5353	6.5362
4th Linear model/2nd tank	0.0118	89.9512	5.8720	5.8729
4th Linear model/3rd tank	0.0204	82.4868	4.7855	4.7865

The best performance concerning the values of RMSE is obtained by the fourth linear model in case of the first and second tank and by the TP model in case of the third tank while, the best performamce in terms of VAF are obtained by the fourth linear model in case of all three tanks. However, the TP model ensures better performance than the nonlinear model and the four linear ones in terms of AIC and BIC in case of all three tanks.

Therefore, the experimental results have shown that the derived TP model expressed in (3.28) approximately mimics the behavior of the laboratory equipment, but exhibiting numerical error. Other numbers of parameters of the TP model would lead to other values in Table 3.2.1.

3.3. The derivation of the TP model for a partial state feedback controlled Magnetic Levitation System

The Magnetic Levitation System (MLS) from Inteco, illustrated in Fig. 3.11, is a laboratory equipment based on the magnetic levitation principle, which includes a metallic frame with one upper electromagnet, Electromagnet 1, and one lower electromagnet, Electromagnet 2. A ferromagnetic sphere levitates between these two electromagnets and its position is measured using position sensors. The communication between the hardware and the software components is ensured by a computer interface.

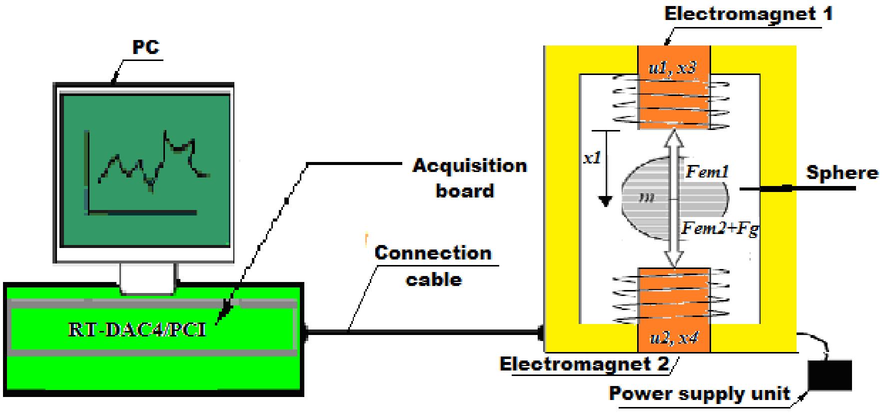

Fig.3.11. Experimental setup for MLS [Int08].

Due to the fact that the MLS is a nonlinear and unstable process, the design of a control structure for the sphere position is a challenging task. So, in order to simplify the further development of control structures, which will be presented in Chapter 4, the fourth state variable of the process is first dropped out resulting the following third-order system with the remaining state variables: the position x_1, the speed v and the intensity of the current in the upper electromagnet i_{EM1}, in terms of neglecting the lower electromagnet. The intensitiy of the current and the signal applied to the lower electromagnet were considered as disturbance inputs, with the following constant numerical values: $i_{EM2} = 0.039$ and $u_{EM2} = 0.005$. Therefore, the reduced nonlinear state-space mathematical model of MLS is:

$$\begin{aligned}
&\dot{x}_1 = v, \\
&\dot{v} = -\frac{i_{EM1}^2 \cdot F_{emP1} \cdot \exp(-x_1 / F_{emP2})}{m \cdot F_{emP2}} + g \\
&\qquad + \frac{i_{EM2}^2(t) \cdot F_{emP1} \cdot \exp(-(x_d - x_1) / F_{emP2}}{m \cdot F_{emP2}}, \\
&\dot{i}_{EM1} = \frac{k_i \cdot u_{EM1} + c_i - i_{EM1}}{\dfrac{f_{iP1}}{f_{iP2}} \cdot \exp(-x_1 / f_{iP2})}, \\
&y = x_1,
\end{aligned} \tag{3.33}$$

where: $x_1 \in [0, 0.0016]$ (m) - the sphere position, $v \in \Re$ (m/s) - the sphere speed, $i_{EM1}, i_{EM2} \in [0.03884, 3.28]$ (A) - the intensities of the currents in the top and bottom electromagnets, $u_{EM1}, u_{EM2} \in [0.00498, 1]$ (V) - the control signals applied to the upper and lower electromagnets, and y (m) - the process output. The MLS process includes the actuators and sensors. The numerical values of the process parameters are determined analytically and experimentally and are given in the following: $D_s = 0.06$ m - the diameter of the sphere, $x_d = 0.09$ m - the distance between electromagnets minus sphere diameter, $g = 9.81$ m/s^2 - the gravity acceleration, $m = 0.0571$ kg - the sphere mass, the parameters $k_i = 0.0243$ (A) and $c_i = 2.5165$ (A) correspond the actuator dynamic analysis, $F_{emP1} = 1.7521 \cdot 10^{-2}$ (H) and $F_{emP2} = 5.8231 \cdot 10^{-3}$ (m) are the electromagnetic forces parameters, $f_{iP1} = 1.4142 \cdot 10^{-4}$ (m s), $f_{iP2} = 4.5626 \cdot 10^{-3}$ (m) [Boj18a].

The third order model given in (3.33) is next linearized at seven operating points (o.p.s.) leading to a set of linearized models, which are controlled using state feedback controllers as shown in [Boj18a], and one of the state feedback controllers is further used. Therefore, the TP model derived in this sub-chapter is obtained for the partial state feedback controlled MLS (psfcMLS).

The mathematical model of the psfcMLS is obtained following two steps, (1) and (2).

Step (1). The third order nonlinear model of MLS (3.32) is linearized around seven o.p.s $P^{(j)} = (x_1^{(j)}, v^{(j)}, i_{EM1}^{(j)}, u_{EM1}^{(j)})^T$ where $j = \overline{1,7}$ is the index of the current o.p. The number of the o.p.s is chosen such that they belong to the steady-state zone of the sphere position sensor input-output map [Boj18a], to cover the usual operating regimes and to avoid the extremities of the input-output map, which create problems in the computation of the process gains. Therefore, the seven o.p.s are $P^{(1)}(0.0063, 0, 1.128, 0.48)$, $P^{(2)}(0.007, 0, 1.145, 0.45)$, $P^{(3)}(0.0077, 0, 1.07, 0.42)$, $P^{(4)}(0.0084, 0, 1, 0.39)$, $P^{(5)}(0.009, 0, 0.9345, 0.36)$, $P^{(6)}(0.0098, 0, 0.89, 0.34)$ and $P^{(7)}(0.0105, 0, 0.83, 0.32)$.

Using the seven o.p.s, the following state-space linearized mathematical model is obtained for MLS:

$$
\begin{aligned}
&\begin{cases} \Delta\dot{\mathbf{x}}^{(j)} = \mathbf{A}^{(j)}\, \Delta\mathbf{x}^{(j)} + \mathbf{b}_{u1}^{(j)} \Delta u_1^{(j)} \\ \Delta y^{(j)} = \mathbf{c}^{T\,(j)} \Delta\mathbf{x}^{(j)} \end{cases}, \\
&\Delta\mathbf{x}^{(j)} = \begin{bmatrix} \Delta x_1^{(j)} & \Delta v^{(j)} & \Delta i_{EM1}^{(j)} \end{bmatrix}^T, \\
&\Delta y^{(j)} = \Delta x_1^{(j)}, \\
&\mathbf{A}^{(j)} = \begin{bmatrix} 0 & 1 & 0 \\ a_{21}^{(j)} & 0 & a_{23}^{(j)} \\ a_{31}^{(j)} & a_{32}^{(j)} & a_{33}^{(j)} \end{bmatrix}, \mathbf{b}_{u1}^{(j)} = \begin{bmatrix} 0 \\ 0 \\ b_{31}^{(j)} \end{bmatrix}, \ \mathbf{c}^{T\,(j)} = \begin{bmatrix} 1 & 0 & 0 \end{bmatrix}, \\
&\mathbf{A}^{(j)} \in \Re^{3x3},\ \mathbf{b}^{(j)} \in \Re^{3x1},\ \mathbf{c}^{T\,(j)} \in \Re^{1x3},\ \Delta\mathbf{x}^{(j)} \in \Re^{3x1},\ \Delta u_1^{(j)} \in \Re,
\end{aligned}
\tag{3.34}
$$

with the matrix parameters

$$a_{21}^{(j)} = \frac{x_{30}^2}{m}\frac{F_{emP1}}{F_{emP2}^2} e^{-\frac{x_{10}}{F_{emP2}}} + \frac{x_{40}^2}{m}\frac{F_{emP1}}{F_{emP2}^2} e^{-\frac{x_d - x_{10}}{F_{emP2}}},\ a_{23}^{(j)} = -\frac{2x_{30}}{m}\frac{F_{emP1}}{F_{emP2}} e^{-\frac{x_{10}}{F_{emP2}}},$$

$$a_{31}^{(j)} = -(k_i u_1 + c_i - x_{30})\frac{x_{10}}{f_{iP1}} \cdot e^{\frac{x_{10}}{f_{iP2}}},\ \ a_{32}^{(j)} = k_i \frac{f_{iP2}}{f_{iP1}} \cdot e^{\frac{x_{10}}{f_{iP2}}}, \tag{3.35}$$

$$a_{33}^{(j)} = -\frac{f_{iP2}}{f_{iP1}} \cdot e^{\frac{x_{10}}{f_{iP2}}}, b_{31}^{(j)} = k_i \cdot \frac{f_{iP2}}{f_{iP1}} \cdot e^{\frac{x_{10}}{f_{iP2}}},$$

where $\Delta x_1^{(j)} = x_1^{(j)} - x_{10}^{(j)}$, $\Delta v^{(j)} = v^{(j)} - v_0^{(j)}$, $\Delta i_{EM1}^{(j)} = i_{EM1}^{(j)} - i_{EM10}^{(j)}$, $\Delta u_{EM1}^{(j)} = u_{EM1}^{(j)} - u_{EM10}^{(j)}$ and $\Delta y^{(j)} = y^{(j)} - y_0^{(j)}$, are the differences of the variables $x_1^{(j)}$, $v^{(j)}$, $i_{EM1}^{(j)}$, $u_{EM1}^{(j)}$ and $y^{(j)}$ with respect to the values at the operating points, $x_{10}^{(j)}$, $v_0^{(j)}$, $i_{EM10}^{(j)}$, $u_{EM10}^{(j)}$ and $y_0^{(j)}$, respectively.

Step (2). The models in (3.34) are stabilized using the pole placement method [Boj18a] and finally the state feedback gain matrix $\mathbf{k}_c^T = [k_{c1} \quad k_{c2} \quad k_{c3}] = [66.63 \quad 1.62 \quad -0.15]$ are obtained. Next, $\mathbf{k}_c^T$ is applied to the reduced nonlinear model of MLS (3.33) and the psfcMLS model is obtained as

$$\begin{aligned}
\dot{x}_1 &= v, \\
\dot{v} &= -\frac{i_{EM1}^2 \cdot F_{emP1} \cdot \exp(-x_1 / F_{emP2})}{m \cdot F_{emP2}} + g \\
&\quad + \frac{i_{EM2}^2 \cdot F_{emP1} \cdot \exp(-(x_d - x_1) / F_{emP2}}{m \cdot F_{emP2}}, \\
\dot{i}_{EM1} &= \frac{k_i \cdot u_{EM1} + k_i \cdot k_{c1} \cdot x_1 + k_i \cdot k_{c2} \cdot v + c_i + (k_i \cdot k_{c3} - 1) i_{EM1}}{\frac{f_{iP1}}{f_{iP2}} \cdot \exp(-x_1 / f_{iP2})}, \\
y &= x_1,
\end{aligned} \tag{3.36}$$

where the control law is given as

$$u_{EM1} = -u + k_{c1} x_1 + k_{c2} v + k_{c3} i_{EM1}, \tag{3.37}$$

and it is also illustrated in the block diagram of the psfcMLS given in Fig. 3.12.

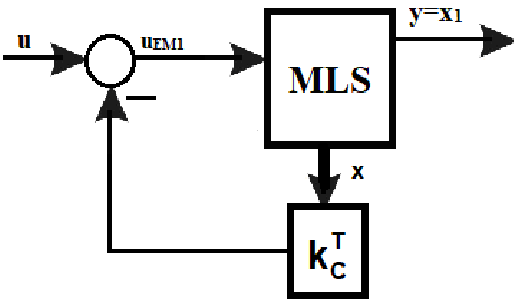

Fig.3.12. Block diagram of psfcMLS.

The LPV model resulted from the psfcMLS model (3.34) is next used in the derivation of the TP model. Therefore, the LPV model of psfcMLS is expressed as:

$$
\begin{aligned}
&\dot{\mathbf{x}} = \mathbf{A}(\mathbf{p})\mathbf{x} + \mathbf{b}(\mathbf{p})u_{EM1}, \\
&y = \mathbf{c}^T\mathbf{x}, \\
&\mathbf{x} = [x_1 \quad v \quad i_{EM1}]^T,\ \mathbf{p} = [p_1 \quad p_2]^T = [x_1 \quad i_{EM1}]^T,
\end{aligned}
\tag{3.38}
$$

where $\mathbf{p}$ is the parameter vector, which contains the first state variable $p_1 = x_1$ and the matrices $\mathbf{A}(\mathbf{p})$, $\mathbf{b}(\mathbf{p})$ and $\mathbf{c}^T$, are [Boj18a]

$$
\begin{aligned}
&\mathbf{A}(\mathbf{p}) = \begin{bmatrix} 0 & 1 & 0 \\ a_{21}(\mathbf{p}) & 0 & a_{23}(\mathbf{p}) \\ a_{31}(\mathbf{p}) & a_{32}(\mathbf{p}) & a_{33}(\mathbf{p}) \end{bmatrix},\ \mathbf{b}(\mathbf{p}) = \begin{bmatrix} 0 \\ 0 \\ b_{31}(\mathbf{p}) \end{bmatrix}, \\
&\mathbf{c}^T = [1\ \ 0\ \ 0], \\
&\mathbf{A}(\mathbf{p}) \in \Re^{3x3},\ \mathbf{b}(\mathbf{p}) \in \Re^{3x1},\ \mathbf{c}^T \in \Re^{1x3},\ u_{EM1} \in \Re,
\end{aligned}
\tag{3.39}
$$

with the elements:

$$
\begin{aligned}
&a_{21}(\mathbf{p}) = \frac{p_2{}^2}{m}\frac{F_{emP1}}{F_{emP2}^2} e^{-\frac{p_1}{F_{emP2}}},\ a_{23}(\mathbf{p}) = -\frac{2p_2}{m}\frac{F_{emP1}}{F_{emP2}} e^{-\frac{p_1}{F_{emP2}}}, \\
&a_{31}(\mathbf{p}) = -(k_i u_{1x} + c_i - i_{EM2})\frac{p_1}{f_{iP1}} \cdot e^{\frac{p_1}{f_{iP2}}} + 66.33 \cdot k_i \cdot \frac{f_{iP2}}{f_{iP1}} \cdot e^{\frac{p_1}{f_{iP2}}}, \\
&a_{32}(\mathbf{p}) = 1.62 \cdot k_i \cdot \frac{f_{iP2}}{f_{iP1}} \cdot e^{\frac{p_1}{f_{iP2}}},\ a_{33}(\mathbf{p}) = -\frac{f_{iP2}}{f_{iP1}} \cdot e^{\frac{p_1}{f_{iP2}}} - 0.15 \cdot k_i \cdot \frac{f_{iP2}}{f_{iP1}} \cdot e^{\frac{p_1}{f_{iP2}}}, \\
&b_{31}(\mathbf{p}) = k_i \cdot \frac{f_{iP2}}{f_{iP1}} \cdot e^{\frac{p_1}{f_{iP2}}}.
\end{aligned}
\tag{3.40}
$$

Introducing in (3.38) the sistem matrix $\mathbf{S}(\mathbf{p}) = [\mathbf{A}(\mathbf{p}) \quad \mathbf{b}(\mathbf{p})] \in \Re^{3\times 4}$, the model is transformed in the qLPV state-space form

$$
\begin{aligned}
&\dot{\mathbf{x}} = \mathbf{S}(\mathbf{p})[\mathbf{x}^T \quad u_{EM1}]^T, \\
&y = \mathbf{c}^T\mathbf{x},
\end{aligned}
\tag{3.41}
$$

with the following LTI models [Hed17a], [Hed19e]:

$$
\begin{aligned}
\dot{\mathbf{x}} &= \mathbf{S}(\mathbf{p}) \bigotimes_{n=1}^{N} \mathbf{w}_n(\mathbf{p}_n)[\mathbf{x}^T \quad u_{EM1}]^T \\
&= \sum_{m_1=1}^{M_1} w_{1,m_1}(p_1)\mathbf{S}_{m_1}[\mathbf{x}^T \quad u_{EM1}]^T, \\
y &= \mathbf{c}^T\mathbf{x}.
\end{aligned}
\tag{3.42}
$$

Finally the TP model derived for psfcMLS model is given as

$$
\begin{aligned}
&\dot{\mathbf{x}} = \sum_{m_1=1}^{3} w_{1,m_1}(p_1)(\mathbf{A}_{m1}\mathbf{x} + \mathbf{b}_{m1}u_{EM1}), \\
&y = \mathbf{c}^T\mathbf{x}.
\end{aligned}
\tag{3.43}
$$

Using the TP Tool described in detail in [Nag07c], the LTI system matrices are obtained and their values are given in Equation (2) in Appendix 2. The weighting functions are illustrated in Fig.3.13.

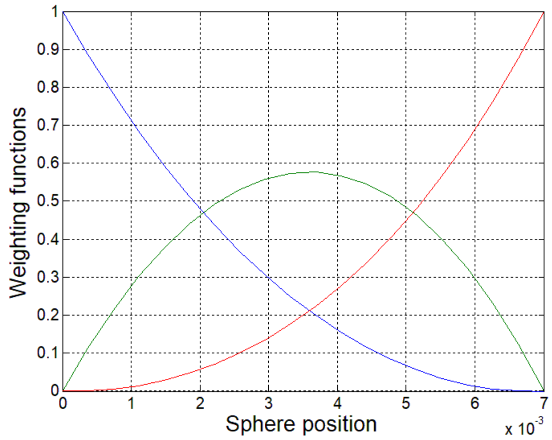

Fig.3.13. W.f.s obtained by TP-based model transformation of psfcMLS [Hed17a], [Hed19e].

Four testing scenarios are conducted in order to test the derived TP model expressed in (3.43) using the open-loop diagram illustrated in Fig.3.14. In order to compare the performance of the TP model with other models derived for psfcMLS, four linear models are also tested in the same scenario as the TP model. The first linear model is represented by the first linearized model presented in (3.34) corresponding to the first o.p. with the numerical values given in Equation (2) in Appendix 1, the second linear model is represented by the second linearized model presented in (3.34) corresponding to the second o.p. with the numerical values given in Equation (2) in Appendix 1, the third linear model is represented by the LTI model resulting from the TP model, characterized by the LTI system matrix $\mathbf{S}_1$ given in Equation (2) in Appendix 2 and the fourth linear model is represented by the LTI model resulting from the TP model, characterized by the LTI system matrix $\mathbf{S}_2$ given in Equation (2) in Appendix 2.

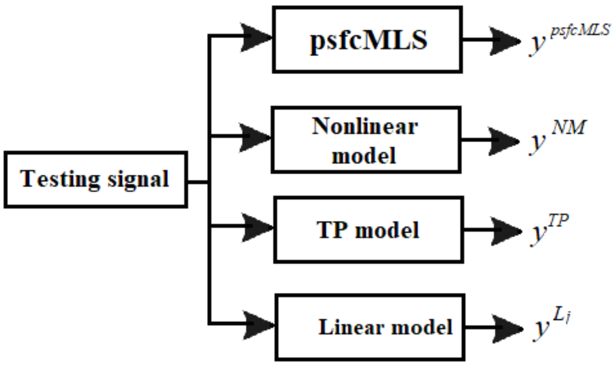

Fig.3.14. Testing block diagram for psfcMLS.

In the first testing scenario a Pseudo Random Binary Signal (PRBS) with a 0.008 m amplitude, which is illustrated in Fig.3.15, is applied to the psfcMLS laboratory equipment, to the nonlinear model given in (3.36), to the TP model given in (3.43) and to the four linear models of psfcMLS on the time horizon of 20 s. The initial state vector matching the experiments is $\mathbf{x}_0 = [0 \quad 0 \quad 0]^T$.

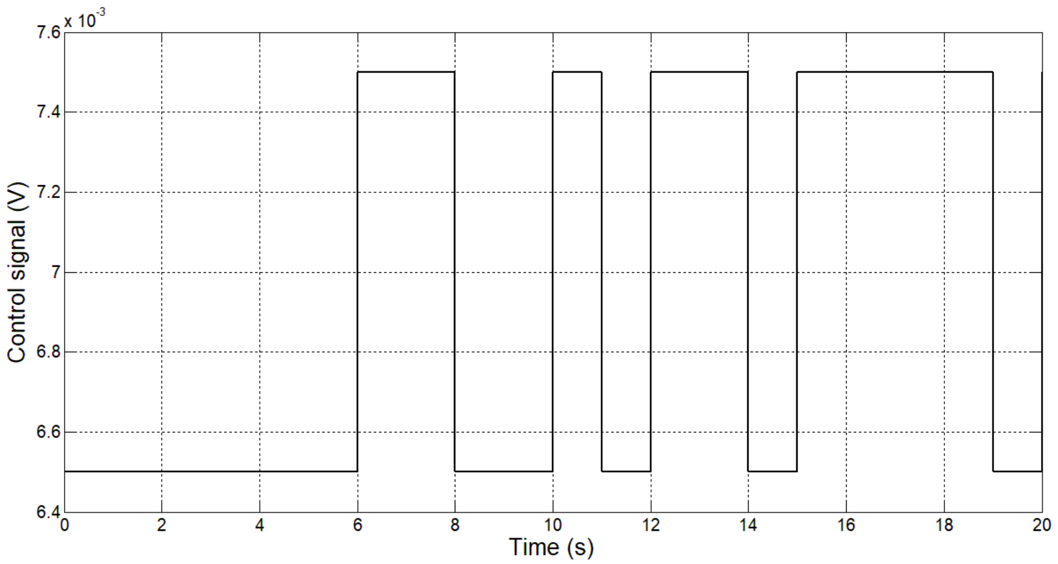

Fig.3.15. PRBS control signal versus time used in the first testing scenario.

The corresponding plots of the sphere position versus time are illustrated in Fig.3.16.

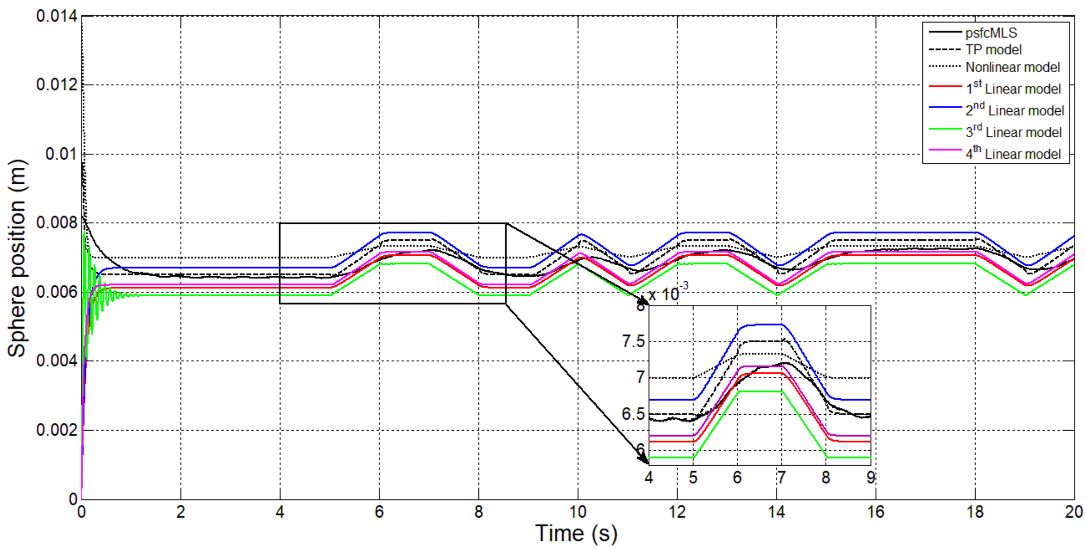

Fig.3.16. Sphere position vs. time for psfcMLS, nonlinear model, TP model, 1st linear model, 2nd linear model, 3rd linear model and 4th linear model in the first testing scenario.

In the second testing scenario, a sine signal with a 0.0015 m amplitude, which is illustrated in Fig.3.17, is applied as control signal and the corresponding plots are illustrated in Fig.3.18.

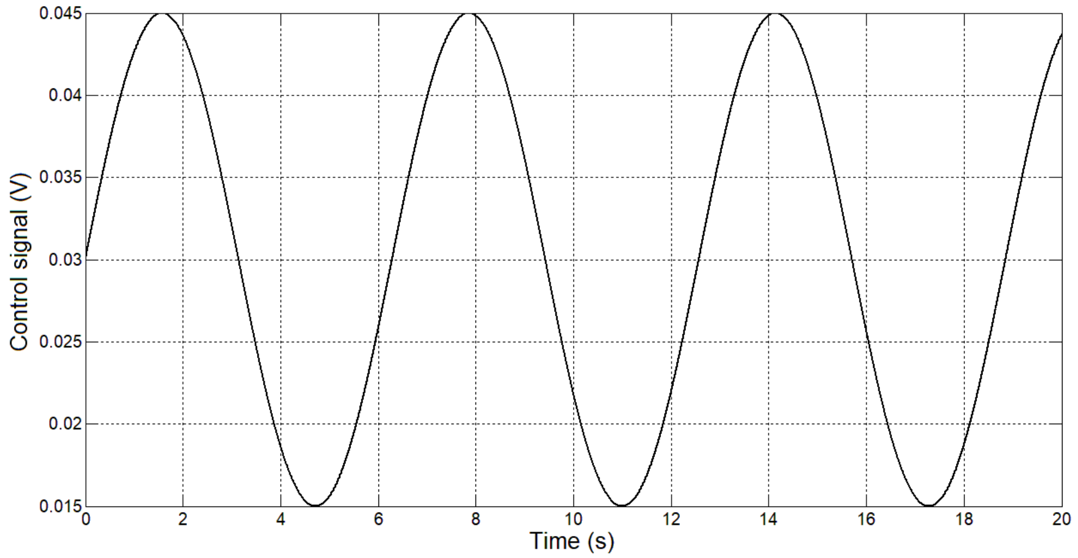

Fig.3.17. Sine control signal versus time used in the second testing scenario.

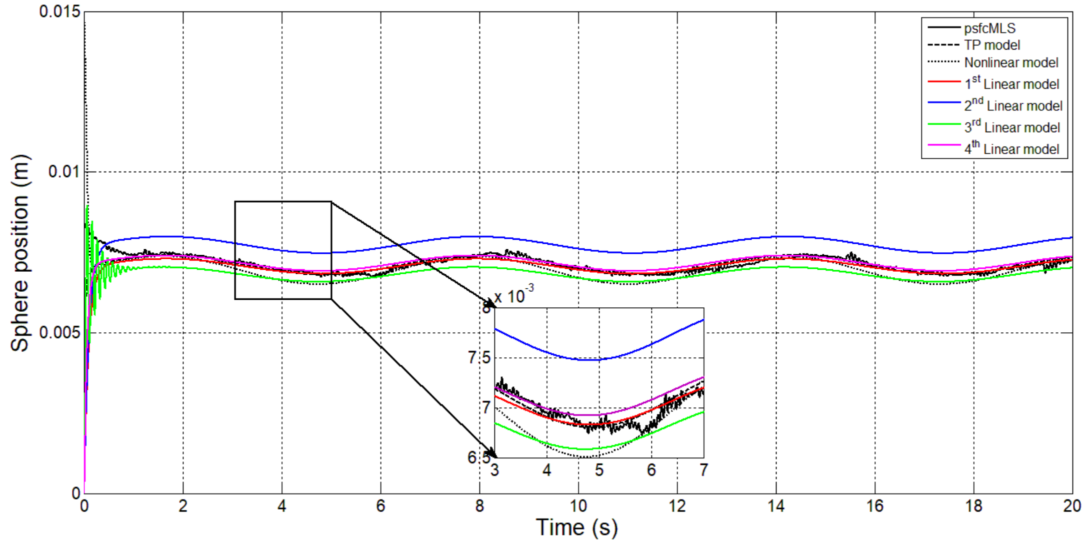

Fig.3.18. Sphere position vs. time for psfcMLS, nonlinear model, TP model, 1st linear model, 2nd linear model, 3rd linear model and 4th linear model in the second testing scenario.

In the third testing scenario, a chirp control signal with a 0.1 initial frequency, which is illustrated in Fig.3.19, is applied as control signal. The plots of the sphere position y versus time are illustrated in Fig.3.20.

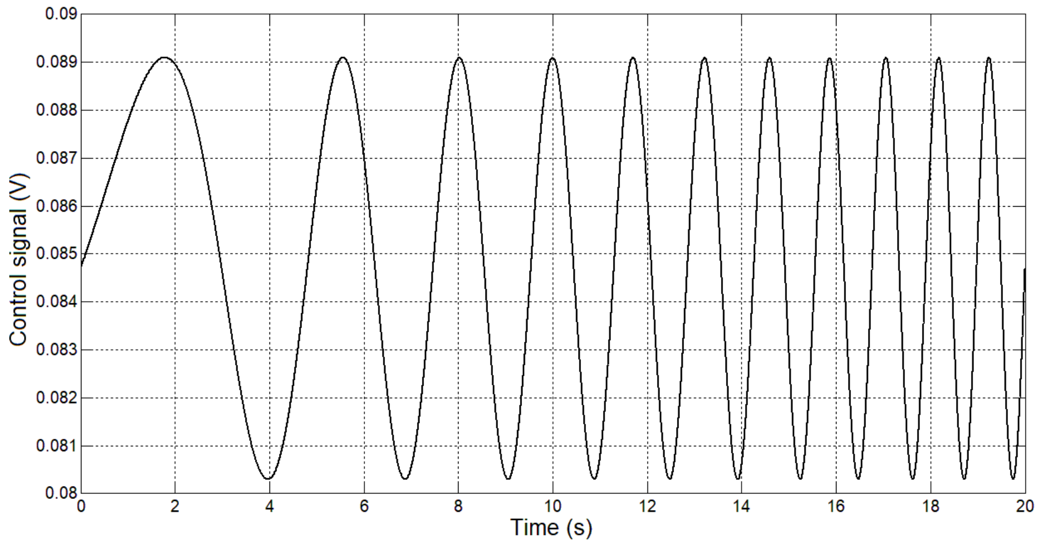

Fig.3.19. Chirp control signal versus time used in the third testing scenario.

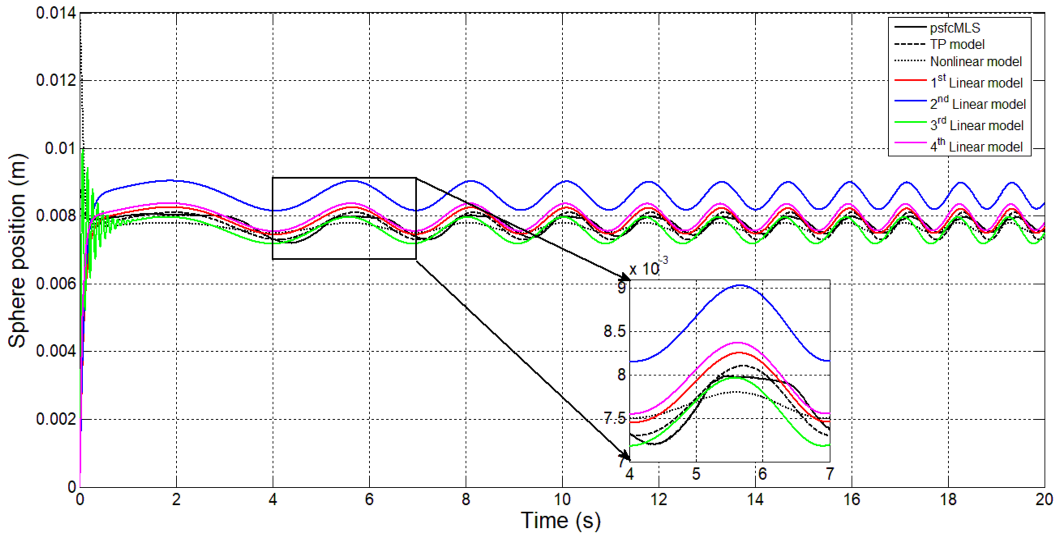

Fig.3.20. Sphere position vs. time for psfcMLS, nonlinear model, TP model, 1st linear model, 2nd linear model, 3rd linear model and 4th linear model in the third testing scenario.

In the fourth testing scenario a Pulse-Width Modulation (PWM) control signal with a 0.0012 m amplitude and a 50 % pulse width, which is illustrated in Fig.3.21, is applied as control signal. The plots of the sphere position y versus time are illustrated in Fig.3.22.

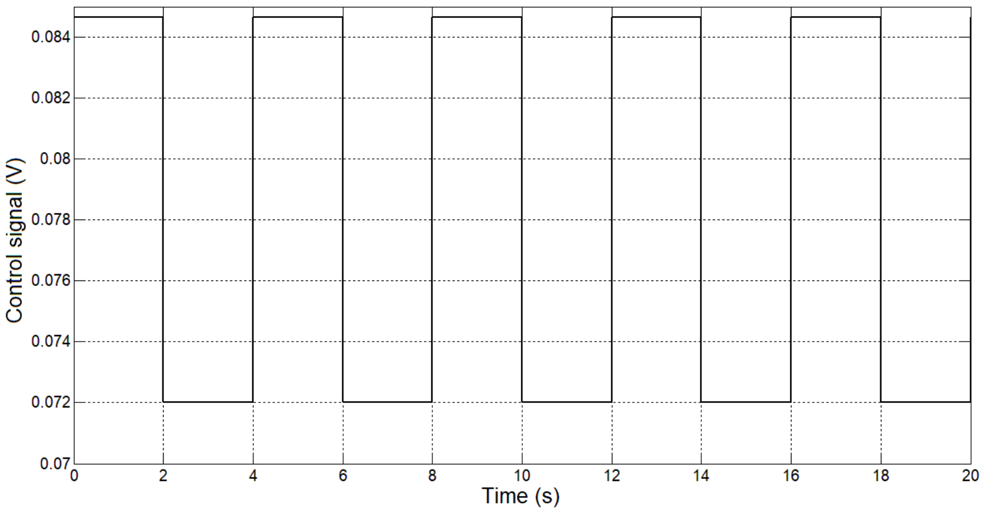

Fig.3.21. PWM control signal versus time used in the fourth testing scenario.

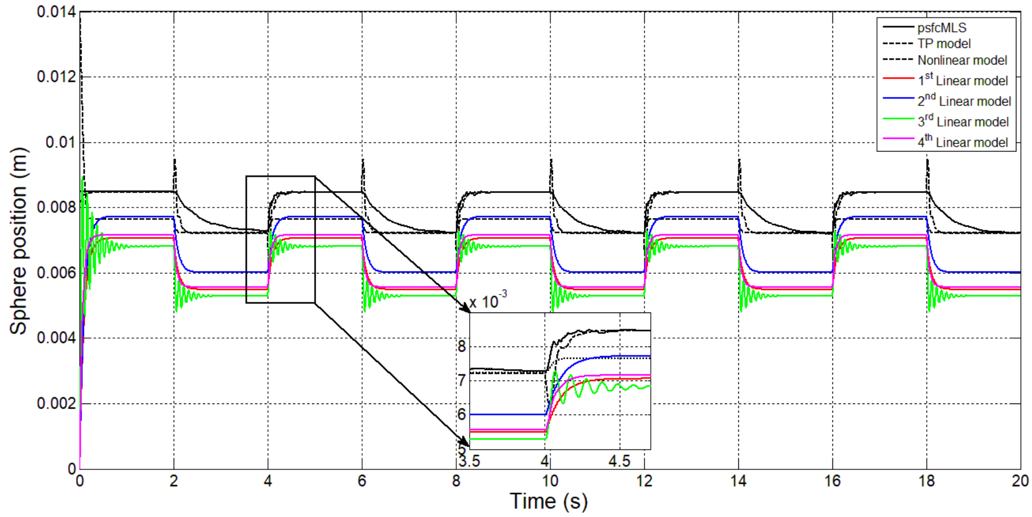

Fig.3.22. Sphere position vs. time for psfcMLS, nonlinear model, TP model, 1st linear model, 2nd linear model, 3rd linear model and 4th linear model in the fourth testing scenario.

The four performance indices introduced in Sub-chapter 3.2, namely RMSE, VAF, AIC and BIC are measured in order to better highlight the performance of the TP model derived for the psfcMLS model in the testing scenario.

The RMSEs, VAF, AIC and BIC were computed using (3.29), (3.31) and (3.32), where the modeling errors are defined as

$$e^{\Psi} = y^{psfcMLS} - y^{\Psi}. \tag{3.44}$$

The superscript $y^{psfcMLS}$ are the outputs of the psfcMLS (i.e. the real-world process), $\psi = psfcMLSm$ indicates the nonlinear psfcMLS model, $\psi = TP$ indicates the TP model, $\psi = L_1$ indicates the first linear model, $\psi = L_2$ indicates the second linear model, $\psi = L_3$ indicates the third linear model, $\psi = L_4$ indicates the fourth linear model, $M = 80001$ is the number of samples and the sampling period $T_s = 0.0025$ s, $k^{TP} = 18$ is the number of parameters of the TP model, $k^{psfcMLSm} = 12$ is the number of parameters of the psfcMLS model, $k^{L_1} = k^{L_2} = k^{L_3} = k^{L_4} = 12$ is the number of parameters of the linear models. The values of the performance indices are given in Table 3.3.1.

Table 3.3.1.
Values of performance indices for MLS.

Model	***Criterion*** RMSE (m)	VAF (%)	AIC	BIC
TP model/ 1st testing scenario	$2.72 \cdot 10^{-4}$	72.61	-7.41	-7.42
TP model/ 2nd testing scenario	$2.05 \cdot 10^{-4}$	11.66	-7.98	-7.97
TP model/ 3rd testing scenario	$1.39 \cdot 10^{-4}$	78.91	-8.79	-8.78
TP model/ 4th testing scenario	$2.98 \cdot 10^{-4}$	83.20	-7.23	-7.21
psfcMLS model/ 1st testing scenario	$7.83 \cdot 10^{-4}$	92.24	-8.30	-8.29
psfcMLS model/ 2nd testing scenario	$6.20 \cdot 10^{-4}$	13.35	-8.77	-8.75
psfcMLS model/ 3rd testing scenario	$4.56 \cdot 10^{-4}$	56.75	-9.38	-9.39
psfcMLS model/ 4th testing scenario	$8.99 \cdot 10^{-4}$	138.45	-8.02	-8.01
1st Linear model/ 1st testing scenario	$6 \cdot 10^{-4}$	6.20	-7.45	-7.44
1st Linear model/ 2nd testing scenario	$5.04 \cdot 10^{-4}$	-45.73	-7.79	-7.78
1st Linear model/ 3rd testing scenario	$4.82 \cdot 10^{-4}$	8.48	-7.88	-7.89
1st Linear model/ 4th testing scenario	$1.8 \cdot 10^{-3}$	66.53	-5.25	-5.26
2nd Linear model/ 1st testing scenario	$6.47 \cdot 10^{-4}$	7.52	-7.29	-7.28
2nd Linear model/ 2nd testing scenario	$7.76 \cdot 10^{-4}$	-38.49	-6.93	-6.94
2nd Linear model/ 3rd testing scenario	$9.65 \cdot 10^{-4}$	8.91	-6.49	-6.48
2nd Linear model/ 4th testing scenario	$1.3 \cdot 10^{-3}$	63.61	-5.95	-5.94
3rd Linear model/ 1st testing scenario	$6.51 \cdot 10^{-4}$	24.79	-7.28	-7.27
3rd Linear model/ 2nd testing scenario	$4.92 \cdot 10^{-4}$	-23.66	-7.84	-7.85
3rd Linear model/ 3rd testing scenario	$4.34 \cdot 10^{-4}$	13.99	-8.09	-8.08
3rd Linear model/ 4th testing scenario	$2 \cdot 10^{-3}$	65.12	-5.04	-5.03
4th Linear model/ 1st testing scenario	$5.17 \cdot 10^{-4}$	13.39	-7.74	-7.73
4th Linear model/ 2nd testing scenario	$4.40 \cdot 10^{-4}$	-40.97	-8.06	-8.05
4th Linear model/ 3rd testing scenario	$4.78 \cdot 10^{-4}$	11.73	-7.91	-7.92
4th Linear model/ 4th testing scenario	$1.7 \cdot 10^{-3}$	67.73	-5.35	-5.36

The best performance concerning the values of RMSE is obtained by the TP model in the third testing scenario. The best performance concerning the values of VAF is obtained by the psfcMLS model in the first testing scenario. The third linear model ensures the best performance in terms of both AIC and BIC in case of the fourth testing scenario.

Therefore, the experimental results have shown that the derived TP model expressed in (3.43) approximately mimics the behavior of the laboratory equipment, but exhibiting numerical error. Other number of parameters of the TP model would lead to other values in Table 3.3.1.

3.4. The derivation of the TP model for Pendulum Cart System

The Pendulum Cart System (PCS) is a challenging nonlinear Single Input-Multi Output. The state-space model that describes the behavior of the nonlinear PCS is [Fee98]:

$$\dot{x}_1 = x_3,$$
$$\dot{x}_2 = x_4,$$
$$\dot{x}_3 = \frac{(l^2 + J/m)(F - T_c - \mu x_4^2 \sin x_2) + l \cos x_2 (\mu g \sin x_2 - f_p x_4)}{J + \mu l \sin^2 x_2}, \quad (3.45)$$
$$\dot{x}_4 = \frac{l \cos x_2 \,(F - T_c - \mu x_4^2 \sin x_2) + \mu g \sin x_2 - f_p x_4}{J + \mu l \sin^2 x_2},$$
$$y = x_1,$$

where $\mathbf{x} = [x_1\ x_2\ x_3\ x_4]^T$ is the state vector, $x_1 = y_1$ (m) is the first process output, i.e. the cart position, x_2 (rad) is the angle between the vertical direction and the pendulum, x_3 (m/s) is the cart velocity, x_4 (rad/s) is the cart pendulum angular velocity, $F = f_1 \cdot u + f_2 \cdot x_3$ (N) is the control force produced by a DC motor which is controlled by a PWM signal with the notations $u\,(\%) \in [-100, 100]$ and next $u \in [-0.5, 0.5]$, $f_1 = 9.4$ (N) is the control force to PWM signal ratio, $f_2 = -0.548$ (N) is the control force to cart velocity ratio, $l = 0.011$ (m) is the distance from axis of rotation to center of mass of system, $J = 0.00282$ $(kg \cdot m^2)$ is the moment of inertia of pendulum with respect to axis of rotation, $m = 0.872$ (kg) is the equivalent mass of cart and pendulum, $\mu = m \cdot l$ (kg·m) is the friction coefficient, $g = 9.81$ (m/s^2) is gravitational acceleration and $T_c = 1.203$ (N) is the friction force.

The block diagram of the PCS laboratory equipment is shown in Fig. 3.23.

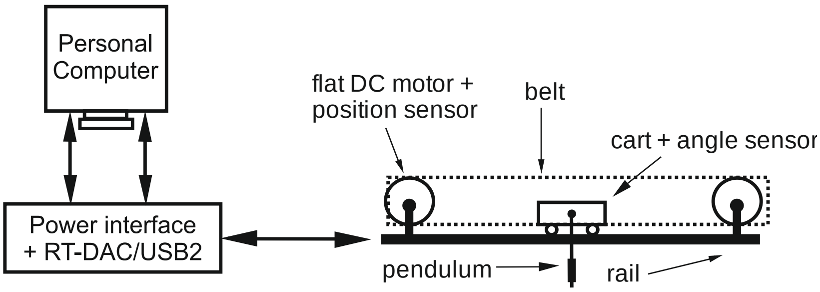

Fig.3.23. Block diagram of PCS [Hed21a].

The PCS has two operation modes, the crane mode and the self erecting mode, which are illustrated in Fig. 3.24. The crane mode is considered in this thesis.

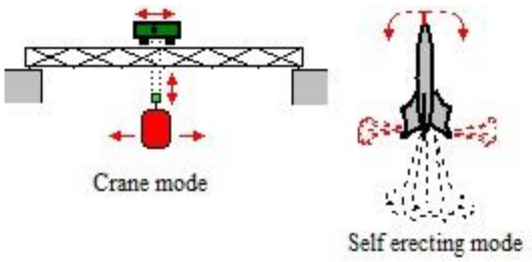

Fig.3.24. Two control problems of PCS [Fee98].

In order to simplify the further development of control structures for the cart position control of PCS, which will be presented in Chapter 4, the nonlinear model is linearized around one operating point (o.p.) $P^{(1)} = (y_1^{(1)}, y_2^{(1)}, y_3^{(1)}, y_3^{(1)}, u^{(1)})^T$. The o.p. is chosen to cover the usual operating regimes and to avoid the extremities of the input-output map, which create problems in the computation of the process gains. Therefore, the o.p. is $P^{(1)}(0, \pi, 0, 0, 0)$.

Using the o.p., the following state-space linearized mathematical model is obtained for PCS:

$$\begin{cases} \Delta\dot{\mathbf{x}}^{(1)} = \mathbf{A}^{(1)}\ \Delta\mathbf{x}^{(1)} + \mathbf{b}^{(1)}\Delta u^{(1)} \\ \Delta y^{(1)} = \mathbf{C}\Delta\mathbf{x}^{(1)} \end{cases},$$

$$\Delta\mathbf{x}^{(1)} = \left[\Delta x_1^{(1)} \quad \Delta x_2^{(1)} \quad \Delta x_3^{(1)} \quad \Delta x_4^{(1)},\right], j = 1$$

$$\mathbf{A}^{(1)} = \begin{bmatrix} 0 & 0 & 1 & 0 \\ 0 & 0 & 0 & 1 \\ 0 & a_{32}^{(1)} & a_{33}^{(1)} & a_{34}^{(1)} \\ 0 & a_{42}^{(1)} & a_{43}^{(1)} & a_{44}^{(1)} \end{bmatrix}, \mathbf{b}^{(1)} = \begin{bmatrix} 0 \\ 0 \\ b_{31}^{(1)} \\ b_{41}^{(1)} \end{bmatrix}, \mathbf{C} = \begin{bmatrix} 1 & 0 & 0 & 0 \\ 0 & 1 & 0 & 0 \\ 0 & 0 & 1 & 0 \\ 0 & 0 & 0 & 1 \end{bmatrix}, \tag{3.46}$$

$$\mathbf{A}^{(1)} \in \Re^{4x4},\ \mathbf{b}^{(1)} \in \Re^{4x1},\ \mathbf{C} \in \Re^{1x4},\ u \in \Re,$$

with the matrix parameters

$$a_{32}^{(1)} = \frac{(l^2 + J/m)(-T_c \mu l \sin(2x_2)) + l\mu g \cos(2x_2)(J\mu l \sin^2(x_2))}{(J + \mu l \sin^2(x_2))^2} + \\ + \frac{l\mu g \cos(2x_2)(l^2 \mu^2 g \cos(x_2)\sin(x_2)\sin(2x_2))}{(J + \mu l \sin^2(x_2))^2},$$

$$a_{33}^{(1)} = \frac{(l^2 + J/m)}{(J + \mu l \sin^2(x_2))^2 f_2},\quad a_{34}^{(1)} = \frac{-l\cos(x_2) f_p}{(J + \mu l \sin^2(x_2))^2}, \tag{3.47}$$

$$a_{42}^{(1)} = \frac{(l\sin(x_2)T_c)(J\mu l \sin^2(x_2))}{(J + \mu l \sin^2(x_2))^2} - \frac{(-l\cos(x_2)T_c)(2\mu l \sin(x_2)\cos(x_2) + J\mu g \cos(x_2))}{(J + \mu l \sin^2(x_2))^2} - \\ - \frac{(-l\cos(x_2)T_c)(\mu^2 g l \cos(x_2)\sin^2(x_2) - 2\mu^2 l \cos(x_2)\sin^2(x_2))}{(J + \mu l \sin^2(x_2))^2},$$

$$a_{43}^{(1)} = \frac{l\cos(x_2)}{(J + \mu l \sin^2(x_2))^2 f_2},\quad a_{44}^{(1)} = \frac{-f_p}{(J + \mu l \sin^2(x_2))^2},$$

$$b_{31}^{(1)} = \frac{(l^2 + J/m)}{(J + \mu l \sin^2(x_2)) f_1},\quad b_{41}^{(1)} = \frac{l\cos(x_2)}{(J + \mu l \sin^2(x_2))^2 f_1},$$

where $\Delta x_1^{(1)} = x_1^{(1)} - x_{10}^{(1)}$, $\Delta x_2^{(1)} = x_2^{(1)} - x_{20}^{(1)}$, $\Delta x_3^{(1)} = x_3^{(1)} - x_{30}^{(1)}$, $\Delta x_4^{(1)} = x_4^{(1)} - x_{40}^{(1)}$, $\Delta u^{(1)} = u^{(1)} - u_0^{(1)}$ are the differences of the variables $x_1^{(1)}$, $x_2^{(1)}$, $x_3^{(1)}$, $x_4^{(1)}$ and $u^{(1)}$ with respect to the values at the o.p., $x_{10}^{(1)}$, $x_{20}^{(1)}$, $x_{30}^{(1)}$, $x_{40}^{(1)}$ and $u_0^{(1)}$, respectively.

After replacing the values of the o.p. in (3.46), one linearized model is obtained for PCS with the corresponding matrices given in Equation (3) in Appendix 1.

Next, the derivation of the TP model for PCS is presented. It starts with the qLPV model of PCS

$$\dot{\mathbf{x}} = \mathbf{A}(\mathbf{p})\mathbf{x} + \mathbf{b}(\mathbf{p})u, \quad \mathbf{x}(0) = \mathbf{x}_0$$
$$y = \mathbf{C}\mathbf{x}, \tag{3.48}$$
$$\mathbf{x} = [x_1 \quad x_2 \quad x_3 \quad x_4]^T,\ \mathbf{p} = p_1 = x_2,$$

where $\mathbf{x}$ denotes the process state vector and $\mathbf{p}$ is the bounded parameter vector (which contains only the second state variable). The matrices $\mathbf{A}(\mathbf{p}), \mathbf{b}(\mathbf{p}), \mathbf{C}$ have the following expressions:

$$\mathbf{A}(\mathbf{p}) = \begin{bmatrix} 0 & 0 & 1 & 0 \\ 0 & 0 & 0 & 1 \\ 0 & a_{32}(\mathbf{p}) & a_{33}(\mathbf{p}) & a_{34}(\mathbf{p}) \\ 0 & a_{42}(\mathbf{p}) & a_{42}(\mathbf{p}) & a_{44}(\mathbf{p}) \end{bmatrix}, \ \mathbf{b}(\mathbf{p}) = \begin{bmatrix} 0 \\ 0 \\ b_{31}(\mathbf{p}) \\ b_{41}(\mathbf{p}) \end{bmatrix},$$
$$\mathbf{C} = \begin{bmatrix} 1 & 0 & 0 & 0 \\ 0 & 1 & 0 & 0 \\ 0 & 0 & 1 & 0 \\ 0 & 0 & 0 & 1 \end{bmatrix}, \tag{3.49}$$
$$\mathbf{A}(\mathbf{p}) \in \Re^{4x4}, \ \mathbf{b}(\mathbf{p}) \in \Re^{4x1}, \ \mathbf{C} \in \Re^{4x4}, \ u \in \Re,$$

and the elements of the matrices are computed according to (3.47).

Introducing in (3.48) the system matrix

$$\mathbf{S}(\mathbf{p}) = [\mathbf{A}(\mathbf{p}) \quad \mathbf{b}(\mathbf{p})] \in \Re^{4\times 5}, \tag{3.50}$$

the model is transformed in the qLPV state-space form

$$\dot{\mathbf{x}} = \mathbf{S}(\mathbf{p})[\mathbf{x}^T \quad u]^T, \ \mathbf{x}(0) = \mathbf{x}_0, \quad y = \mathbf{C}\mathbf{x}. \tag{3.51}$$

The purpose of TP-based Model Transformation is to obtain LTI models as follows [Bar04b]:

$$\dot{\mathbf{x}} = \sum_{m_1=1}^{M_1} w_{m_1}(p_1)\mathbf{S}_{m_1}[\mathbf{x}^T \quad u]^T, \quad y = \mathbf{C}\mathbf{x}, \tag{3.52}$$

where $\mathbf{S}_{m_1} = [\mathbf{A}_{m_1} \ \ \mathbf{b}_{m_1}]$ are the LTI vertex systems from which the system tensor $\mathbf{S}$ is made of, $w_{m_1}(p_1)$ are the values of the weighting functions, $M_1 = 5$ is the number of singular values.

The TP model derived for PCS is expressed as

$$\dot{\mathbf{x}} = \sum_{m_1=1}^{5} w_{m_1}(p_1)(\mathbf{A}_{m_1}\mathbf{x}^T + \mathbf{b}_{m_1}u), \quad y = \mathbf{C}\mathbf{x}. \tag{3.53}$$

Using the TP Tool described in detail in [Nag07c], the LTI system matrices are obtained and their values are given in Equation (3) in Appendix 2. The weighting functions are illustrated in Fig.3.25.

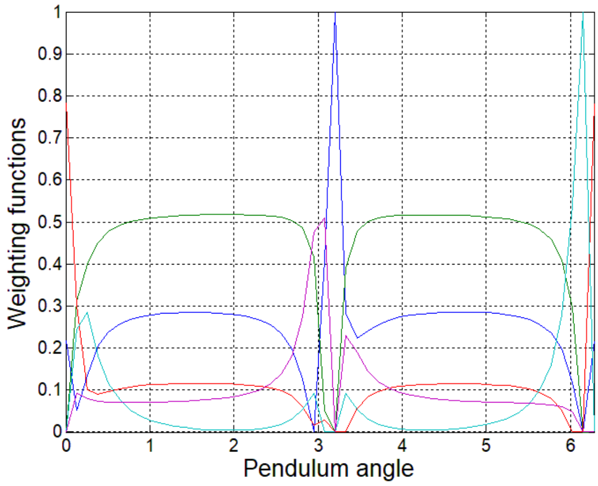

Fig.3.25. Weighting functions for pendulum angle.

Two testing scenarios were conducted in order to test the derived TP model for PCS given in (3.53). In order to compare the performance of the TP model with other models derived for PCS, the nonlinear model given in (3.45), the first linearized model presented in (3.47) with the numerical values given in Equation (3) in Appendix 1, the second linear model represented by the LTI model resulting from the TP model, characterized by the LTI system matrix $\mathbf{S}_1$ given in Equation (3) in Appendix 2, the third linear model represented by the LTI model resulting from the TP model, characterized by the LTI system matrix $\mathbf{S}_2$ given in Equation (3) in Appendix 2 and the fourth linear model represented by the LTI model resulting from the TP model, characterized by the LTI system matrix $\mathbf{S}_3$ given in Equation (3) in Appendix 2, were also tested using the testing block diagram illustrated in Fig. 3.26.

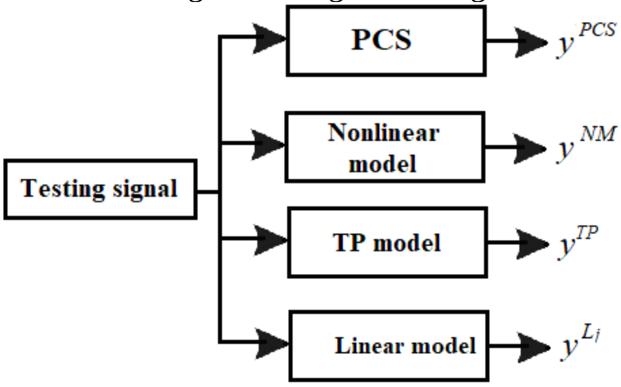

Fig.3.26. Testing block diagram for PCS.

In the first testing scenario a sine signal with a 0.4 m amplitude, which is illustrated in Fig. 3.27, is applied to the PCS laboratory equipment, to the nonlinear model given in (3.45), to the TP model given in (3.53) and to the four linear models of PCS on the time horizon of 20 s. The initial state vector matching the experiments is $\mathbf{x}_0 = [0 \quad \pi \quad 0 \quad 0]^T$.

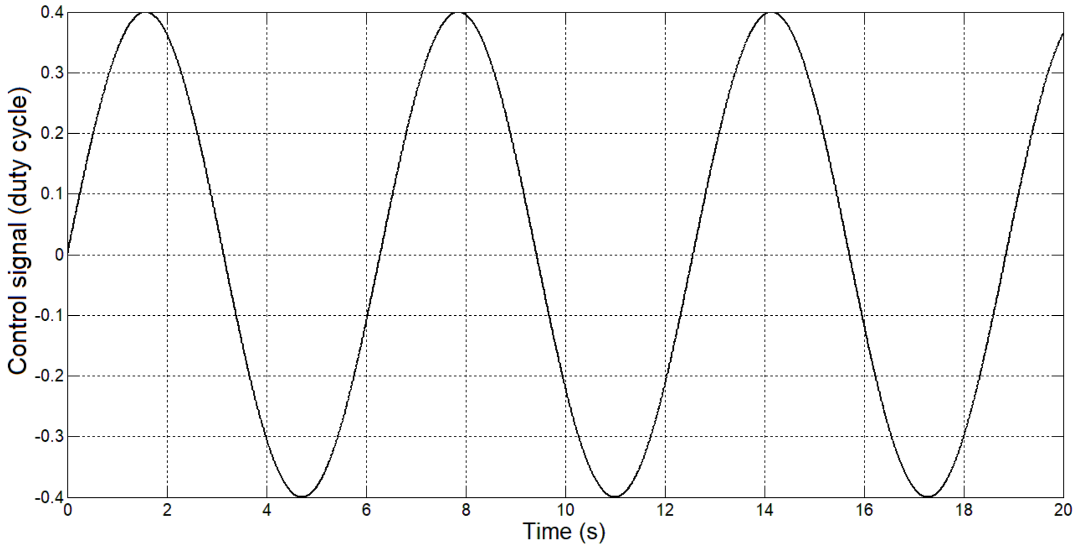

Fig.3.27. Sine control signal versus time used in the first testing scenario.

The plot of the cart position obtained after conducting the first testing scenario is illustrated in Fig. 3.28.

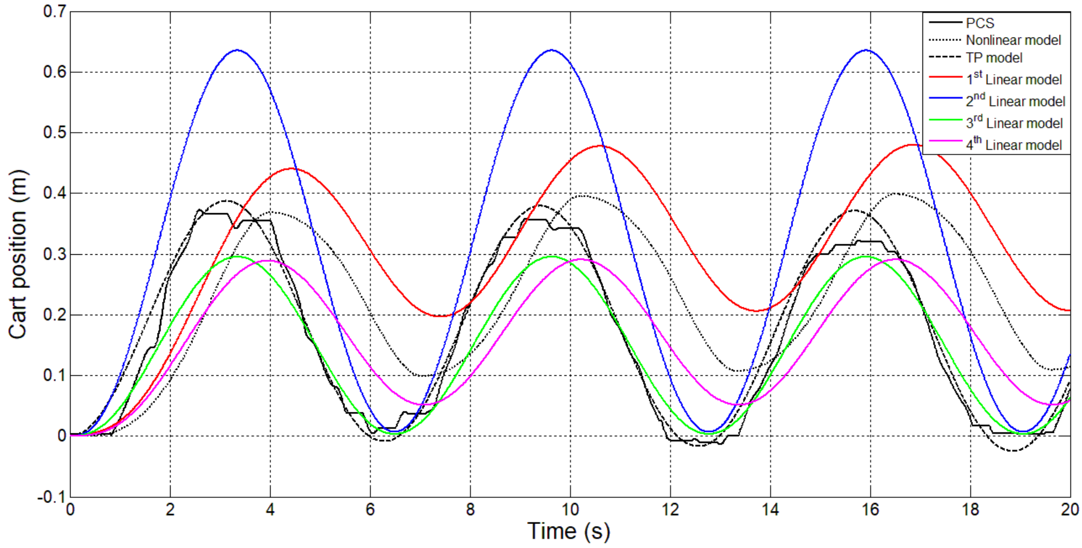

Fig.3.28. Cart position vs. time for PCS, nonlinear model, TP model, 1st linear model, 2nd linear model, 3rd linear model and 4th linear model in the first testing scenario.

In the second testing scenario a random signal, which is illustrated in Fig. 3.29, is applied to the PCS laboratory equipment, to the nonlinear model given in (3.45), to the TP model given in (3.53) and to the four linear models of PCS on the time horizon of 20 s. The initial state vector matching the experiments is $\mathbf{x}_0 = [0 \quad \pi \quad 0 \quad 0]^T$.

The plot of the cart position obtained after conducting the second testing scenario is illustrated in Fig. 3.30.

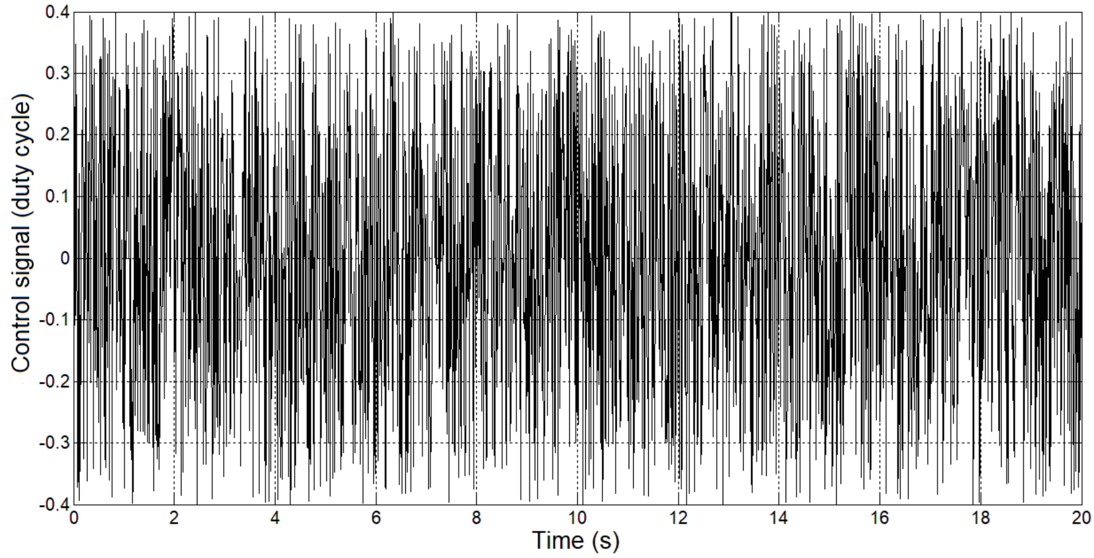

Fig.3.29. Random control signal versus time used in the second testing scenario.

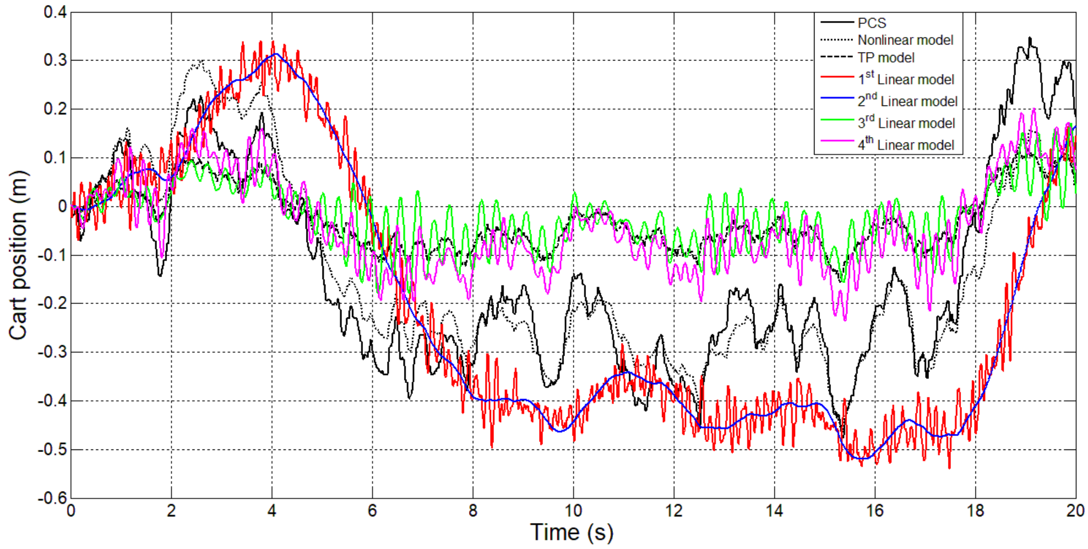

Fig.3.30. Cart position vs. time for PCS, nonlinear model, TP model, 1st linear model, 2nd linear model, 3rd linear model and 4th linear model in the second testing scenario.

The four performance indices introduced in Sub-chapter 3.2, namely RMSE, VAF, AIC and BIC are measured in order to better highlight the performance of the TP model derived for the PCS model in the testing scenarios.

The RMSEs, VAF, AIC and BIC were computed using (3.29), (3.31) and (3.32), where the modeling errors are defined as

$$e^{\psi} = y^{PCS} - y^{\psi}. \tag{3.54}$$

The superscript y^{PCS} are the outputs of the PCS (i.e. the real-world process), $\psi = NM$ indicates the nonlinear PCS model, $\psi = TP$ indicates the TP model, $\psi = L_1$ indicates the first linear model, $\psi = L_2$ indicates the second linear model, $\psi = L_3$ indicates the third linear model, $\psi = L_4$ indicates the fourth linear model, $M = 2001$ is the number of samples and the sampling period $T_s = 0.01$ s, $k^{TP} = 40$ is the number of parameters of the TP model, $k^{NM} = 8$ is the number of parameters of the psfcMLS model, $k^{L_1} = k^{L_2} = k^{L_3} = k^{L_4} = 8$ is the number of parameters of the linear models. The values of the performance indices are given in Table 3.4.1.

Table 3.4.1.
Values of performance indices for PCS.

Model	Criterion			
	RMSE (m)	**VAF (%)**	**AIC**	**BIC**
TP model/ 1st testing scenario	0.1707	41.8467	16.4648	16.4686
TP model/ 2nd testing scenario	0.1822	-429.3567	16.5949	16.5987
PCS model/ 1st testing scenario	0.2127	21.7093	0.9046	0.9084
PCS model/ 2nd testing scenario	0.1904	-969.8976	0.6825	0.6863
1st Linear model/ 1st testing scenario	0.2895	14.6536	1.5207	1.5245
1st Linear model/ 2nd testing scenario	0.2125	42.1668	0.9028	0.9066
2nd Linear model/ 1st testing scenario	0.3269	27.0985	1.7638	1.7676
2nd Linear model/ 2nd testing scenario	0.2092	44.2180	0.8106	0.8744
3rd Linear model/ 1st testing scenario	0.1242	52.7107	-0.1714	-0.1676
3rd Linear model/ 2nd testing scenario	0.1949	-495.4938	0.7295	0.7333
4th Linear model/ 1st testing scenario	0.1385	40.9879	0.0457	0.0495
4th Linear model/ 2nd testing scenario	0.1561	-58.6528	0.2849	0.2887

The best performance concerning the values of RMSE is obtained by the third linear model in the first testing scenario and concerning the VAF is obtained by the third linear model in the first testing scenario.The best values for AIC and BIC are obtained for the fourth linear model in the first testing scenario. Therefore, the experimental results have shown that the derived TP model expressed in (3.53) approximately mimics the behavior of the laboratory equipment, but exhibiting numerical error. Other number of parameters of the TP model would lead to other values in Table 3.4.1.

3.5. Chapter conclusions

In this chapter the main steps of the TP-based Model Transformation modeling algorithm along with the derivation of TP models for three systems, namely Vertical Three Tank System, partial state feedback controlled Magnetic Levitation System and Pendulum Cart System were presented.

In Sub-chapter 3.1, the steps of the TP-based Model Transformation modeling algorithm were presented in detail using some particular examples for a better illustration.

In Sub-chapter 3.2, the derivation of the TP model for a Vertical Three Tank System was presented. In order to carry out a comparative analysis, four linear models were also derived for V3TS: the first two linear models were obtained by linearization around two o.p.s and the next two linear models were extracted from the LTI system matrices of the TP model. Finally, the derived TP model was tested along with the nonlinear model of the V3TS, with four linear models and with the laboratory equipment using a PRBS and four performance indices, namely RMSE, VAF, AIC and BIC were computed. The experimental results and the values of the performance indices, given in Table 3.2.1, have shown that the TP model ensures good modeling performance but exhibiting numerical error. The best performance concerning the values of RMSE is obtained by the fourth linear model in case of the first and second tank and by the TP model in case of the third tank while, the best performamce in terms of VAF are obtained by the fourth linear model in case of all three tanks.

However, the TP model ensures better performance than the nonlinear model and the four linear ones in terms of AIC and BIC in case of all three tanks.

In Sub-chapter 3.3, the derivation of the TP model for a partial state feedback controlled Magnetic Levitation System was presented. In order to carry out a comparative analysis, four linear models were also derived for psfcMLS: the first two linear models were obtained by linearization around two o.p.s and the next two linear models were extracted from the LTI system matrices of the TP model. Finally, the derived TP model was tested along with the nonlinear model of the psfcMLS, with four linear models and with the laboratory equipment in the same four testing scenarios using PRBS, sine, chirp and PWM input signals. Also the four performance indices, namely RMSE, VAF, AIC and BIC were computed. The best performance concerning the values of RMSE is obtained by the TP model in the third testing scenario. The best performance concerning the values of VAF is obtained by the psfcMLS model in the first testing scenario. The third linear model ensures the best performance in terms of both AIC and BIC in case of the fourth testing scenario. The experimental results and the values of the performance indices, given in Table 3.3.1, have shown that the TP model ensures good modeling performance but exhibiting nonzero numerical errors.

Sub-chapter 3.4 was dedicated to the derivation of the TP model for a Pendulum Cart System. In order to carry out a comparative analysis, four linear models were also derived for PCS: the first linear model was obtained by linearization around one o.p. and the next three linear models were extracted from the LTI system matrices of the TP model. Finally, the derived TP model was tested along with the nonlinear model of the PCS, with four linear models and with the laboratory equipment in the same two testing scenarios using sineand random input signals. Also the four performance indices, namely RMSE, VAF, AIC and BIC were computed. The experimental results have shown that the derived TP model expressed in (3.53) approximately mimics the behavior of the laboratory equipment, but exhibiting numerical error. Other number of parameters of the TP model would lead to other values in Table 3.4.1.

The experimental results have shown that:

- Both the accuracy and the performance of a TP model depend the most on how well the LPV model, which is used in the TP-based Model Transformation modeling algorithm, mimics the behavior of the real world process. Therefore, the best results have been achieved by the TP model derived for the V3TS.
- The performance of the TP model also depends on other elements such as: the number of varying parameters, the number of singular values or the types of weighting functions.

The contributions presented in this chapter are:

- The derivation and validation of a TP model for a Vertical Three Tank system laboratory equipment.
- The derivation and validation of a TP model for a partial state feedback controlled Magnetic Levitation System.
- The derivation and validation of a TP model for a Pendulum Cart system laboratory equipment.

These contributions were published in the papers:

1. **E.-L. Hedrea**, R.-E. Precup, C.-A. Bojan-Dragos and C. Hedrea, "Tensor product-based model transformation technique applied to modeling vertical three tank systems," in Proc. IEEE 12th International Symposium on Applied

Computational Intelligence and Informatics, Timisoara, Romania, 2018, pp. 63-68, **indexed in Clarivate Analytics Web of Science, cited in:**

1. Z.J. Zhao, X.K. Zhang and Z. Li, "Tank-level control of liquefied natural gas carrier based on Gaussian function nonlinear decoration," Journal of Marine Science and Engineering, vol. 8, no. 9, 2020, **indexed in Clarivate Analytics Web of Science, impact factor = 2.458 according to Journal Citation Reports (JCR) published by Clarivate Analytics in 2021**.

2. **E.-L. Hedrea**, R.-E. Precup, C.-A. Bojan-Dragos and O. Tanasoiu, "Tensor product-based model transformation technique applied to modeling magnetic levitation systems," in Proc. IEEE 23rd International Conference on Intelligent Engineering Systems, Gödöllö, Hungary, 2019, pp. 179-184, **indexed in Clarivate Analytics Web of Science**.
3. **E.-L. Hedrea**, R.-E. Precup and C.-A. Bojan-Dragos, "Results on tensor product-based model transformation of magnetic levitation systems," Acta Polytehnica Hungarica, vol. 16, no. 9, pp. 93-111, 2019, **indexed in Clarivate Analytics Web of Science, impact factor = 1.806, Journal rank = Q3 according to Journal Citation Reports (JCR) published by Clarivate Analytics in 2021, cited in:**
   1. X. Pan, Y. Wang, S. He and K.-S. Chin, "A dynamic programming algorithm based clustering model and its application to interval type-2 fuzzy large-scale group decision-making problem," IEEE Transactions on Fuzzy Systems, vol. 30, no.1, pp. 108-120, 2022, **indexed in Clarivate Analytics Web of Science, impact factor = 12.029 according to Journal Citation Reports (JCR) published by Clarivate Analytics in 2021**.
   2. S. Yan, W. Sun, X, Yu and H. Gao, "Adaptive sensor fault accommodation for vehicle active suspensions via partial measurement information," IEEE Transactions on Cybernetics, doi: 10.1109/TCYB.2021.3072219, 2021, **indexed in Clarivate Analytics Web of Science, impact factor = 11.448 according to Journal Citation Reports (JCR) published by Clarivate Analytics in 2021**.
   3. Y.R. Liu, L. Wang, Z.P. Qiu and X. Chen, "A dynamic force reconstruction method based on modified Kalman filter using acceleration responses under multi-source uncertain samples," Mechanical Systems and Signal Processing, vol. 159, 2021, **indexed in Clarivate Analytics Web of Science, impact factor = 6.823 according to Journal Citation Reports (JCR) published by Clarivate Analytics in 2021**
   4. E. Nsugbe, O.W. Samuel, M.G. Asogbon and G.L. Li, "Contrast of multi-resolution analysis approach to transhumeral phantom motion decoding," CAAI Transactions on Intelligence Technology, 2021, pp. 1-16, **indexed in Clarivate Analytics Web of Science, without impact factor**.
   5. C.J. Qin, G. Shi, J.F. Tao, H.G. Yu, Y.R. Jin, J.B. Lei and C.L. Liu, "Precise cutterhead torque prediction for shield tunneling machines a novel neural network," Mechanical Systems and Signal Processing, vol. 151, 2021, **indexed in Clarivate Analytics Web of Science, impact factor = 6.823 according to Journal Citation Reports (JCR) published by Clarivate Analytics in 2021**.

6. Q. Zhang, J.H. Zhou, B. Zhang and E.H. Wu, "DsNet: Dual stack network for detecting diabetes mellitus and chronic kidney disease," Information Sciences, vol. 547, pp. 945-962, 2021, **indexed in Clarivate Analytics Web of Science, impact factor = 6.795 according to Journal Citation Reports (JCR) published by Clarivate Analytics in 2021**.
7. A.B. Csapo, "Cyclical inverse interpolation: An approach for the inverse interpolation of black-box models using tensor product representations," Asian Journal of Control, vol. 23, pp. 1301-1312, 2021, **indexed in Clarivate Analytics Web of Science, impact factor = 3.452 according to Journal Citation Reports (JCR) published by Clarivate Analytics in 2021**.
8. T.T. Ngoc, L.V. Dai and C.M. Thuyen, "Support vector regression based on grid gearch method of hyperparameters for load forecasting," Acta Polytechnica Hungarica, vol. 18, no. 2, pp. 143-158, 2021, **indexed in Clarivate Analytics Web of Science, impact factor = 1.806 according to Journal Citation Reports (JCR) published by Clarivate Analytics in 2021**.
9. A. Boonyaprapasorn, S. Kuntanapreeda, P.S. Ngiamsunthorn, E. Pengwang and T. Sangpet, "Tensor product model transformation-based control for fractional-order biological pest control systems," Asian Journal of Control, vol. 23, no. 2, pp. 1340-1351, 2020, **indexed in Clarivate Analytics Web of Science, impact factor = 3.452 according to Journal Citation Reports (JCR) published by Clarivate Analytics in 2021**.
10. Y.Y. He and W.Y. Zhang, "Probability density forecasting of wind power based on multi-core parallel quantile regression neural network," Knowledge-Based Systems, vol. 209, no. 8, 2020, **indexed in Clarivate Analytics Web of Science, impact factor = 8.038 according to Journal Citation Reports (JCR) published by Clarivate Analytics in 2021**.
11. R.C. Suganthe, R.S. Latha, M. Geetha and G.R. Sreekanth, "Diagnosis of Alzheimer's disease from brain magnetic resonance imaging images using deep learning algorithms," Advances in Electrical and Computer Engineering, vol. 20, no. 3, pp. 57-64, 2020, **indexed in Clarivate Analytics Web of Science, impact factor = 1.221 according to Journal Citation Reports (JCR) published by Clarivate Analytics in 2021**.
12. T. Pramanik, G. Muhiuddin, A.M. Alanazi and M. Pal, "An extension of fuzzy competition graph and its uses in manufacturing industries," Mathematics, vol. 8, no. 6, 2020, **indexed in Clarivate Analytics Web of Science, impact factor = 2.258 according to Journal Citation Reports (JCR) published by Clarivate Analytics in 2021**.
13. F. Christudas and A.V. Dhanraj, "System identification using long short term memory recurrent neural networks for real time conical tank system," Romanian Journal of Information Science and Technology, vol. 23, no. T, pp. T57-T77, 2020, **indexed in Clarivate Analytics Web of Science, impact factor = 0.643 according to Journal Citation Reports (JCR) published by Clarivate Analytics in 2021**.

14. M. Turkiewicz, E. Prociow and A. Dziedzic, "Thermovoltaic effect in a multilayer junction structure with an oxide insulation barrier," Acta Polytechnica Hungarica, vol. 17, no. 9, pp. 125-140, 2020, **indexed in Clarivate Analytics Web of Science, impact factor = 1.806 according to Journal Citation Reports (JCR) published by Clarivate Analytics in 2021**.
15. M. Seo, J. Ban, B.Y. Koo and S.W. Kim, "Static model identification for Sendzimir rolling mill using noise corrupted operation data," IEEE Acces, vol. 8, pp. 150685-150695, 2020, **indexed in Clarivate Analytics Web of Science, impact factor = 3.367 according to Journal Citation Reports (JCR) published by Clarivate Analytics in 2021**.

4. **E.-L. Hedrea**, R.-E. Precup, E.M. Petriu, C.-A. Bojan-Dragos and C. Hedrea, "Tensor product-based model transformation approach to cart position modeling and control in pendulum-cart systems," Asian Journal of Control, vol. 23, no. 3, pp. 1238-1248, 2021, **indexed in Clarivate Analytics Web of Science, impact factor = 3.452 according to Journal Citation Reports (JCR) published by Clarivate Analytics in 2021**.

4. TP-based Model Transformation technique used in control system design

4.1. The TP-based Model Transformation control algorithm

Based on the Linear Time Invariant (LTI) system matrices resulted from the Tensor Product (TP)-based Model Transformation, the Parallel Distributed Compensation (PDC) technique along with Linear Matrix Inequalities (LMIs) are involved in the TP controller design and tuning. Therefore, the input of the TP controller design approach is the core tensor made by the LTI system matrices, and the outputs are the LTI feedback gains which are stored in the tensor of the TP controller. Therefore, the steps of the TP-based model transformation control algorithm, illustrated in Fig. 4.1, are considered and are presented in detail in the following paragraphs. The PDC technique and the LMIs are used in order to design a TP-based controller which can fulfill the following control system performance specifications:

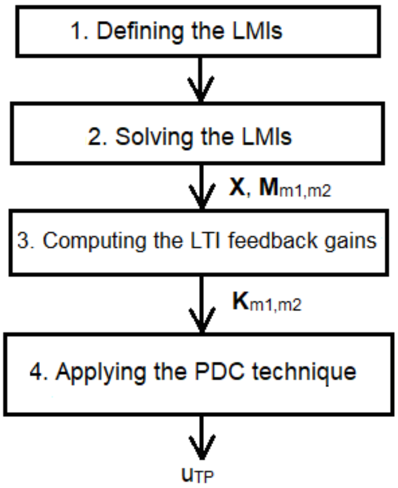

Fig.4.1. The TP-based model transformation control algorithm diagram.

i. The asymptotic stability of the control system;
ii. Constraints on the control signal.

In this regard, the following controller design approach steps are detailed in the following paragraphs. In order to ensure homogeneity of presentation, the same particular case a process with two varying parameters, presented in Sub-chapter 3.1, is used.

The two parameters, ϕ and μ, introduced in the first step of the TP-based model transformation control algorithm are used as initial data of the controller design algorithm. They are chosen by the designer in order to express the control system performance specifications i. and ii.

The number of LMIs is not a parameter imposed as initial data of the controller design algorithm. This number depends on the dimension of the core tensor $\mathcal{S}$ of the derived TP model according to the modeling algorithm presented in Sub-chapter 3.1.

1. Defining the LMIs.

Let us consider the TP-based model given in (3.18) for a particular system with two varying parameters. The goal of the LMI-based controller design is to determine one LTI feedback gain, which is stored in tensor $\mathbf{K}$ of the controller, for each LTI system matrix, which is stored in tensor $\mathbf{S}$ of the TP model given in (3.18). Therefore, in order to design a TP-based controller which fulfills the two requirements presented above, the following LMIs are defined.

The control system specification i., namely the asymptotic stability of the closed-loop control system, is equivalent to the existence of $\mathbf{X}=\mathbf{P}^{-1}>0$ (where $\mathbf{P}$ is a positive definite matrix) and $\mathbf{M}_{m1,m2}$ that satisfy the following LMIs [Bar13]:

$$\begin{aligned}&-\mathbf{X}\mathbf{A}_{m1,m2}^{T}-\mathbf{A}_{m1,m2}\mathbf{X}+\mathbf{M}_{m1,m2}^{T}\mathbf{X}_{m1,m2}^{T}+\mathbf{B}_{m1,m2}\mathbf{M}_{m1,m2}>0,\\&-\mathbf{X}\mathbf{A}_{m1,m2}^{T}-\mathbf{A}_{m1,m2}\mathbf{X}-\mathbf{X}\mathbf{A}_{s}^{T}-\mathbf{A}_{s}\mathbf{X}+\mathbf{M}_{s}^{T}\mathbf{B}_{m1,m2}^{T}+\mathbf{B}_{m1,m2}\mathbf{M}_{s}\\&+\mathbf{M}_{m1,m2}^{T}\mathbf{B}_{s}^{T}+\mathbf{B}_{s}\mathbf{M}_{m1,m2}\geq 0,\end{aligned}\tag{4.1}$$

where $m1=1...M_1, m2=1...M_2$ and the matrices $\mathbf{A}_{m1,m2}$ and $\mathbf{B}_{m1,m2}$ are defined in Sub-chapter 3.1.

Next, the objective of the control system performance specification ii., i.e. to constrai the control signal, is considered. Assuming that $\|\mathbf{x}(0)\|_2\leq\phi$, where $\mathbf{x}(0)$ is unknown, but the upper bound ϕ is known, the constraint $|u|\leq\mu$ is enforced at all time moments if the following LMIs are satisfied [Bar13]:

$$\begin{aligned}&\phi^2\mathbf{I}\leq\mathbf{X},\\&\begin{pmatrix}\mathbf{X} & \mathbf{M}_{m1,m2}^{T}\\ \mathbf{M}_{m1,m2}^{T} & \mu^2\mathbf{I}\end{pmatrix}\geq 0,\end{aligned}\tag{4.2}$$

where $m1=1...M_1, m2=1...M_2$.

2. Solving the LMIs.

The LMIs defined in step 1 are solved using a dedicated LMI software or toolbox. In this thesis the YalmipR2015 solver was used. Therefore, the two matrices $\mathbf{M}_{m1,m2}$ and $\mathbf{X}$ are computed as solutions of the LMIs.

3. Computing the LTI feedback gains.

Based on the solutions of the previous LMIs, the LTI feedback gains are computed and stored in the TP controller tensor as

$$\mathbf{K}_{m1,m2}=\mathbf{M}_{m1,m2}\mathbf{X}^{-1}.\tag{4.3}$$

4. Applying the PDC technique.

Finally, the control signal applied to the process with two varying parameters is expressed as:

$$\begin{aligned}&u=r-u_{TP},\\&u_{TP}=\left[\sum_{m1=1}^{M_1}\sum_{m2=1}^{M_2}w_{1,m1}(p_1)w_{2,m2}(p_2)\mathbf{K}_{m1,m2}\right]\mathbf{x},\end{aligned}\tag{4.4}$$

where r is the reference input and u_{TP} is the control law of the TP controller based on the feedback gain tensor obtained after the application of the PDC technique.

4.2. The TP-based Model Transformation used for level control of Vertical Three Tank System

Starting with the TP model derived for the V3TS given in Equation (3.26) in Sub-chapter 3.2 and following the control design steps given in Sub-chapter 4.1, the PDC technique is applied as follows in order to design a TP-based controller for the level control of V3TS.

Since, as shown in Sub-chapter 3.1, the parameter vector consists of one parameter, that means $M_2 = 1$ in the design approach and all subscripts $m1, m2$ of the matrices in the design approach will be replaced in this sub-chapter with $m1$. This is justified because $m2 = 1$, so it does not make sense anymore to use the subscript $m2$ as follows.

The two control system performance specifications presented in the previous sub-chapter are considered. The control system performance specification i., which consists in guaranteeing the asymptotic stabilization of the control system, is solved using the PDC design framework. Therefore for each LTI vertex system of the convex TP model one LTI feedback gain is determined. The asymptotic stability of the closed-loop control system is equivalent to the existence of $\mathbf{X} = \mathbf{P}^{-1} > 0$ (where $\mathbf{P}$ is a positive definite matrix) and $\mathbf{M}_{m1}$ that satisfy the LMIs given in (4.1) [Bar13].

The state feedback gain matrices $\mathbf{K}_{m1}$ that correspond to each LTI vertex system are next computed as [Hed17b], [Hed19a]:

$$\mathbf{K}_{m1} = \mathbf{M}_{m1}\mathbf{X}^{-1}. \tag{4.5}$$

The objective of the control system performance specification ii. is to constrain the control signal. It is assumed that $\|\mathbf{x}(0)\|_2 \le \phi$, where $\mathbf{x}(0)$ is unknown, but the upper bound ϕ is known. The constraint $|u| \le \mu$ is enforced at all time moments if the LMIs given in (4.2) are satisfied [Bar13].

Considering the following numerical values for $\phi = 0.05 > 0$ and $\mu = 1$, the matrices $\mathbf{X}$ and $\mathbf{M}_{m1}$ are computed by solving the seven LMIs, namely two plus two in (4.1) plus one plus two in (4.2), using the YalmipR2015 solver. The solutions are next substituted in (4.5) leading to the values of the LTI feedback gains which are given in Equation (1) in Appendix 3.

Finally, the resulted TP controller is introduced in the Single Input Multiple Output (SIMO) closed-loop control system structure (TPCS), where $\mathbf{y}_i^{TP} = \begin{bmatrix} y_1^{TP} & y_2^{TP} & y_3^{TP} \end{bmatrix}^T$ represents the controlled output vector. The TPCS is illustrated in Fig. 4.2.

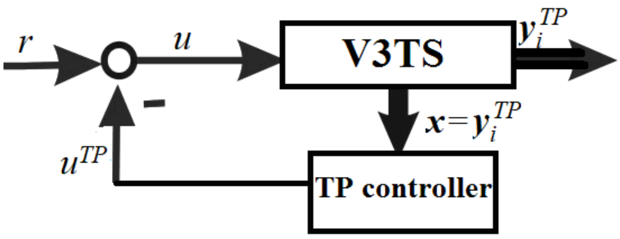

Fig.4.2. Block diagram of the TPCS designed for V3TS [Hed19a].

Using the PDC technique, the following state feedback control law results for V3TS [Hed17b], [Hed19a]:

$$u = r - u_{TP},$$
$$u_{TP} = [\sum_{m1=1}^{2} w_{1,m1}(p_1)\mathbf{K}_{m1}]\mathbf{x}. \tag{4.6}$$

In order to compare the performance of the TP-based controller designed for V3TS with similar control structures, four state feedback control structures (SFCSs) are designed considering the same control performace specifications as the ones considered for the TP-CS, i.e. the asymptotic stabilization of the control system and the constraint applied to the control signal.

The general block diagram of the four SFCSs is illustrated in Fig.4.3, where $j = \overline{1,4}$ denotes the number of linear models, $u^{(j)}$ is the control signal, r is the reference input, $u_x^{(j)}$ is the state feedback controller matrix product output, $\mathbf{y}_i^{(j)} = \begin{bmatrix} y_1^{(j)} & y_2^{(j)} & y_3^{(j)} \end{bmatrix}^T$ is the controlled output vector.

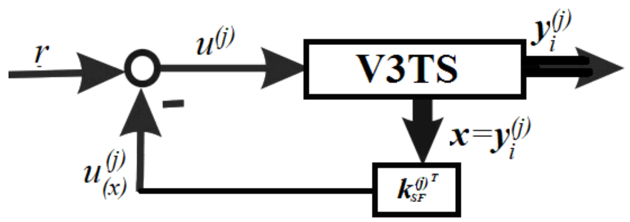

Fig.4.3. General block diagram of the four SFCSs designed for V3TS [Hed17b], [Hed19a].

The fair comparison of the TP controller and the linear state feedback controller makes use of the same design approach applied in the nonlinear case (i.e. the TP controller) and the four linear cases. In this regard, the computation of the state feedback gain matrices $\mathbf{k}_{SF}^{(j)T}$ is similar with the one of the LTI feedback gains of the TP controller. These matrices result after solving the following LMIs that correspond to (4.1):

$$\begin{aligned}
&-\mathbf{X}^{(j)}\mathbf{A}^{(j)} - \mathbf{A}^{(j)}\mathbf{X}^{(j)} + \mathbf{M}^{(j)}\mathbf{X}^{(j)T} + \mathbf{b}^{(j)}\mathbf{M}^{(j)} > 0,\\
&-\mathbf{X}^{(j)}\mathbf{A}^{(j)} - \mathbf{A}^{(j)}\mathbf{X}^{(j)} - \mathbf{X}^{(j)}\mathbf{A}^{(j)T} - \mathbf{A}^{(j)}\mathbf{X}^{(j)} + \mathbf{M}^{(j)T}\mathbf{b}^{(j)T}\\
&+\mathbf{b}^{(j)}\mathbf{M}^{(j)} + \mathbf{M}^{(j)T}\mathbf{b}^{(j)T} + \mathbf{b}^{(j)}\mathbf{M}^{(j)} \geq 0
\end{aligned} \tag{4.7}$$

in order to ensure the asymptotic stabilization of the control system (i.e. the performance specification i.), and the following LMIs that correspond to (4.2):

$$\begin{aligned}
&\phi^2\mathbf{I} \leq \mathbf{X}^{(j)},\\
&\begin{pmatrix} \mathbf{X}^{(j)} & \mathbf{M}^{(j)T} \\ \mathbf{M}^{(j)T} & \mu^2\mathbf{I} \end{pmatrix} \geq 0
\end{aligned} \tag{4.8}$$

in order to fulfill the constraint imposed to the modulus of the control signal in terms of the control system performance specification ii., where $\mathbf{A}^{(j)}$ and $\mathbf{b}^{(j)}$ result in accordance with Sub-chapter 3.2, and ϕ and μ are the same parameters as the ones chosen in the design of the TP controller.

Finally the state feedback gain matrices are computed for each of the four linear models of V3TS derived in Sub-chapter 3.2, as:

$$\mathbf{k}_{SF}^{(j)^T} = \mathbf{M}^{(j)}\mathbf{X}^{(j)^{-1}}. \tag{4.9}$$

Considering the same numerical values as in case of the TPCS, i.e. $\phi = 0.05$ and $\mu = 1$, which take into consideration the real operating conditions of the world laboratory equipment, the matrices $\mathbf{X}^{(j)}$ and $\mathbf{M}^{(j)}$ are computed, after solving four LMIs for each linear model of V3TS, namely two in (4.7) plus one plus one in (4.8), using the YalmipR2015 solver. The solutions are next substituted in (4.9) leading to the values of the state feedback gains which are given in Equation (1) in Appendix 4.

In order to highlight the performance of the five CSs designed for V3TS, namely the first one represented by the TPCS, the second one represented by the first SFCS, the third one represented by the second SFCS, the fourth one represented by the third SFCS and the fifth one represented by the fourth SFCS, two testing scenarios (simulation and experiment) were considered by employing a staircase change for the reference input ($r_1 = 0.2$ m, $r_2 = 0.4$ m, $r_3 = 0.1$ m) on the time horizon of 3000 s. In case of the simulation scenario each controller is tested on its corresponding derived model presented in Sub-chapter 3.2 and in case of the experimental scenario each controller is tested on the V3TS laboratory equipment. The initial state vector matching the simulations and experiments is $\mathbf{x}_0 = [0 \quad 0 \quad 0]^T$. The responses of the controlled outputs and control signals of the control structures responses are plotted in Figs.4.4-4.7 in the simulation scenario and in Figs. 4.8-4.11 in the experimental scenario.

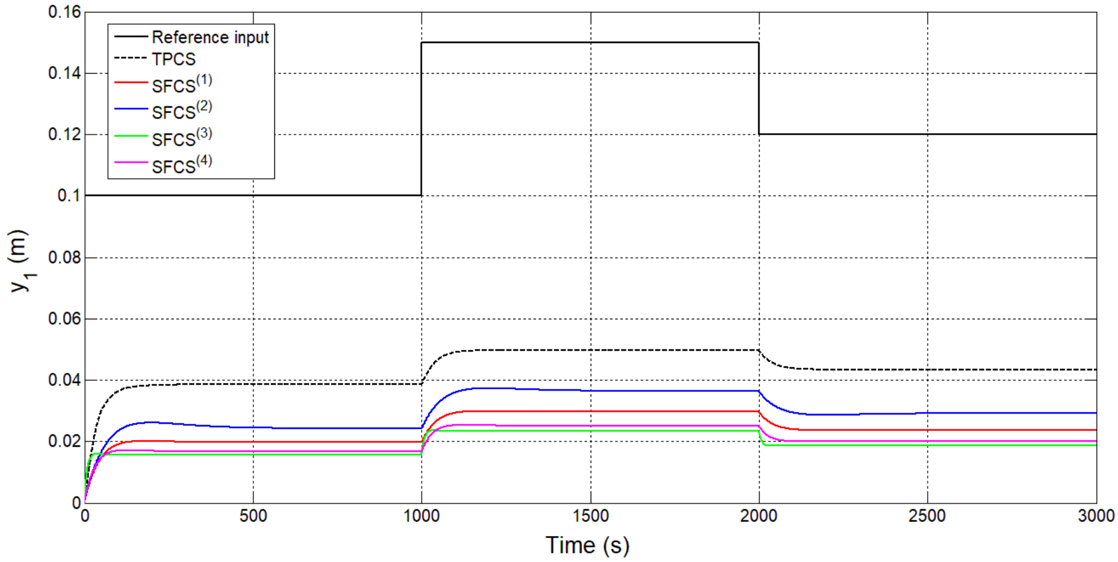

Fig.4.4. First tank fluid levels (y_1) versus time in case of TPCS and the four SFCSs with staircase reference input in the simulation scenario.

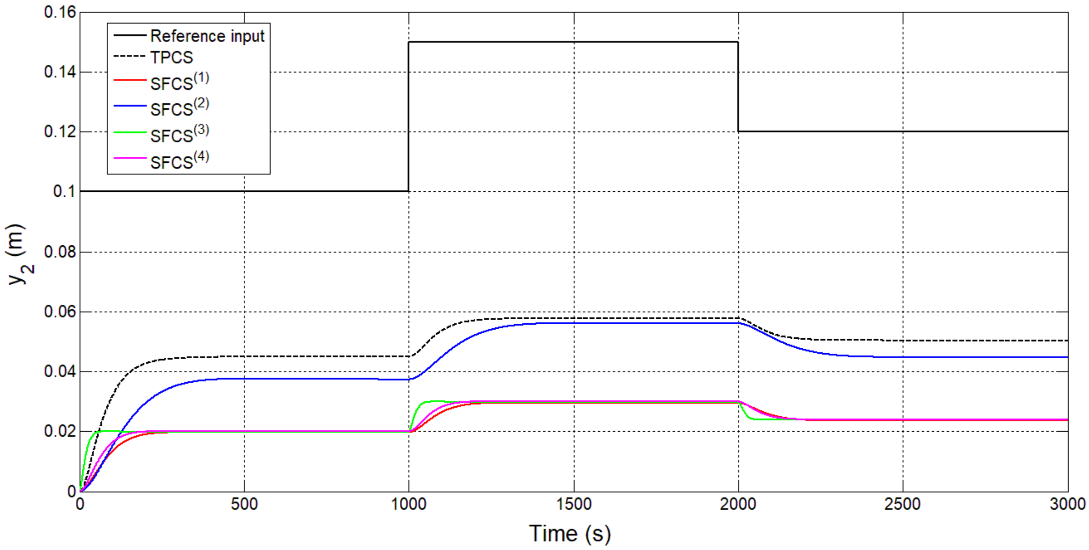

Fig.4.5. Second tank fluid levels (y_2) versus time in case of TPCS and the four SFCSs with staircase reference input in the simulation scenario.

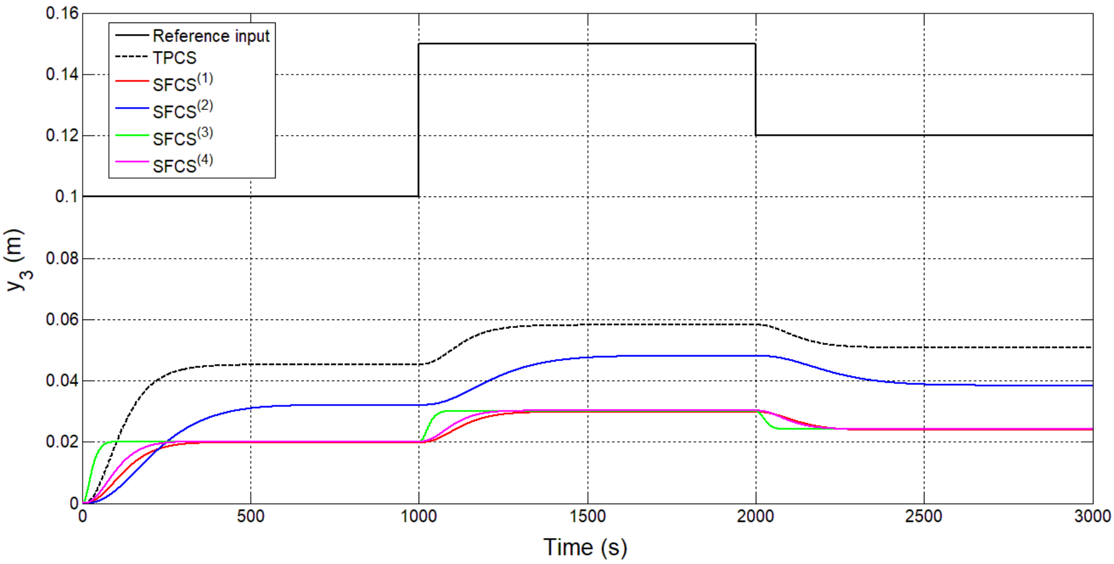

Fig.4.6. Third tank fluid levels (y_3) versus time in case of TPCS and the four SFCSs with staircase reference input in the simulation scenario.

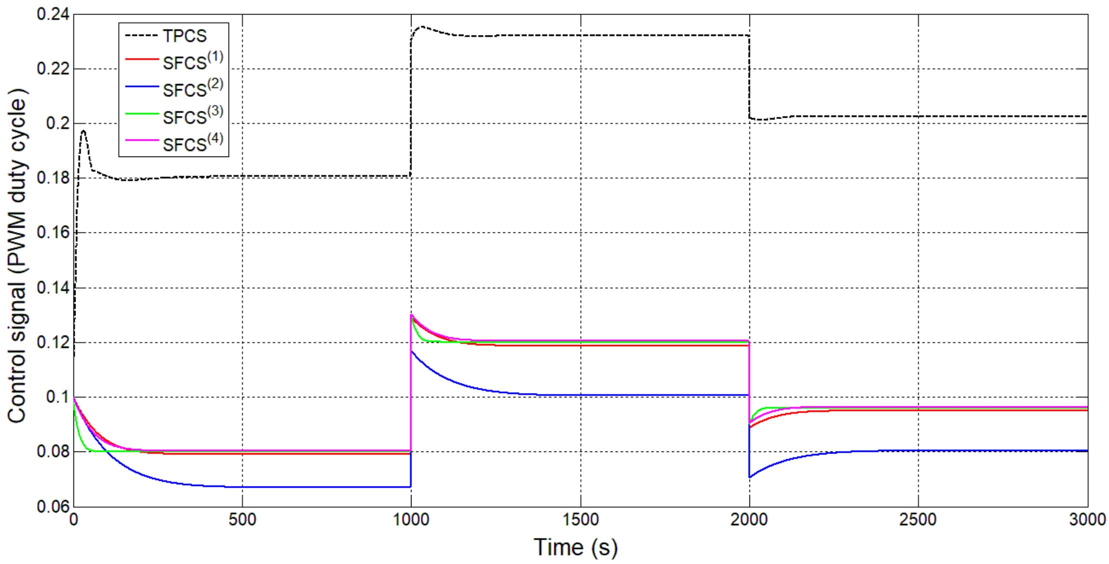

Fig.4.7. Control signal versus time in case of TPCS and the four SFCSs with staircase reference input in the simulation scenario.

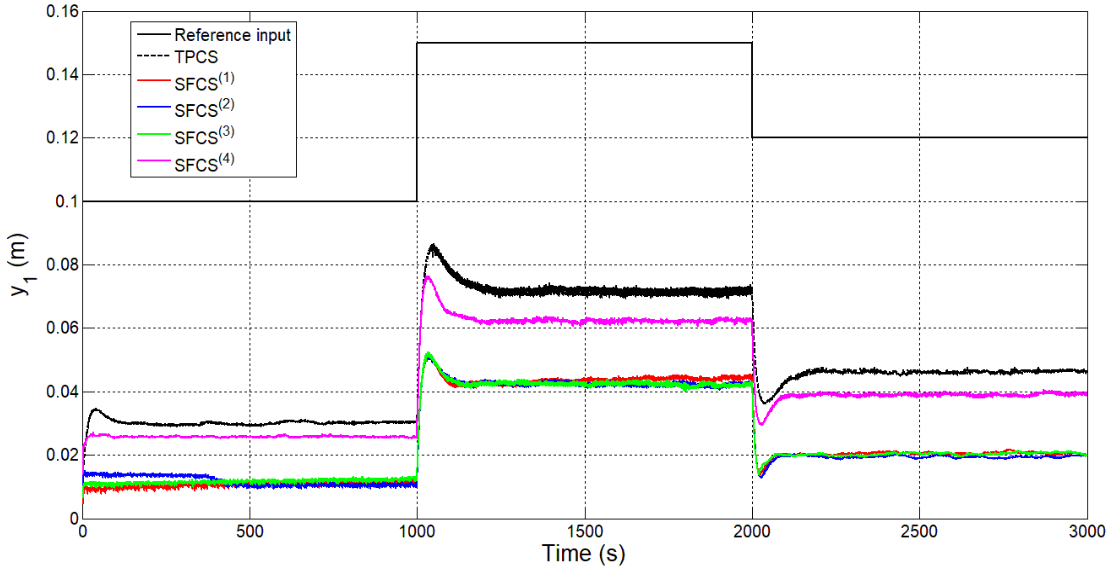

Fig.4.8. First tank fluid levels (y_1) versus time in case of TPCS and the four SFCSs with staircase reference input in the experimental scenario.

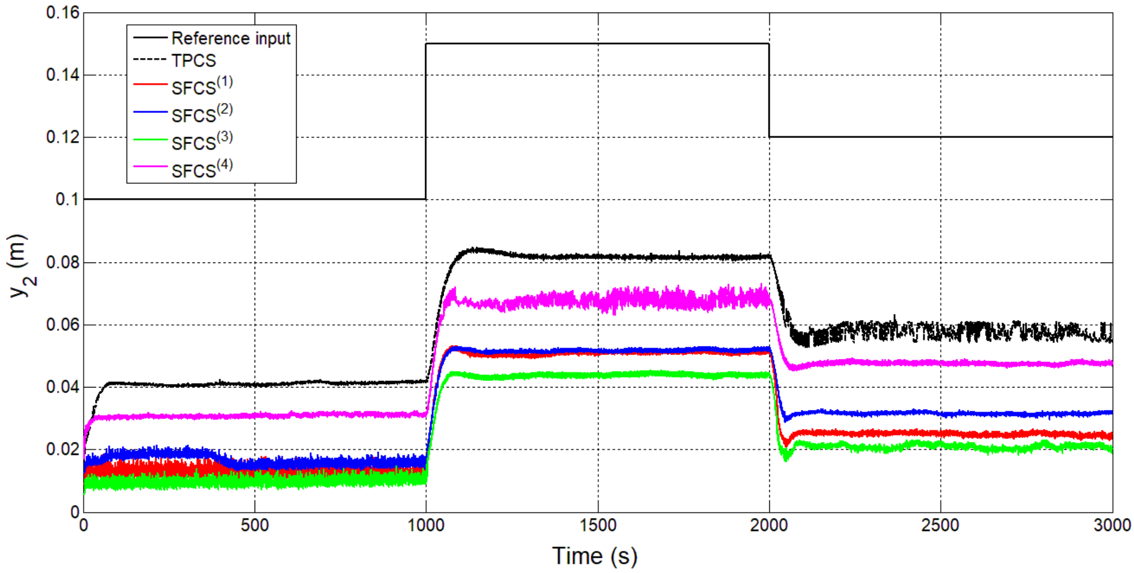

Fig.4.9. Second tank fluid levels (y_2) versus time in case of TPCS and the four SFCSs with staircase reference input in the experimental scenario.

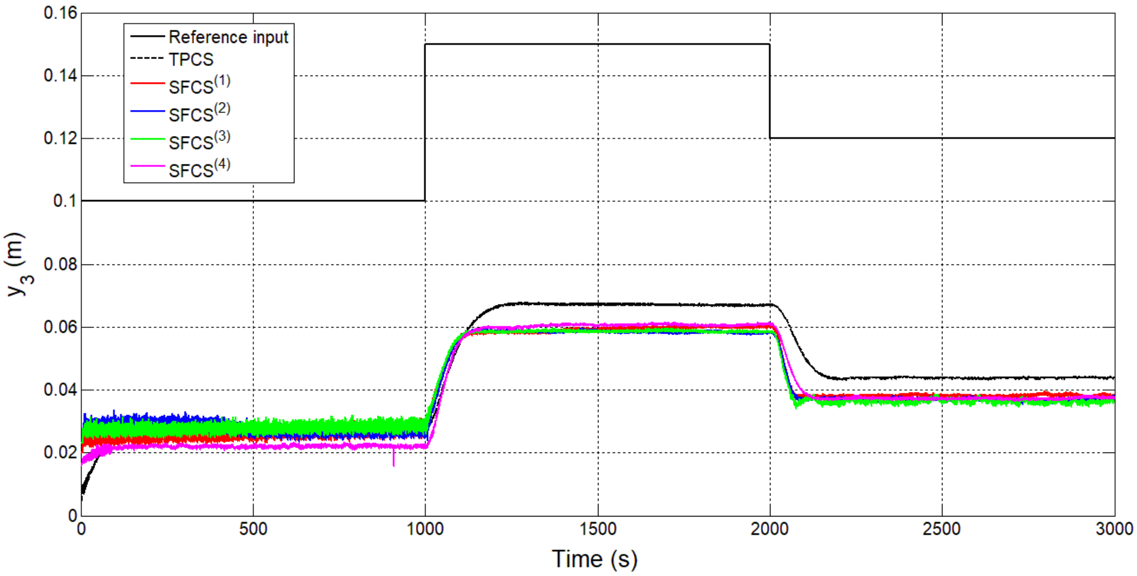

Fig.4.10. Third tank fluid levels (y_3) versus time in case of TPCS and the four SFCSs with staircase reference input in the experimental scenario.

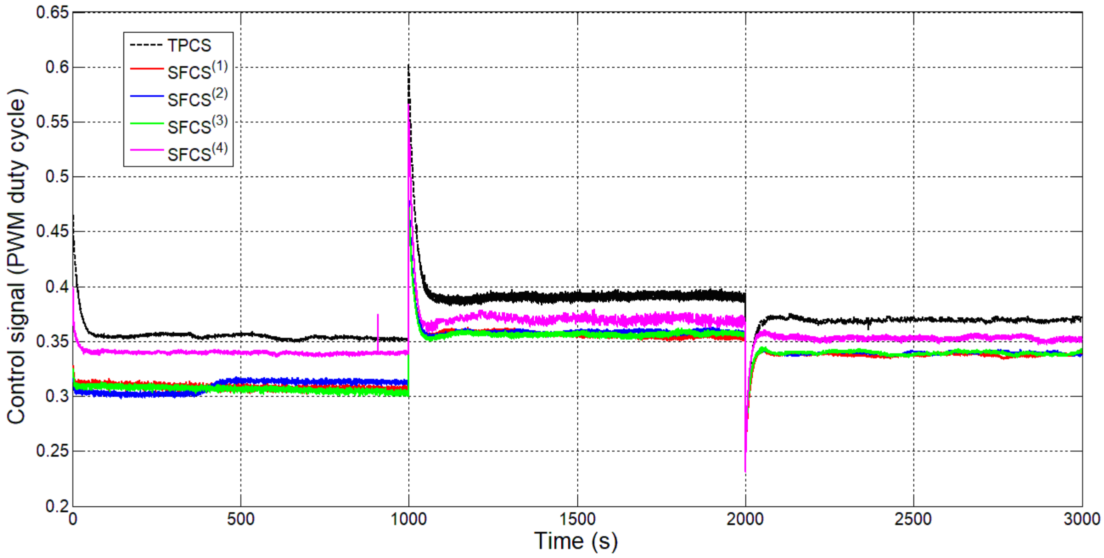

Fig.4.11. Control signal versus time in case of TPCS and the four SFCSs with staircase reference input in the experimental scenario.

The simulation and the experimental results show that all the five CSs designed for V3TS fulfill the control system performance specification i., i.e. the stabilization of the CS, and the control system specification ii., i.e. the control signal is constrained. However, they do not ensure zero steady-state control error. Therefore, each of the five CSs is included in a cascade control system structure with a PID controller the outer control loop.

At first the TPCS, considered as controlled plant, is included in three Single Input Single Output (SISO) cascade control system (PID-TPCS) structures with PID controllers in the outer control loop. The state feedback gain matrices given in Equation (1) in Appendix 3 are employed in the computation of the following third-order benchmark type closed-loop t.f.s of the inner control loop, $H_{TPCS_i}(s)$ with respect of each of the three outputs of V3TS [Hed19a]:

$$H_{TPCS_i}(s) = k_{TPCS_i} / [(1+T_{c1}^{(TPCS_i)}s)(1+T_{c2}^{(TPCS_i)}s)(1+T_{c3}^{(TPCS_i)}s)], \qquad (4.10)$$

where the numerical values of the parameters are given in Table 4.2.1 and are obtained after a simple least-squares-based experimental approximation of the inner control loop illustrated in Fig. 4.12.

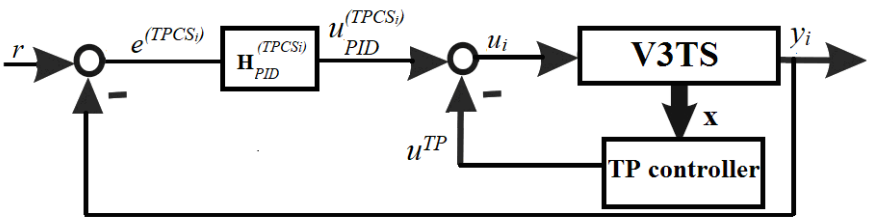

Fig.4.12. Block diagram of the SISO PID-TPCSs designed for V3TS [Hed19a].

Table 4.2.1.

Values of parameters of the third order t.f.s. computed for TPCS.

TPCS output, y_i	k_{TPCS_i}	$T_{c1}^{(TPCS_i)}$	$T_{c2}^{(TPCS_i)}$	$T_{c3}^{(TPCS_i)}$
y_1	0.17	12	3	2
y_2	0.11	25	22	3
Y_3	0.21	52	48	4

The PID controllers were designed using Kessler's Modulus Optimum method (MO-m), having the general t.f.s:

$$H_{PID}^{(TPCS_i)}(s) = k_r^{(TPCS_i)}(1 + sT_{r1}^{(TPCS_i)})(1 + sT_{r2}^{(TPCS_i)}) / [s(1 + sT_d^{(TPCS_i)})], \qquad (4.11)$$

where the tuning parameters were computed as [Kes55]:

$$\begin{aligned} & k_r^{(TPCS_i)} = 0.1 / \left(2k_{TPCS_i} T_{c3}^{(TPCS_i)}\right), \\ & T_{r1}^{(TPCS_i)} = T_{c1}^{(TPCS_i)},\ T_{r2}^{(TPCS_i)} = T_{c2}^{(TPCS_i)},\ T_d^{(TPCS_i)} = 0.1 \cdot T_{c3}^{(TPCS_i)}. \end{aligned} \qquad (4.12)$$

The numerical values of the parameters are given in Table 4.2.2.

Table 4.2.2.

Values of parameters of the PID controllers designed for TPCS.

TPCS output, y_i	$k_r^{(TPCS_i)}$	$T_{r1}^{(TPCS_i)}$	$T_{r2}^{(TPCS_i)}$	$T_d^{(TPCS_i)}$
y_1	0.1471	12	3	0.2
y_2	0.1515	25	22	0.3
y_3	0.0595	52	48	0.4

The control signals applied to V3TS are computed by combining the output of the TP-based controller, u_{TP}, and the outputs of the PID controllers, $u_{PID}^{(TPCS_i)}$.

Next, the four SFCSs, as controlled plants, are also included in twelve Single Input Single Output (SISO) cascade control system (PID-SFCS) structures with PID controllers in the outer control loop. The equivalent state feedback gain matrices given in Equation (1) in Appendix 4 are employed in the computation of the following third-order benchmark type closed-loop t.f.s of the inner control loop, $H_{SFCS_i}^{(j)}(s)$ with respect of each of the three outputs of V3TS [Hed19a]:

$$H_{SFCS_i}^{(j)}(s) = k_{SFCS_i}^{(j)} / [(1 + T_{c1_i}^{(j)} s)(1 + T_{c2_i}^{(j)} s)(1 + T_{c3_i}^{(j)} s)], \qquad (4.13)$$

where the numerical values of the parameters are given in Table 4.2.3. These parameters are obtained by a simple least-squares-based experimental approximation of the inner control loop illustrated in Fig. 4.13.

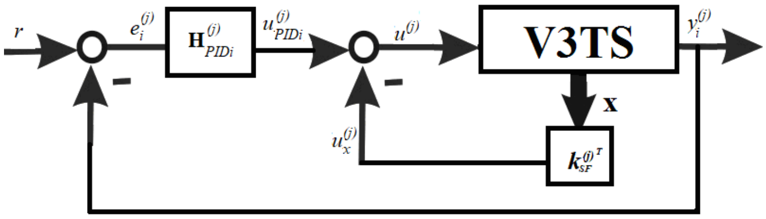

Fig.4.13. Block diagram of the SISO PID-SFCSs designed for V3TS [Hed19a].

The four PID controllers are also designed using the MO-m, with the general t.f.:

$$H_{PID_i}^{(j)}(s) = k_{r_i}^{(j)}(1 + sT_{r1_i}^{(j)})(1 + sT_{r2_i}^{(j)}) / [s(1 + sT_{d_i}^{(j)})], \qquad (4.14)$$

where the tuning parameters were computed as [Kes55]:

$$\begin{aligned} & k_{r_i}^{(j)} = 0.1 / \left(2k_{SFCS_i} T_{c3_i}^{(j)}\right), \\ & T_{r1_i}^{(j)} = T_{c1_i}^{(j)},\ T_{r2_i}^{(j)} = T_{c2_i}^{(j)},\ T_{d_i}^{(j)} = 0.1 \cdot T_{c3_i}^{(j)}. \end{aligned} \qquad (4.15)$$

The numerical values of the parameters are given in Table 4.2.4.

Table 4.2.3.

Values of parameters of the third order t.f.s. computed for SFCSs.

SFCS$^{(j)}$	SFCS output, y_i	$k_{SFCS_i}^{(j)}$	$T_{c1_i}^{(j)}$	$T_{c2_i}^{(j)}$	$T_{c3_i}^{(j)}$
SFCS$^{(1)}$	y_1	0.25	57	55	2
	y_2	0.29	48	41	2.5
	y_3	0.39	56	55	9
SFCS $^{(2)}$	y_1	0.27	45	41	3
	y_2	0.25	54	47	2
	y_3	0.78	64	61	2
SFCS $^{(3)}$	y_1	0.42	55	51	1.5
	y_2	0.21	39	35	4
	y_3	0.28	59	58	4
SFCS $^{(4)}$	y_1	0.21	65	61	3
	y_2	0.21	55	51	1.5
	y_3	0.23	65	57	8

Table 4.2.4.

Values of parameters of the PID controllers designed for SFCSs.

PID-SFCS$^{(j)}$	y_i	$k_{r_i}^{(j)}$	$T_{r1_i}^{(j)}$	$T_{r2_i}^{(j)}$	$T_{d_i}^{(j)}$
PID-SFCS $^{(1)}$	y_1	0.1	57	55	0.2
	y_2	0.0690	48	41	0.25
	y_3	0.0142	56	55	0.9
PID-SFCS $^{(2)}$	y_1	0.0617	45	41	0.3
	y_2	0.1	54	47	0.2
	y_3	0.0321	64	61	0.2
PID-SFCS $^{(3)}$	y_1	0.0794	55	51	0.15
	y_2	0.0595	39	35	0.4
	y_3	0.0446	59	58	0.4
PID-SFCS $^{(4)}$	y_1	0.0794	65	61	0.3
	y_2	0.1587	55	51	0.15
	y_3	0.0272	65	57	0.8

The control signals applied to V3TS are computed by combining the output variable of the state feedback controller, $u_x^{(j)}$, and ones of the PID controllers, $u_{PID_i}^{(j)}$.

The five control structures, namely PI-TPCS and the four PID-SFCSs, were tested in the same two testing scenario used for TPCS and the four SFCSs, i.e. simulation and experiment. Each PID controller is tested on its corresponding control structure with the t.f.s. given in (4.10) and (4.13) as resulting from the block diagrams in Figs. 4.12 and 4.13. The same values of the parameters of the PID controllers were used both in simulations and experiments. The initial state vector matching the simulations and experiments is $\mathbf{x}_0 = [0 \quad 0 \quad 0]^T$. The responses of the controlled outputs and the control signals of the control structures are plotted in Figs. 4.14-4.19 in the simulation scenario and in Figs. 4.20-4.25 in the experimental scenario.

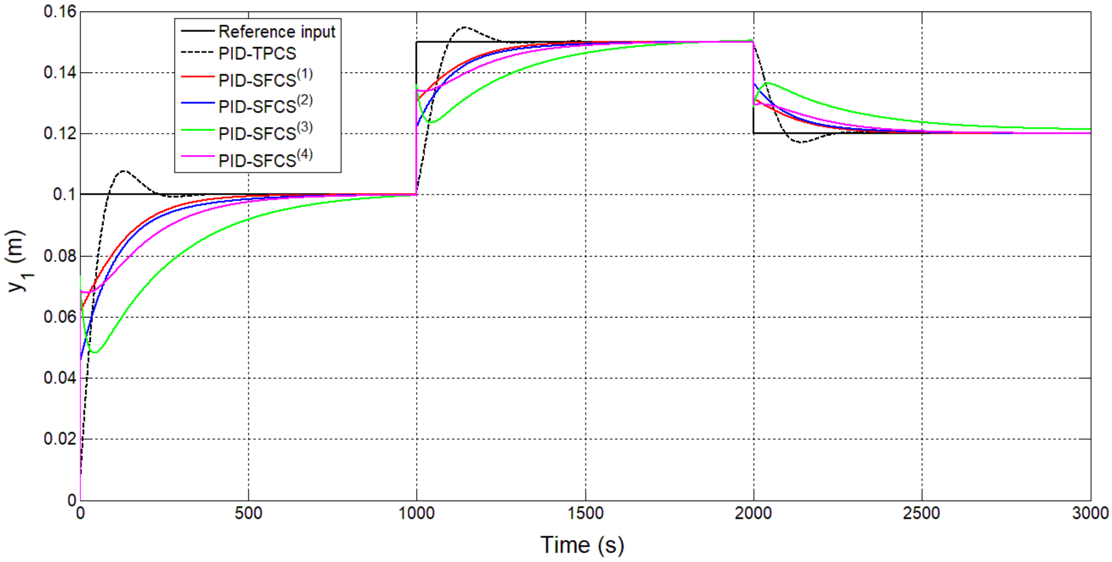

Fig.4.14. First tank fluid levels (y_1) versus time in case of PID-TPCS and the PID-SFCSs designed for the liquid level control of the first tank in the simulaton scenario.

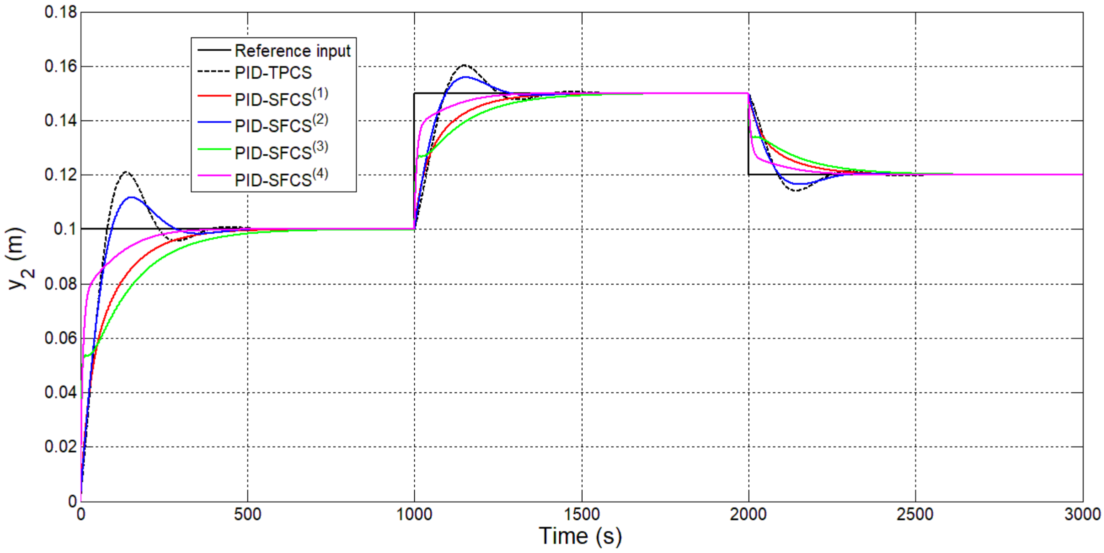

Fig.4.15. Second tank fluid levels (y_2) versus time of PID-TPCS and the PID-SFCSs designed for the liquid level control of the second tank in the simulaton scenario.

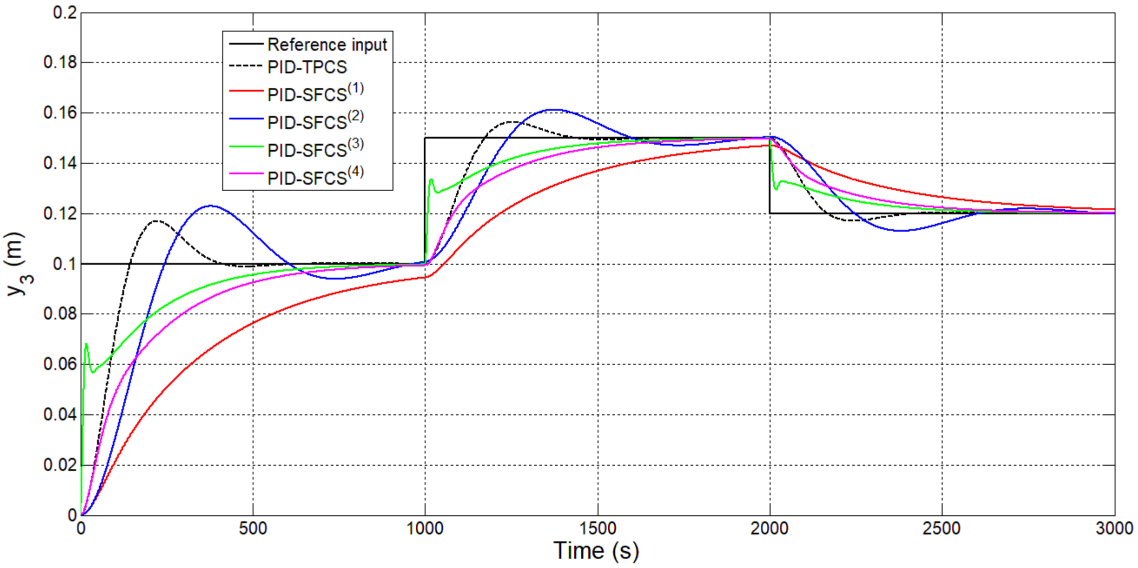

Fig.4.16. Third tank fluid levels (y_3) versus time of PID-TPCS and the PID-SFCSs designed for the liquid level control of the third tank in the simulaton scenario.

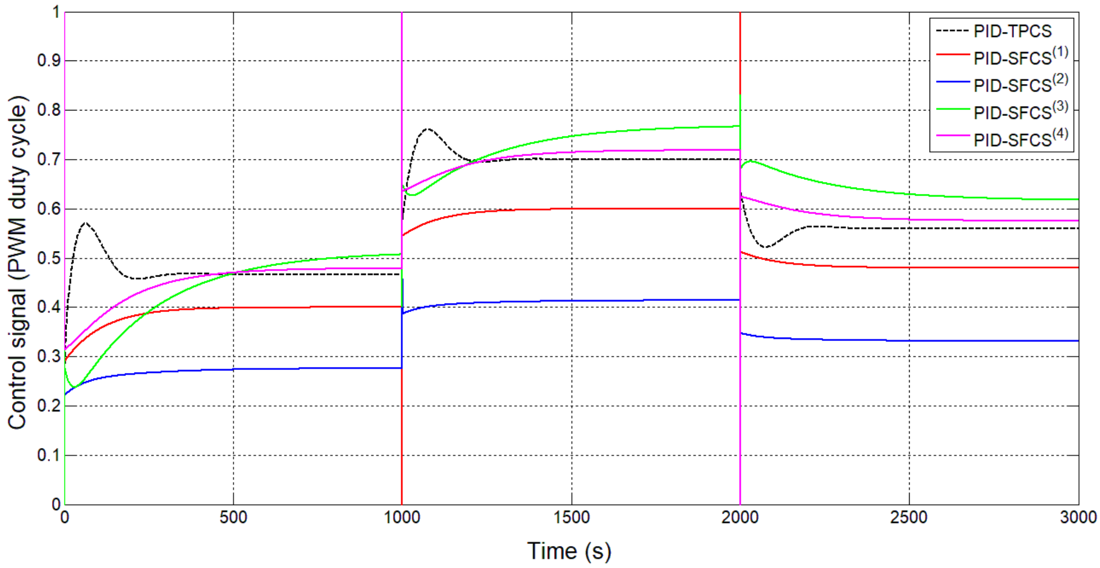

Fig.4.17. Control signal versus time in case of PID-TPCS and the PID-SFCSs designed for the level control of the first tank in the simulaton scenario.

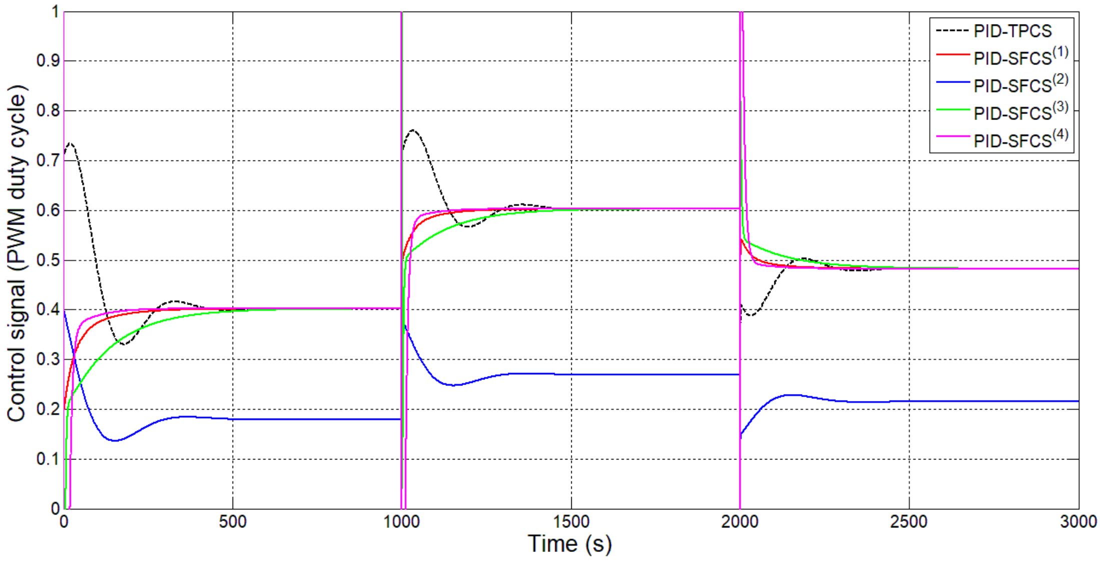

Fig.4.18. Control signal versus time in case of PID-TPCS and the PID-SFCSs designed for the level control of the second tank in the simulaton scenario.

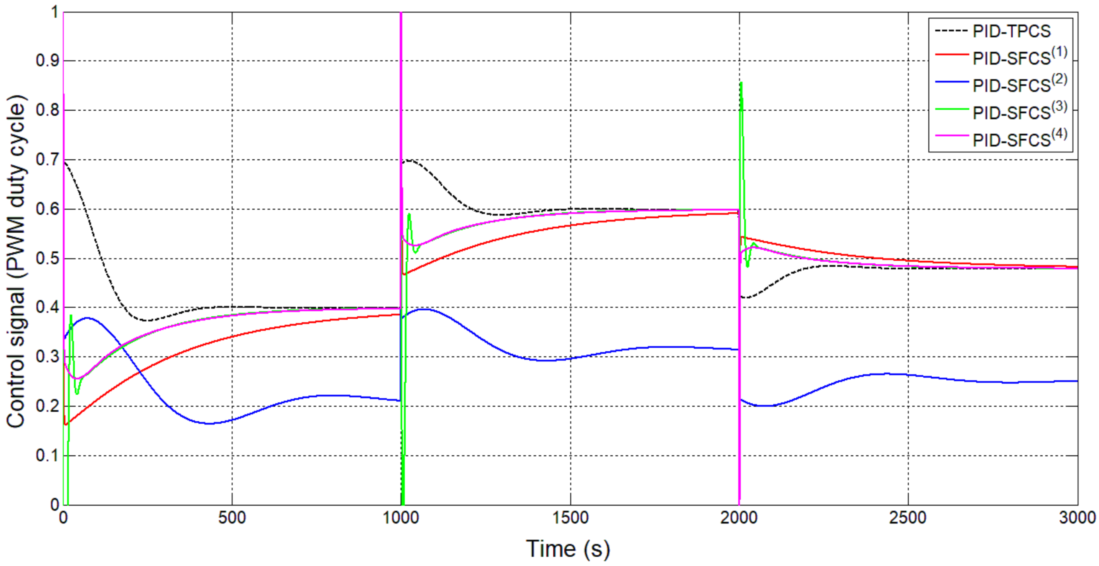

Fig.4.19. Control signal versus time in case of PID-TPCS and the PID-SFCSs designed for the level control of the third tank in the simulaton scenario.

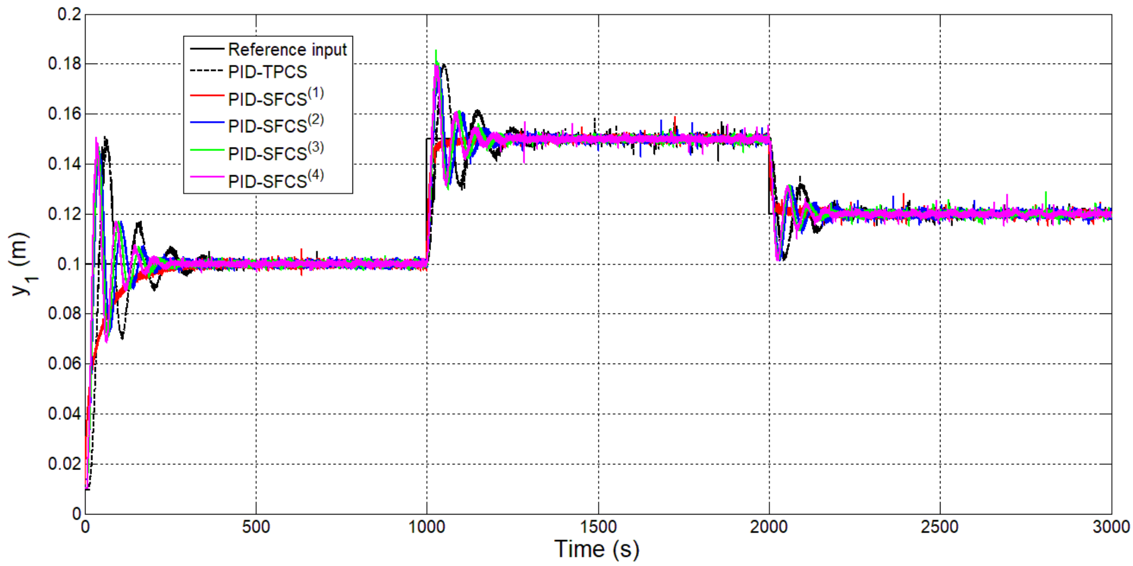

Fig.4.20. First tank fluid levels (y_1) versus time in case of PID-TPCS and the PID-SFCSs designed for the liquid level control of the first tank in the experimental scenario.

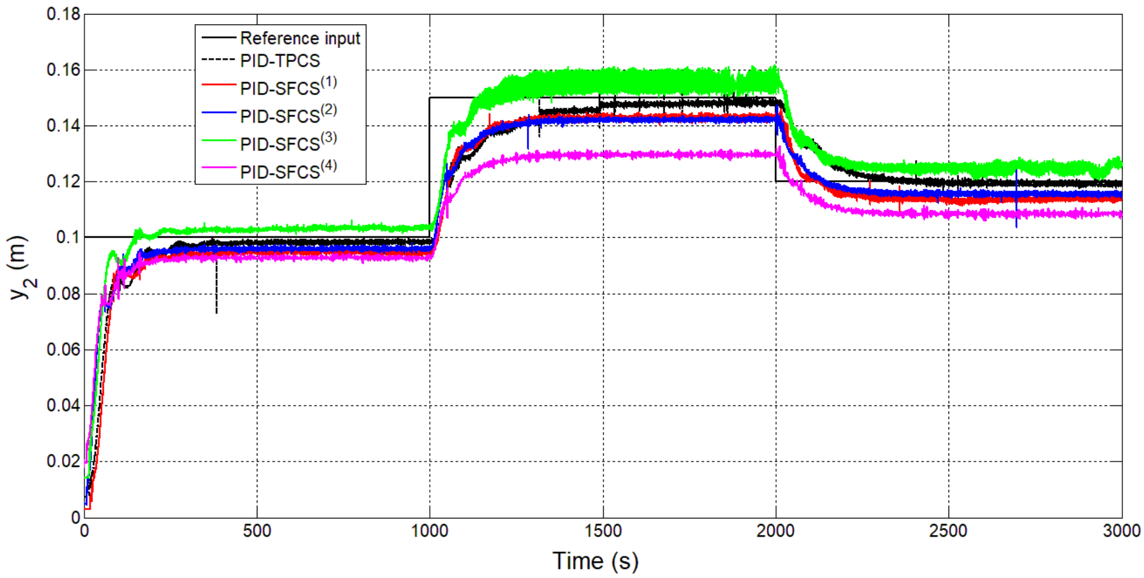

Fig.4.21. Second tank fluid levels (y_2) versus time of PID-TPCS and the PID-SFCSs designed for the liquid level control of the second tank in the experimental scenario.

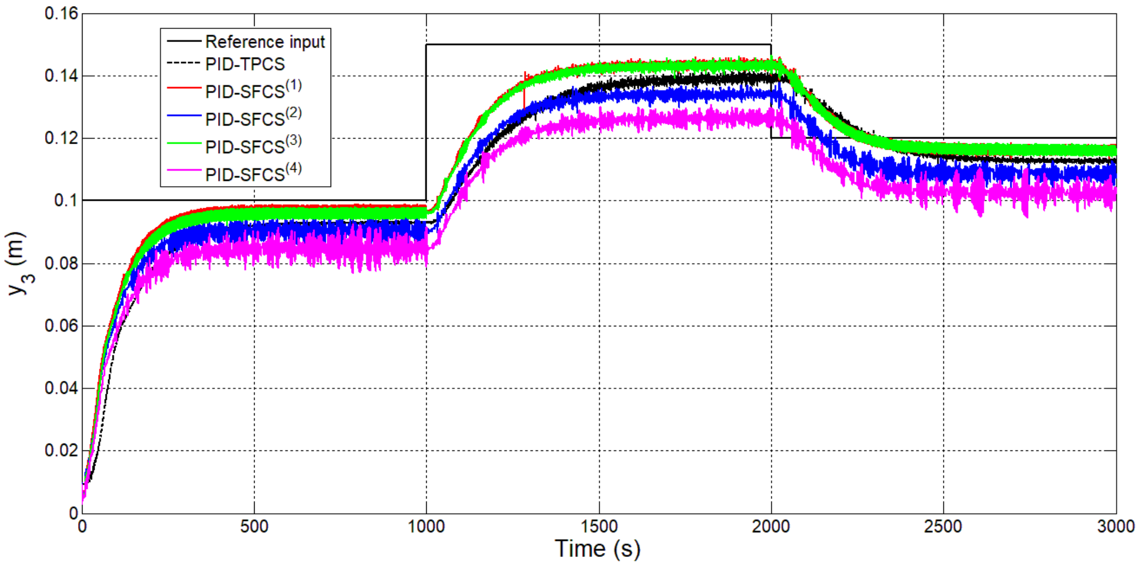

Fig.4.22. Third tank fluid levels (y_3) versus time of PID-TPCS and the PID-SFCSs designed for the liquid level control of the third tank in the experimental scenario.

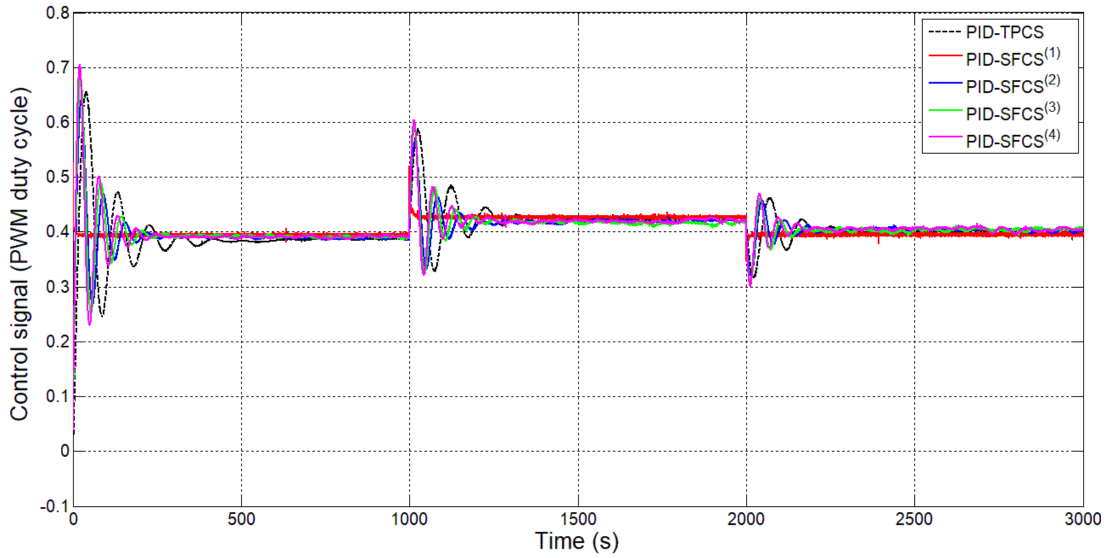

Fig.4.23. Control signal versus time in case of PID-TPCS and the PID-SFCSs designed for the level control of the first tank in the experimental scenario.

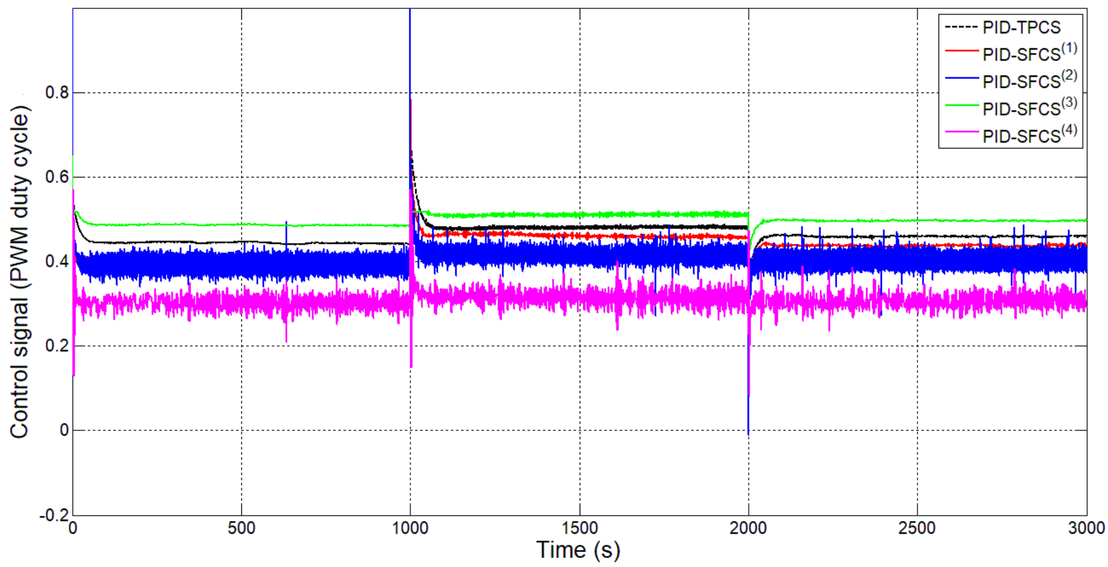

Fig.4.24. Control signal versus time in case of PID-TPCS and the PID-SFCSs designed for the level control of the second tank in the experimental scenario.

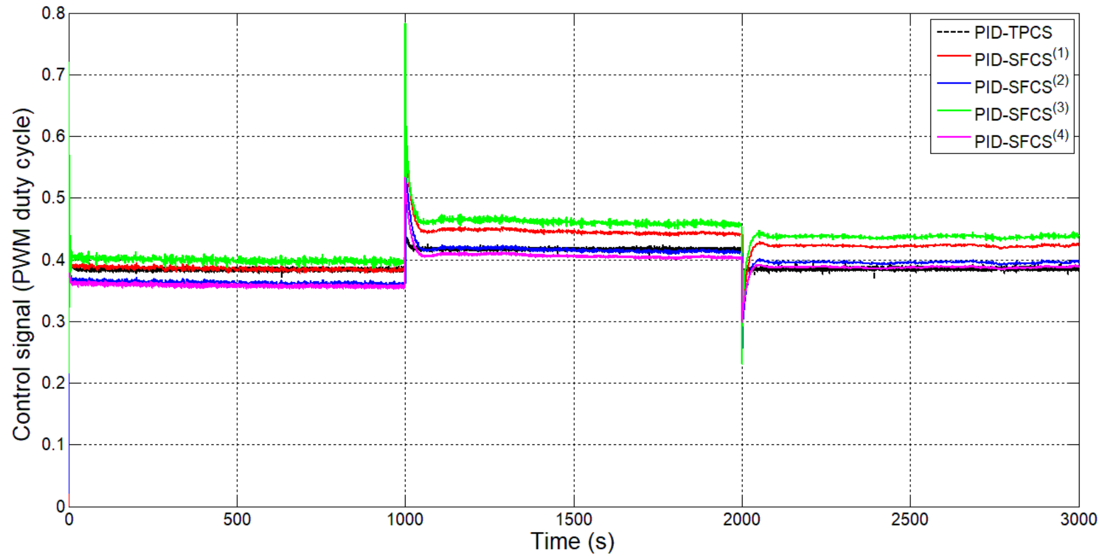

Fig.4.25. Control signal versus time in case of PID-TPCS and the PID-SFCSs designed for the level control of the third tank in the experimental scenario.

The simulation and the experimental results show that all the CSs designed for V3TS fulfill both the control system performance specifications, i.e. the stabilization of the CS and the constraint applied on the control signal and they also ensure zero steady-state control error.

In order to highlight the performance of the ten derived control structures for V3TS, four performance indices, namely the Mean Square Error (MSE), the Mean Square Control Effort (MSU), the settling time and the overshoot are computed.

The MSEs are computed as

$$MSE = \frac{1}{M} \sum_{k=1}^{M} e_i^{\psi\,2}(k), \qquad (4.16)$$

where e_i^{ψ} represents the control error, which in case of V3TS is defined as

$$e_i^{\psi} = r - y_i^{\psi}. \qquad (4.17)$$

The superscript $\psi = TPCS$ indicates the TP-based control structure, $\psi = SFCS^{(j)}$ indicates the four state feedback control structures, $\psi = PID - TPCS_i$ indicates the PID and TP-based control structures, $\psi = PID - SFCS_i^{(j)}$ indicates the PID and state feedback control structures, y_i^{ψ} are the outputs of the V3TS system, r is the reference input, i represents the number of tank, $M = 30001$ is the number of samples and the sampling period $T_s = 0.1$ s.

The MSUs are computed as

$$MSU = \frac{1}{M}\sum_{k=1}^{M} u_i^{\psi\,2}(k), \tag{4.18}$$

where u_i^{ψ} represents the control signal applied in case of the control structures designed for V3TS.

The values of the three performance indices are given in Table 4.2.5 in the simulation scenario and in Table 4.2.6 in the experimental scenario.

Table 4.2.5.
Values of control system performance indices for V3TS in the simulation scenario.

Control structures	**Performance indices**								
	y_i	**MSE (m^2)**	**MSU**	**Settling time (s)**			**Overshoot (%)**		
				r_1	r_2	r_3	r_1	r_2	r_3
TPCS	y_1	$6.6 \cdot 10^{-3}$	0.0425	150	150	150	0	0	0
	y_2	$5.7 \cdot 10^{-3}$	0.0425	300	300	200	0	0	0
	y_3	$5.7 \cdot 10^{-3}$	0.0425	400	400	400	0	0	0
SFCS$^{(1)}$	y_1	$10.1 \cdot 10^{-3}$	0.0099	250	200	200	0	0	0
	y_2	$10.2 \cdot 10^{-3}$	0.0099	250	250	250	0	0	0
	y_3	$10.3 \cdot 10^{-3}$	0.0099	300	300	300	0	0	0
SFCS$^{(2)}$	y_1	$9 \cdot 10^{-3}$	0.0073	500	500	500	0	0	0
	y_2	$6.5 \cdot 10^{-3}$	0.0073	450	450	450	0	0	0
	y_3	$7.8 \cdot 10^{-3}$	0.0073	600	600	600	0	0	0
SFCS$^{(3)}$	y_1	$11.1 \cdot 10^{-3}$	0.0100	50	50	50	0	0	0
	y_2	$10.1 \cdot 10^{-3}$	0.0100	70	70	70	0	0	0
	y_3	$10 \cdot 10^{-3}$	0.0100	100	100	100	0	0	0
SFCS$^{(4)}$	y_1	$10.9 \cdot 10^{-3}$	0.0102	150	150	100	0	0	0
	y_2	$10.1 \cdot 10^{-3}$	0.0102	250	250	250	0	0	0
	y_3	$10.1 \cdot 10^{-3}$	0.0102	250	250	250	0	0	0
PID-TPCS	y_1	$9.62 \cdot 10^{-5}$	0.3443	250	250	250	10	5	5
	y_2	$1.33 \cdot 10^{-4}$	0.2642	500	500	500	15	10	10
	y_3	$2.75 \cdot 10^{-4}$	0.2606	500	500	450	20	10	10
PID-SFCS$^{(1)}$	y_1	$4.8 \cdot 10^{-5}$	0.2459	600	600	600	0	0	0
	y_2	$1.43 \cdot 10^{-4}$	0.2496	650	650	650	0	0	0
	y_3	$8.49 \cdot 10^{-4}$	0.2210	1000	1000	1000	0	0	0
PID-SFCS$^{(2)}$	y_1	$7.9 \cdot 10^{-5}$	0.1174	600	600	600	0	0	0
	y_2	$1.2 \cdot 10^{-4}$	0.0534	650	650	650	10	7	7
	y_3	$5.16 \cdot 10^{-4}$	0.0764	1000	1000	1000	25	15	15
PID-SFCS$^{(3)}$	y_1	$7.87 \cdot 10^{-5}$	0.3946	600	600	600	0	0	0
	y_2	$1.14 \cdot 10^{-4}$	0.2426	650	650	650	0	0	0
	y_3	$1.46 \cdot 10^{-4}$	0.2364	900	900	600	0	0	0
PID-SFCS$^{(4)}$	y_1	$6.86 \cdot 10^{-5}$	0.3467	600	600	600	0	0	0
	y_2	$4.12 \cdot 10^{-5}$	0.2488	550	650	650	0	0	0
	y_3	$3.95 \cdot 10^{-4}$	0.2367	900	800	800	0	0	0

Table 4.2.6.

Values of control system performance indices for V3TS in the experimental scenario.

Control structures	y_i	**MSE (m^2)**	**MSU**	**Settling time (s)**			**Overshoot (%)**		
				r_1	r_2	r_3	r_1	r_2	r_3
TPCS	y_1	$5.5\cdot10^{-3}$	0.1394	200	250	300	10	10	10
	y_2	$4.1\cdot10^{-3}$	0.1394	200	250	250	3	5	5
	y_3	$6.1\cdot10^{-3}$	0.1394	250	300	250	0	0	0
SFCS$^{(1)}$	y_1	$9.7\cdot10^{-3}$	0.1123	200	250	300	0	10	10
	y_2	$8.8\cdot10^{-3}$	0.1123	100	200	250	5	5	5
	y_3	$6.9\cdot10^{-3}$	0.1123	100	200	100	0	0	0
SFCS$^{(2)}$	y_1	$9.8\cdot10^{-3}$	0.1133	200	250	300	0	10	10
	y_2	$8.2\cdot10^{-3}$	0.1133	100	200	250	0	5	5
	y_3	$6.9\cdot10^{-3}$	0.1133	100	200	100	0	0	0
SFCS$^{(3)}$	y_1	$9.8\cdot10^{-3}$	0.1123	200	250	300	0	10	10
	y_2	$9.8\cdot10^{-3}$	0.1123	100	200	250	0	5	5
	y_3	$6.9\cdot10^{-3}$	0.1123	100	200	100	0	0	0
SFCS$^{(4)}$	y_1	$10.9\cdot10^{-3}$	0.1261	200	250	300	10	10	10
	y_2	$6.6\cdot10^{-3}$	0.1261	100	200	250	0	5	5
	y_3	$7.1\cdot10^{-3}$	0.1261	100	200	100	0	0	0
PID-TPCS	y_1	$1.29\cdot10^{-4}$	0.1663	500	450	300	25	15	10
	y_2	$4.13\cdot10^{-4}$	0.2146	300	500	400	0	0	0
	y_3	$4.85\cdot10^{-4}$	0.1567	550	600	550	0	0	0
PID-SFCS$^{(1)}$	y_1	$5.04\cdot10^{-5}$	0.1647	500	450	300	0	0	0
	y_2	$2.50\cdot10^{-4}$	0.1882	300	500	400	0	0	0
	y_3	$2.95\cdot10^{-4}$	0.1753	550	600	550	0	0	0
PID-SFCS$^{(2)}$	y_1	$7.64\cdot10^{-5}$	0.1656	500	450	300	25	15	10
	y_2	$1.71\cdot10^{-4}$	0.1643	300	500	400	0	0	0
	y_3	$4.60\cdot10^{-4}$	0.1538	550	600	550	0	0	0
PID-SFCS$^{(3)}$	y_1	$7.68\cdot10^{-5}$	0.1661	500	450	300	25	15	10
	y_2	$1.50\cdot10^{-4}$	0.2478	300	500	400	0	0	0
	y_3	$3.12\cdot10^{-4}$	0.1882	550	600	550	0	0	0
PID-SFCS$^{(4)}$	y_1	$7.00\cdot10^{-5}$	0.1674	500	450	300	25	15	10
	y_2	$3.14\cdot10^{-5}$	0.0953	300	500	400	0	0	0
	y_3	$6.94\cdot10^{-4}$	0.1482	550	600	550	0	0	0

The best performance concerning the MSE is achieved by the first PID-SFCS for the first tank in the simulation scenario and by the fourth PID-SFCS for the second tank in the experimental scenario. The best settling time is achived by the third SFCS in case of all three tanks in the simulation scenario and by the four SFCSs for the third tank in the experimental scenario. The best performance in terms of MSU is obtained by the second SFCS in case of all three tanks in the simulation scenario and by the fourth PID-SFCS for the second tank in the experimental scenario. The overshoot is present in case of the PID-TPCS and the second PID-SFCS in the simulation scenario and in case of TPCS and the four SFCSs for the first and second tank and by the PID-TPCS, the second, the third and the fourth PID-SFCS for the first tank in the experimental scenario. Its smallest value is obtained for the PID-SFCS in case of the first two tanks, by the PID-TPCS in case of the third tank in the simulation scenario and by the TPCS and the four SFCSs for the second tank in the experimental scenario. The first five CSs, namely the TPCS and the SFCSs do not ensure zero steady-state control error. Therefore, the implementation of the cascade control system structures is justified. Other numbers of parameters of the TP model derived for V3TS would lead to other values of the LTI feedback gains which would lead to other values of the performance indices given in Table 4.2.5 and Table 4.2.6.

4.3. The TP-based Model Transformation used for position control of a partial state feedback controlled Magnetic Levitation System

The Magnetic Levitation System is an important benchmark used to test various linear and nonlinear modeling and control approaches. Some representative control approaches are state-PI and PID feedback control [Wib13], [Boj16], fuzzy control [Yu10], [Mah15], [Zho18], gain scheduling control [Boj18a] and neural networks control [Mil17]. The combination of the tensor product-based model transformation technique with the gain scheduling technique applied to the postion control of the psfcMLS is given in [Hed18b] and with fuzzy control is presented in [Hed18c] and [Hed19c]. The big number of control solutions for the Magnetic Levitation System shows the increasing interest in this field.

In this Sub-chapter, several TP-based and state feedback-based control solutions designed for the sphere position control of psfcMLS are presented.

Starting with the TP model derived for psfcMLS given in Equation (3.43) in Sub-chapter 3.3 and following the control design steps given in Sub-chapter 4.1, the PDC technique is applied as follows in order to design a TP-based controller for the sphere position control of psfcMLS.

Since, as shown in Sub-chapter 3.1, the parameter vector consists of one parameter, that means $M_2 = 1$ in the design approach, all subscripts $m1, m2$ of the matrices in the design approach will be replaced in this Sub-chapter with $m1$. This is justified because $m2 = 1$, so it does not make sense anymore to use the subscript $m2$ as follows.

The two control system performance specifications presented in the previous Sub-chapter are considered. The control system performance specification i., which consists in guaranteeing the asymptotic stabilization of the control system, is solved using the PDC design framework. Therefore for each LTI vertex system of the convex TP model one LTI feedback gain is determined. The asymptotic stability of the closed-loop control system is equivalent to the existence of $\mathbf{X} = \mathbf{P}^{-1} > 0$ (where $\mathbf{P}$ is a positive definite matrix) and $\mathbf{M}_{m1}$ that satisfy the LMIs given in (4.1) [Bar13].

The state feedback gain matrices $\mathbf{K}_{m1}$ that correspond to each LTI vertex system are next computed as [Hed17a], [Hed19d]:

$$\mathbf{K}_{m1} = \mathbf{M}_{m1}\mathbf{X}^{-1}. \qquad (4.19)$$

The objective of the control system performance specification ii. is to constrain the control signal. It is assumed that $\|\mathbf{x}(0)\|_2 \le \phi$, where $\mathbf{x}(0)$ is unknown, but the upper bound ϕ is known. The constraint $|u| \le \mu$ is enforced at all time moments if the LMIs given in (4.2) are satisfied [Bar13].

Considering the numerical values $\phi = 0.0001 > 0$ and $\mu = 1$, the matrices $\mathbf{X}$ and $\mathbf{M}_{m1}$ are computed by solving the seven LMIs, namely three plus three in (4.1) plus two plus three in (4.2), using the YalmipR2015 solver. The solutions are next substituted in (4.5) leading to the values of the LTI feedback gains which are given in Equation (2) in Appendix 3.

Finally, the resulted TP controller is introduced in the Single Input Multiple Output (SIMO) closed-loop control system structure (TPCS), where $\mathbf{y}^{TP}$ represents the controlled output. The TPCS is illustrated in Fig. 4.26.

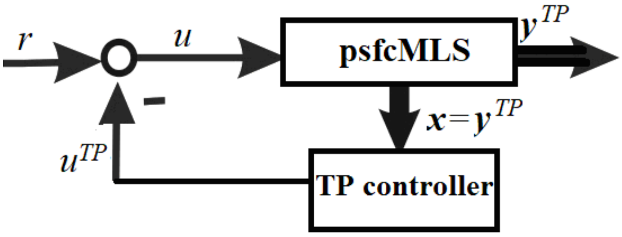

Fig.4.26. Block diagram of the TPCS designed for psfcMLS [Hed17a].

Using the PDC technique, the following state feedback control law results for psfcMLS [Hed17a], [Hed19d]:

$$u = r - u_{TP},$$
$$u_{TP} = [\sum_{m1=1}^{3} w_{1,m1}(p_1)\mathbf{K}_{m1}]\mathbf{x}. \tag{4.20}$$

In order to compare the performance of the TP-based controller designed for psfcMLS with similar control structures, four state feedback control structures (SFCSs) are designed considering the same control performace specifications i. and ii. as the ones considered for the TP-CS, i.e. the asymptotic stabilization of the control system and the constraint applied to the control signal.

The general block diagram of the four SFCSs is illustrated in Fig.4.27, where $j = \overline{1,4}$ denotes the number of linear models, $u^{(j)}$ is the control signal, r is the reference input, $u_x^{(j)}$ is the state feedback controller matrix product output, $y^{(j)}$ is the controlled output.

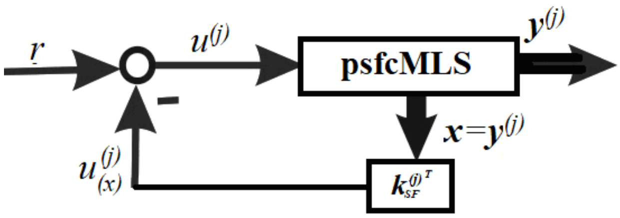

Fig.4.27. General block diagram of the four SFCSs designed for psfcMLS.

The fair comparison of the TP controller and the linear state feedback controller makes use of the same design approach applied in the nonlinear case (i.e. the TP controller) and the four linear cases. In this regard, the computation of the state feedback gain matrices $\mathbf{k}_{SF}^{(j)^T}$ is similar with the one of the LTI feedback gains of the TP controller. These matrices result after solving the following two LMIs (for each j) that correspond to (4.1):

$$\begin{aligned}
&-\mathbf{X}^{(j)}\mathbf{A}^{(j)} - \mathbf{A}^{(j)}\mathbf{X}^{(j)} + \mathbf{M}^{(j)}\mathbf{X}^{(j)^T} + \mathbf{b}^{(j)}\mathbf{M}^{(j)} > 0,\\
&-\mathbf{X}^{(j)}\mathbf{A}^{(j)} - \mathbf{A}^{(j)}\mathbf{X}^{(j)} - \mathbf{X}^{(j)}\mathbf{A}^{(j)^T} - \mathbf{A}^{(j)}\mathbf{X}^{(j)} + \mathbf{M}^{(j)^T}\mathbf{b}^{(j)^T}\\
&+\mathbf{b}^{(j)}\mathbf{M}^{(j)} + \mathbf{M}^{(j)^T}\mathbf{b}^{(j)^T} + \mathbf{b}^{(j)}\mathbf{M}^{(j)} \geq 0
\end{aligned} \tag{4.21}$$

in order to ensure the asymptotic stabilization of the control system (i.e. the performance specification i.), and the following two LMIs (for each *j*) that correspond to (4.2):

$$\phi^2 \mathbf{I} \le \mathbf{X}^{(j)},$$
$$\begin{pmatrix} \mathbf{X}^{(j)} & \mathbf{M}^{(j)T} \\ \mathbf{M}^{(j)T} & \mu^2 \mathbf{I} \end{pmatrix} \ge 0 \quad (4.22)$$

in order to fulfill the constraint imposed to the modulus of the control signal in terms of the control system performance specification ii., where $\mathbf{A}^{(j)}$ and $\mathbf{b}^{(j)}$ result in accordance with Sub-chapter 3.3, and ϕ and μ are the same parameters as the ones chosen in the design of the TP controller.

Finally the state feedback gain matrices are computed for each of the four linear models of psfcMLS derived in Sub-chapter 3.3, as:

$$\mathbf{k}_{SF}^{(j)T} = \mathbf{M}^{(j)} \mathbf{X}^{(j)-1}. \quad (4.23)$$

Considering the same numerical values as in case of the TPCS, i.e. $\phi = 0.0001$ and $\mu = 1$, which take into consideration the real operating conditions of the world laboratory equipment, the matrices $\mathbf{X}^{(j)}$ and $\mathbf{M}^{(j)}$ are computed, after solving four LMIs for each linear model of psfcMLS, namely two in (4.21) plus one plus one in (4.22), using the YalmipR2015 solver. The solutions are next substituted in (4.23) leading to the values of the state feedback gains which are given in Equation (2) in Appendix 4.

In order to highlight the performance of the five CSs designed for psfcMLS, namely the first one represented by the TPCS, the second one represented by the first SFCS, the third one represented by the second SFCS, the fourth one represented by the third SFCS and the fifth one represented by the fourth SFCS, two testing scenarios (one simulation one plus one experimental one) were considered by employing a staircase change for the reference input ($r_1 = 0.006$ m, $r_2 = 0.008$ m, $r_3 = 0.007$ m) on the time horizon of 20 s. In case of the simulation scenario each controller is tested on its corresponding derived model presented in Sub-chapter 3.3 and in case of the experimental scenario each controller is tested on the psfcMLS laboratory equipment. The initial state vector matching the simulations and experiments is $\mathbf{x}_0 = [0 \quad 0 \quad 0]^T$. The responses of the controlled outputs and the control signals (or control inputs) of the control structures are plotted in Fig.4.28 and Fig. 4.29 in the simulation scenario and in Fig.4.30 and Fig.4.31 in the experimental scenario.

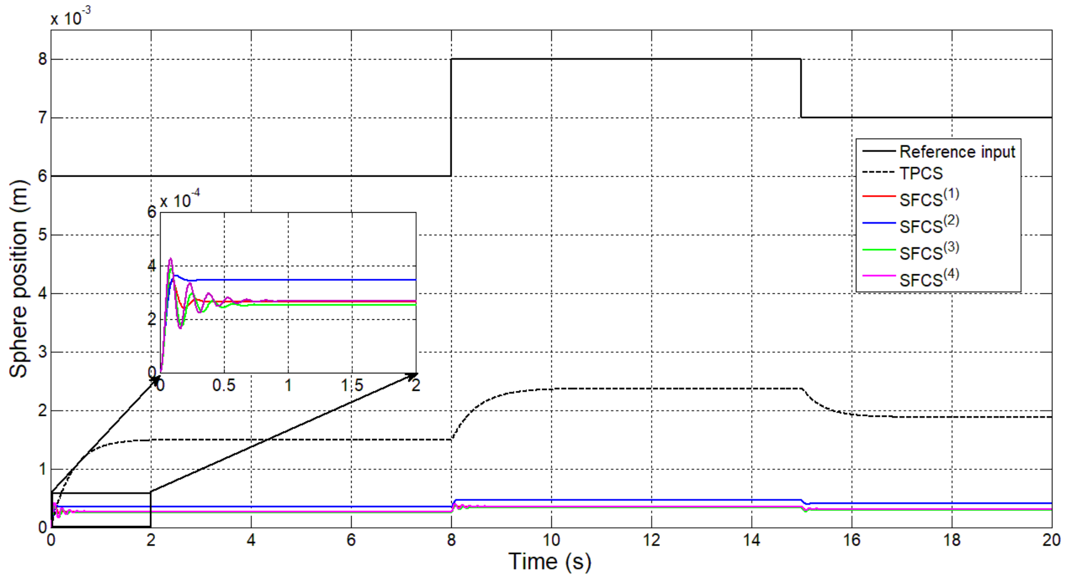

Fig.4.28. Sphere position versus time in case of TPCS and the four SFCSs with staircase reference input in the simulation scenario.

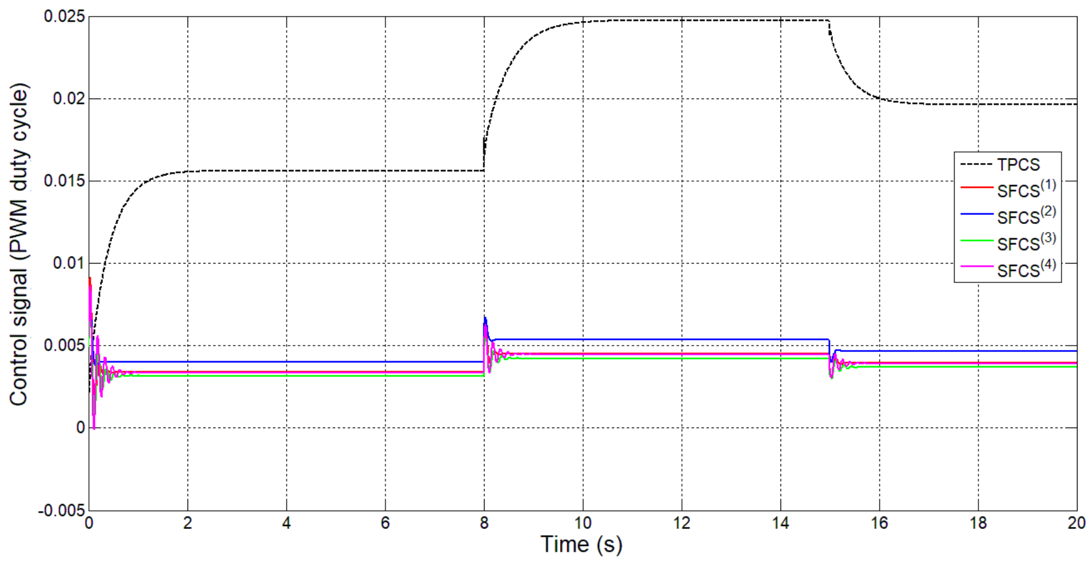

Fig.4.29. Control signal versus time in case of TPCS and the four SFCSs with staircase reference input in the simulation scenario.

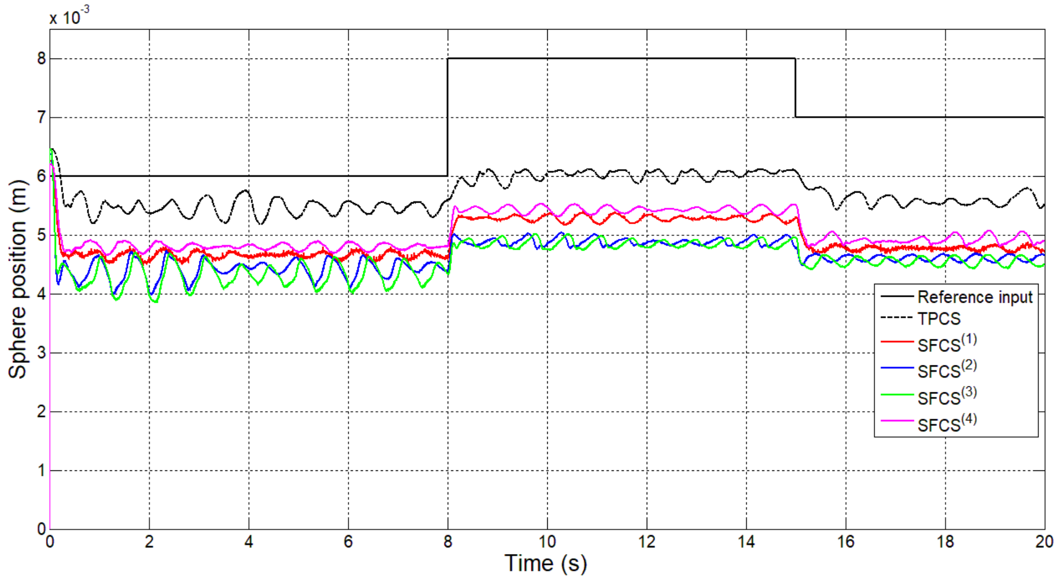

Fig.4.30. Sphere position versus time in case of TPCS and the four SFCSs with staircase reference input in the experimental scenario.

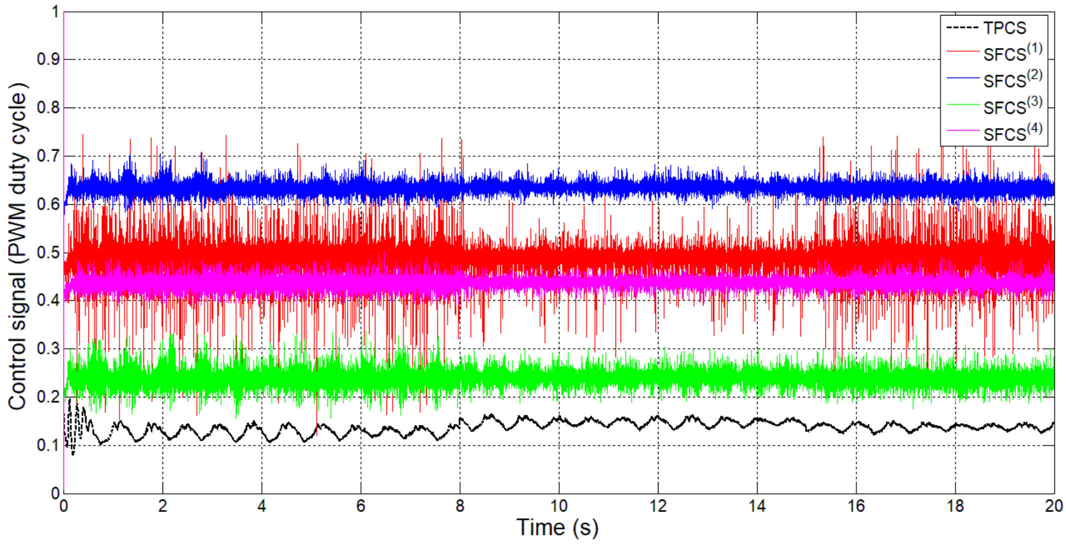

Fig.4.31. Control signal versus time in case of TPCS and the four SFCSs with staircase reference input in the experimental scenario.

The simulation and the experimental results show that all the five CSs designed for psfcMLS fulfill the control system performance specification i., i.e. the stabilization of the CS, and the control system specification ii., i.e. the control signal is constrained. However, they do not ensure zero steady-state control error. Therefore, each of the five CSs is included in a cascade control system structure with a PI controller in the outer control loop.

At first the TPCS, considered as controlled plant, is included in a Single Input Single Output (SISO) cascade control system (PI-TPCS) structure with PI controller in the outer control loop. The state feedback gain matrices given in Equation (2) in Appendix 3 are employed in the computation of the following second-order benchmark type closed-loop t.f.s of the inner control loop, $H_{TPCS}(s)$:

$$H_{TPCS}(s) = k_{TPCS} / [(1 + T_{c1}^{(TPCS)} s)(1 + T_{c2}^{(TPCS)} s)], \tag{4.24}$$

where the numerical values of parameters are obtained by a simple least-squares-based approximation of the inner control loop illustrated in Fig. 4.32 and the following parameters are obtained: $k_{TPCS} = 2$, $T_{c1}^{(TPCS)} = 0.5$ s, $T_{c1}^{(TPCS)} = 0.01$ s .

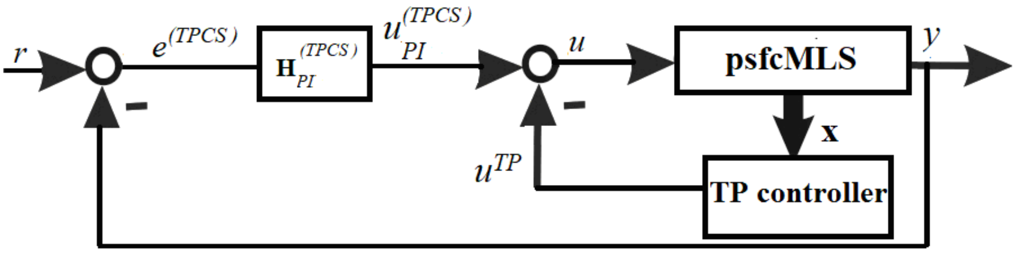

Fig.4.32. Block diagram of the SISO PI-TPCSs designed for psfcMLS.

Due to the fact that the PI controller designed for TPCS in the simulation scenario did not ensure good performance when tested on the real time laboratory equipment, another simple least-squares-based experimental approximation of the inner control loop illustrated in Fig. 4.32 is applied using the experimental data presented in Fig. 4.30, and the following values of the parameters of the second-order benchmark type closed-loop t.f.s of the inner control loop are obtained: $k_{TPCS} = 4.2$, $T_{c1}^{(TPCS)} = 0.7$ s, $T_{c1}^{(TPCS)} = 0.03$ s.

The PI controllers are designed using Kessler's Modulus Optimum method (MO-m), with the general t.f.s:

$$H_{PI}^{(TPCS)}(s) = k_r^{(TPCS)}(1 + sT_r^{(TPCS)})/(sT_r^{(TPCS)}), \tag{4.25}$$

where the tuning parameters were computed as [Kes55]:

$$\begin{aligned} &k_r^{(TPCS)} = 1/\left(2k_{TPCS}T_\Sigma^{(TPCS)}\right), \\ &T_r^{(TPCS)} = T_{c1}^{(TPCS)},\ T_\Sigma^{(TPCS)} = T_{c2}^{(TPCS)}. \end{aligned} \tag{4.26}$$

The numerical values of the parameters are $k_r^{(TPCS)} = 25$, $T_r^{(TPCS)} = 0.5$ s in the simulation scenario and $k_r^{(TPCS)} = 3.96$ and $T_r^{(TPCS)} = 0.7$ s in the experimental scenario.

The control signals applied to psfcMLS are computed by combining the output of the TP-based controller, u_{TP}, and the output of the PI controller, $u_{PI}^{(TPCS)}$.

Next, the four SFCSs designed above, as controlled plants, are also included in four Single Input Single Output (SISO) cascade control system (PI-SFCS) structures with PI controllers in the outer control loop. The equivalent state feedback gain matrices given in Equation (2) in Appendix 4 are employed in the computation of the following second-order benchmark type closed-loop t.f.s of the inner control loop, $H_{SFCS}^{(j)}(s)$:

$$H_{SFCS}^{(j)}(s) = k_{SFCS}^{(j)} /[(1 + T_{c1}^{(j)}s)(1 + T_{c2}^{(j)}s)], \tag{4.27}$$

where the numerical values of the parameters are given in Table 4.3.1 in the simulation scenario. These parameters are obtained by a simple least-squares-based experimental approximation of the inner control loop illustrated in Fig. 4.33.

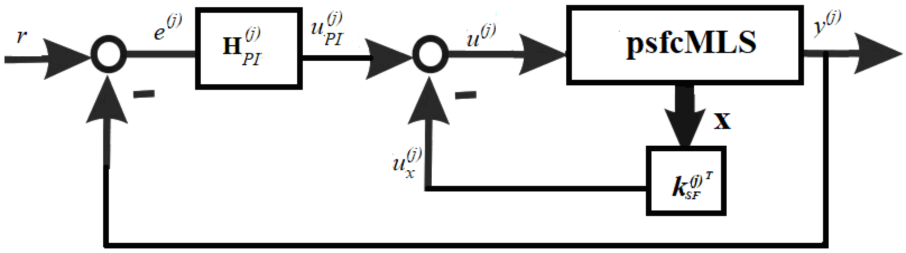

Fig.4.33. Block diagram of the SISO PI-SFCSs designed for psfcMLS.

Table 4.3.1.
Values of parameters of the second order t.f.s. computed for SFCSs in the simulation scenario.

SFCS$^{(j)}$	$k_{SFCS}^{(j)}$	$T_{c1}^{(j)}$ (s)	$T_{c2}^{(j)}$ (s)
SFCS$^{(1)}$	0.55	0.60	0.030
SFCS$^{(2)}$	0.41	0.57	0.035
SFCS$^{(3)}$	2.35	0.75	0.028
SFCS$^{(4)}$	2.50	0.65	0.040

Due to the fact that the PI controllers designed for SFCSs in the simulation scenario did not ensure good performance when tested on the real time laboratory equipment, another simple least-squares-based experimental approximation of the inner control loop illustrated in Fig. 4.33 is applied using the experimental data presented in Fig. 4.30, and the values of the parameters of of the second-order benchmark type closed-loop t.f.s of the inner control loop are given in Table 4.3.2.

Table 4.3.2.
Values of parameters of the second order t.f.s. computed for SFCSs in the experimental scenario.

SFCS$^{(j)}$	$k_{SFCS}^{(j)}$	$T_{c1}^{(j)}$ (s)	$T_{c2}^{(j)}$ (s)
SFCS$^{(1)}$	1.55	0.8	0.020
SFCS$^{(2)}$	2.41	0.54	0.026
SFCS$^{(3)}$	0.85	0.65	0.040
SFCS$^{(4)}$	1.50	0.76	0.034

The PI controllers are also designed using the MO-m, with the general t.f.:

$$H_{PI}^{(j)}(s) = k_r^{(j)}(1 + sT_r^{(j)})/(sT_r^{(j)}), \tag{4.28}$$

where the tuning parameters were computed as [Kes55]:

$$\begin{aligned} &k_r^{(j)} = 1/\left(2k_{SFCS}T_\Sigma^{(j)}\right), \\ &T_r^{(j)} = T_{c1}^{(j)},\, T_\Sigma^{(j)} = T_{c2}^{(j)}. \end{aligned} \tag{4.29}$$

The numerical values of the parameters are given in Table 4.3.3 in the simulation scenario and in Table 4.3.4 in the experimental scenario.

The control signals applied to psfcMLS are computed by combining the output variable of the state feedback controller, $u^{(j)}$, and the output variables of the PI controllers, $u_{PI}^{(j)}$.

Table 4.3.3.
Values of parameters of the PI controllers designed for psfcMLS in the simulation scenario.

PI-SFCS$^{(j)}$	$k_r^{(j)}$	$T_r^{(j)}$ (s)
PI-SFCS $^{(1)}$	30.3	0.6
PI-SFCS $^{(2)}$	34.84	0.57
PI-SFCS $^{(3)}$	7.59	0.75
PI-SFCS $^{(4)}$	5	0.65

Table 4.3.4.
Values of parameters of the PI controllers designed for psfcMLS in the experimental scenario.

PI-SFCS $^{(j)}$	$k_r^{(j)}$	$T_r^{(j)}$ (s)
PI-SFCS $^{(1)}$	16.12	0.8
PI-SFCS $^{(2)}$	7.97	0.54
PI-SFCS $^{(3)}$	14.70	0.65
PI-SFCS $^{(4)}$	9.80	0.76

The five control structures, namely PI-TPCS and the four PI-SFCSs, were tested in the same two testing scenario used for TPCS and the four SFCSs, i.e. simulation and experiment. Each PI controller is tested on its corresponding control structure with the t.f.s. given in (4.24) and (4.27) as resulting from the block diagrams in Figs. 4.32 and 4.33. The initial state vector matching the simulations is $\mathbf{x}_0 = [0 \quad 0 \quad 0]^T$. The responses of the controlled outputs and the control signals of the control structures are plotted in Fig. 4.34 and Fig. 4.35 in the simulation scenario and in Fig. 4.36 and Fig. 4.37 in the experimental scenario.

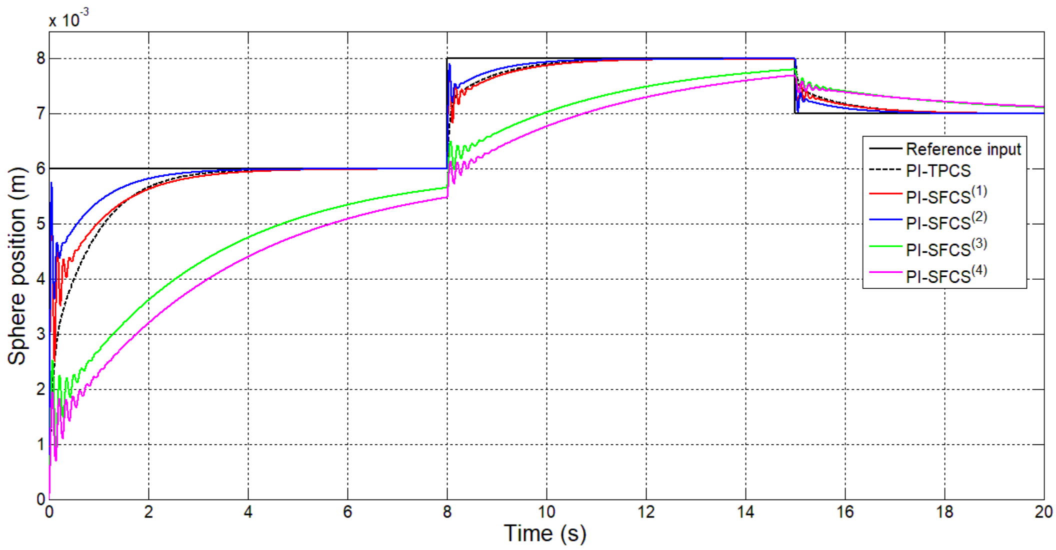

Fig.4.34. Sphere position versus time in case of PI-TPCS and the PI-SFCSs designed for the sphere position control of psfcMLS in the simulation scenario.

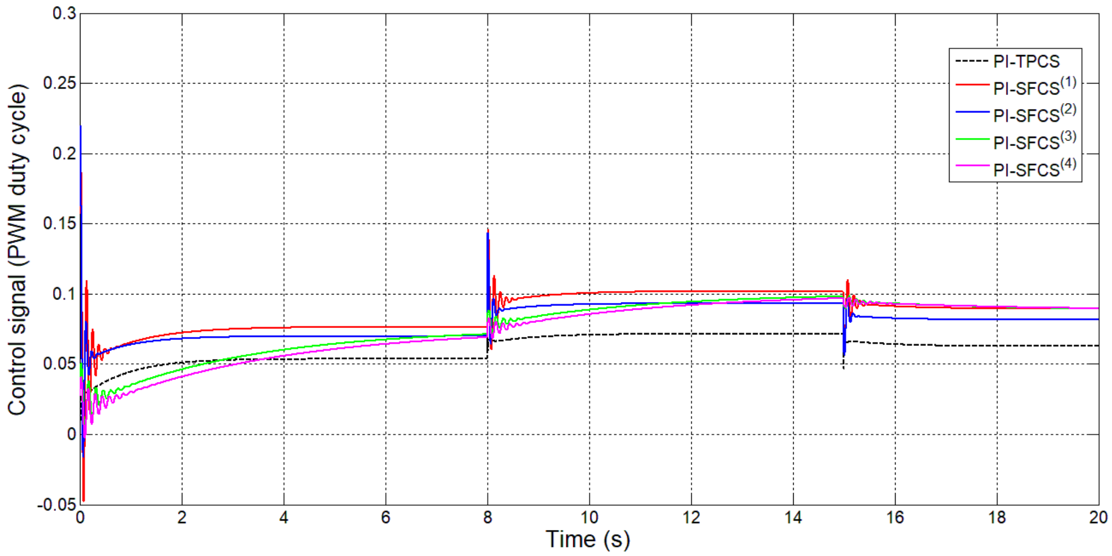

Fig.4.35. Control signal versus time in case of PI-TPCS and the PI-SFCSs designed for the sphere position control of psfcMLS in the simulation scenario.

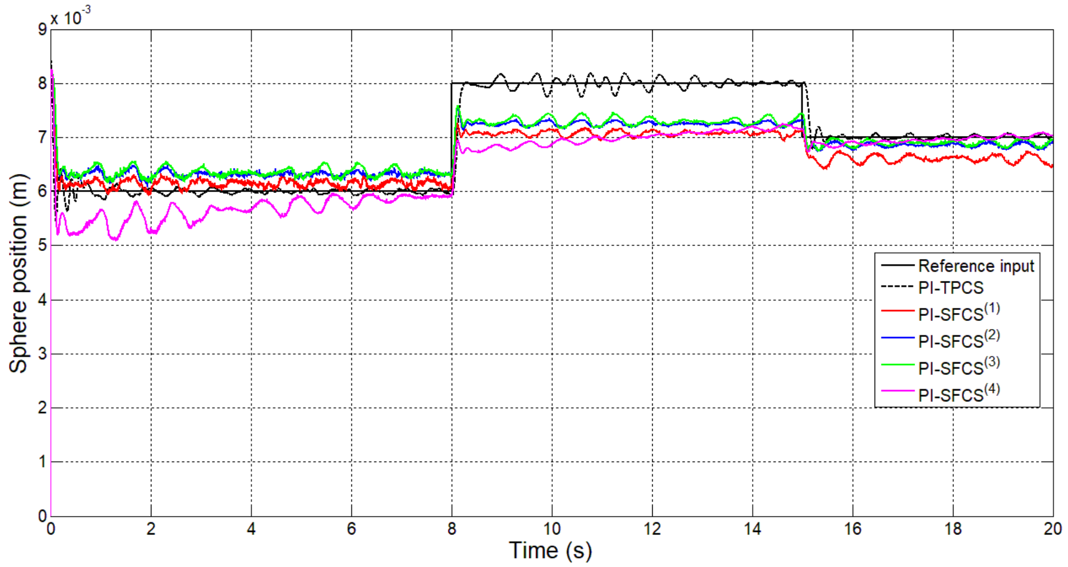

Fig.4.36. Sphere position versus time in case of PI-TPCS and the PI-SFCSs designed for the sphere position control of psfcMLS in the experimental scenario.

The simulation and the experimental results show that all the CSs designed for psfcMLS fulfill both the control system performance specifications i. and ii., i.e. the stabilization of the CS and the constraint applied on the control signal and they also ensure zero steady-state control error.

In order to highlight the performance of the ten derived control structures for psfcMLS, four performance indices, namely the Mean Square Error (MSE), the Mean Square Control Effort (MSU), the settling time and the overshoot are computed.

The MSEs are computed as using (4.16), where e_i^{ψ} represents the control error, which in case of psfcMLS is defined as

$$e^{\psi} = r - y^{\psi}. \tag{4.30}$$

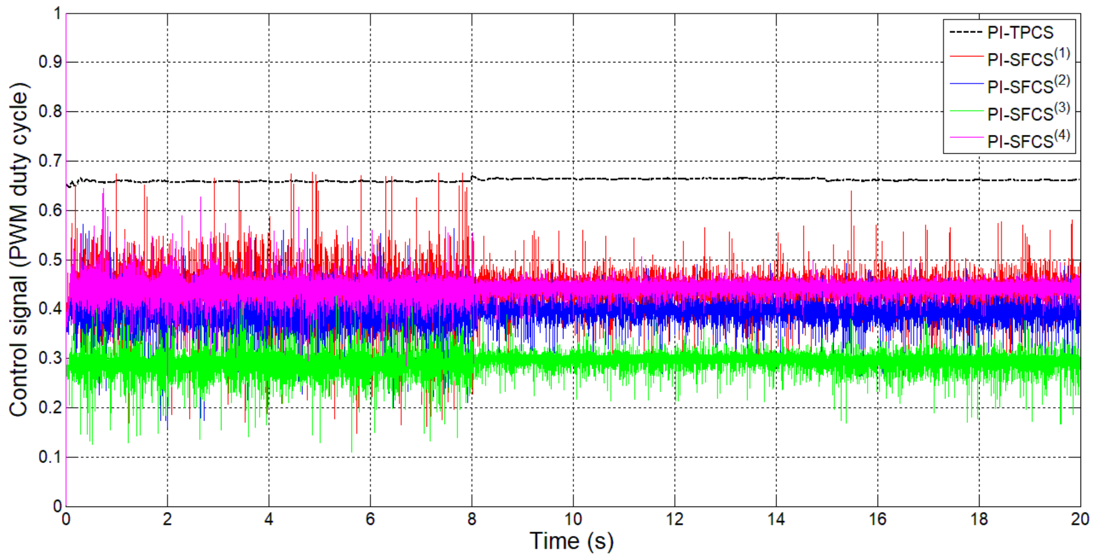

Fig.4.37. Control signal versus time in case of PI-TPCS and the PI-SFCSs designed for the sphere position control of psfcMLS in the experimental scenario.

The MSUs are computed using (4.18) where u^{ψ} represents the control signal applied in case of the control structures designed for psfcMLS.

The superscript $\psi = TPCS$ indicates the TP-based control structure, $\psi = SFCS^{(j)}$ indicates the four state feedback control structures, $\psi = PI - TPCS$ indicates the PI and TP-based control structure, $\psi = PI - SFCS^{(j)}$ indicates the PI and state feedback control structures, y^{ψ} is the first output of the psfcMLS system, i.e. the sphere position, r is the reference input, $M = 80001$ is the number of samples and the sampling period $T_s = 0.00025$ s.

The values of the four performance indices are given in Table 4.3.5 in the simulation scenario and in Table 4.3.6 in the experimental scenario.

Table 4.3.5.
Values of control system performance indices for psfcMLS
in the simulation scenario.

Control structures	**Performance indices**							
	MSE (m^2)	**MSU (%^{2})**	**Settling time (s)**			**Overshoot (%)**		
			r_1	r_2	r_3	r_1	r_2	r_3
TPCS	$2.62 \cdot 10^{-5}$	$3.96 \cdot 10^{-4}$	2	2	2	0	0	0
SFCS$^{(1)}$	$4.48 \cdot 10^{-5}$	$1.57 \cdot 10^{-5}$	1	1	1	0	0	0
SFCS$^{(2)}$	$4.35 \cdot 10^{-5}$	$2.20 \cdot 10^{-5}$	1	1	1	0	0	0
SFCS$^{(3)}$	$4.50 \cdot 10^{-5}$	$1.37 \cdot 10^{-5}$	1	1	1	0	0	0
SFCS$^{(4)}$	$4.47 \cdot 10^{-5}$	$1.55 \cdot 10^{-5}$	1	1	1	0	0	0
PI-TPCS	$3.84 \cdot 10^{-7}$	$3.8 \cdot 10^{-3}$	4	3	3	0	0	0
PI-SFCS$^{(1)}$	$2.28 \cdot 10^{-7}$	$7.8 \cdot 10^{-3}$	4	3	4	0	0	0
PI-SFCS$^{(2)}$	$1.28 \cdot 10^{-7}$	$6.6 \cdot 10^{-3}$	4	3	4	0	0	0
PI-SFCS$^{(3)}$	$1.90 \cdot 10^{-6}$	$6.4 \cdot 10^{-3}$	8	7	4	0	0	0
PI-SFCS$^{(4)}$	$2.57 \cdot 10^{-6}$	$6 \cdot 10^{-3}$	8	7	4	0	0	0

Table 4.3.6.
Values of control system performance indices for psfcMLS
in the experimental scenario.

Control structures	Performance indices							
	MSE (m^2)	MSU ($\%^2$)	Settling time (s)			Overshoot (%)		
			r_1	r_2	r_3	r_1	r_2	r_3
TPCS	$1.99 \cdot 10^{-6}$	$1.91 \cdot 10^{-4}$	2	2	2	0	0	0
SFCS$^{(1)}$	$4.56 \cdot 10^{-6}$	$2.4 \cdot 10^{-1}$	2	2	2	0	0	0
SFCS$^{(2)}$	$5.85 \cdot 10^{-6}$	$4.03 \cdot 10^{-1}$	2	2	2	0	0	0
SFCS$^{(3)}$	$6.13 \cdot 10^{-6}$	$5.86 \cdot 10^{-2}$	2	2	2	0	0	0
SFCS$^{(4)}$	$3.98 \cdot 10^{-6}$	$1.92 \cdot 10^{-1}$	2	2	2	0	0	0
PI-TPCS	$4.68 \cdot 10^{-8}$	$4.3 \cdot 10^{-1}$	2	2	2	20	2	2
PI-SFCS$^{(1)}$	$4.90 \cdot 10^{-6}$	$5.0 \cdot 10^{-3}$	2	2	2	5	0	0
PI-SFCS$^{(2)}$	$3.12 \cdot 10^{-7}$	$1.56 \cdot 10^{-1}$	2	2	2	10	0	5
PI-SFCS$^{(3)}$	$2.60 \cdot 10^{-7}$	$8.69 \cdot 10^{-2}$	2	2	2	5	0	2
PI-SFCS$^{(4)}$	$2.60 \cdot 10^{-7}$	$1.97 \cdot 10^{-1}$	6	2	2	0	0	0

In the simulation scenario, the best performance concerning the MSE is achieved by the second PI-SFCS while in the experimental scenario the best performance in terms of MSE is achived by the PI-TPCS. The best performance in terms of MSU is obtained by the first SFCS in the simulation scenario and by the TPCS in the experimental scenario. The best settling time is achived by all the four SFCSs in the simulation scenario and the settling time was similar for all CSs in the experimental scenario. The overshoot was present only in case of the PI-TPCS and of the first three SFCSs in the experimental scenario. The first five CSs, namely the TPCS and the SFCSs do not ensure zero steady-state control error in both testing scenarios. Therefore, the implementation of the cascade control system structures is justified. Other numbers of parameters of the TP model derived for psfcMLS would lead to other values of the LTI feedback gains which would lead to other values of the performance indices given in Table 4.3.5 and Table 4.3.6.

4.4. The TP-based Model Transformation used for position control of Pendulum Cart System

Starting with the TP model derived for PCS given in Equation (3.53) in Sub-chapter 3.4 and following the control design steps given in Sub-chapter 4.1, the PDC technique is applied as follows in order to design a TP-based controller for the cart position control of PCS.

Since, as shown in Sub-chapter 3.1, the parameter vector consists of one parameter, that means $M_2 = 1$ in the design approach, all subscripts $m1, m2$ of the matrices in the design approach will be replaced in this sub-chapter with $m1$. This is justified because $m2 = 1$, so it does not make sense anymore to use the subscript $m2$ as follows.

The two control system performance specifications presented in the previous Sub-chapter are considered. The control system performance specification i., which consists in guaranteeing the asymptotic stabilization of the control system, is solved using the PDC design framework. Therefore for each LTI vertex system of the convex TP model one LTI feedback gain is determined. The asymptotic stability of the closed-loop control system is equivalent to the existence of $\mathbf{X} = \mathbf{P}^{-1} > 0$ (where $\mathbf{P}$ is a positive definite matrix) and $\mathbf{M}_{m1}$ that satisfy the LMIs given in (4.1) [Bar13].

The state feedback gain matrices $\mathbf{K}_{m1}$ that correspond to each LTI vertex system are next computed as [Hed21a]:

$$\mathbf{K}_{m1} = \mathbf{M}_{m1}\mathbf{X}^{-1}. \tag{4.31}$$

The objective of the control system performance specification ii. is to constrain the control signal. It is assumed that $\| \mathbf{x}(0) \|_2 \leq \phi$, where $\mathbf{x}(0)$ is unknown, but the upper bound ϕ is known. The constraint $|u| \leq \mu$ is enforced at all time moments if the LMIs given in (4.2) are satisfied [Bar13].

Considering the numerical values $\phi = 0.01 > 0$ and $\mu = 1$, the matrices $\mathbf{X}$ and $\mathbf{M}_{m1}$ are computed by solving the seven LMIs, namely three plus three in (4.1) plus two plus three in (4.2), using the YalmipR2015 solver. The solutions are next substituted in (4.5) leading to the values of the LTI feedback gains which are given in Equation (3) in Appendix 3.

Finally, the resulted TP controller is introduced in the Single Input Multiple Output (SIMO) closed-loop control system structure (TPCS), where $\mathbf{y}^{TP}$ represents the controlled output. The TPCS is illustrated in Fig. 4.38.

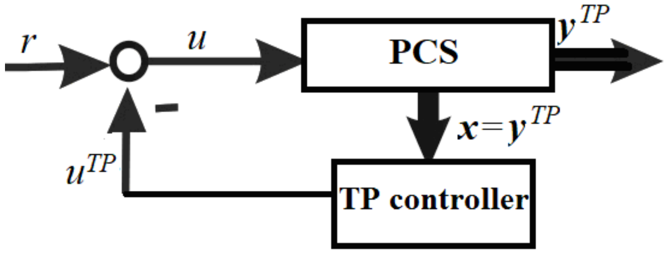

Fig.4.38. Block diagram of the TPCS designed for PCS [Hed21a].

Using the PDC technique, the following state feedback control law results for PCS [Hed21a]:

$$u = r - u_{TP},$$
$$u_{TP} = [\sum_{m1=1}^{5} w_{1,m1}(p_1)\mathbf{K}_{m1}]\mathbf{x}. \quad (4.32)$$

In order to compare the performance of the TP-based controller designed for PCS with similar control structures, four state feedback control structures (SFCSs) are designed considering the same control performace specifications i. and ii. as the ones considered for the TP-CS, i.e. the asymptotic stabilization of the control system and the constraint applied to the control signal.

The general block diagram of the four SFCSs is illustrated in Fig. 4.39, where $j = \overline{1,4}$ denotes the number of linear models, $u^{(j)}$ is the control signal, r is the reference input, $u_x^{(j)}$ is the state feedback controller matrix product output, $y^{(j)}$ is the controlled output.

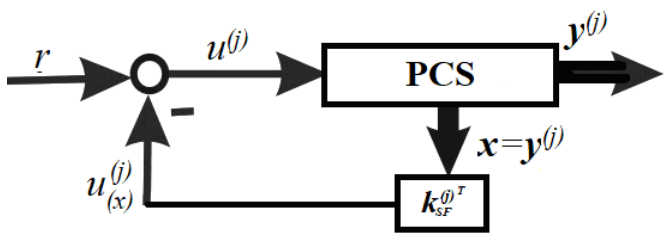

Fig.4.39. General block diagram of the four SFCSs designed for PCS.

The fair comparison of the TP controller and the linear state feedback controller makes use of the same design approach applied in the nonlinear case (i.e. the TP controller) and the four linear cases. In this regard, the computation of the state feedback gain matrices $\mathbf{k}_{SF}^{(j)T}$ is similar with the one of the LTI feedback gains of the TP controller. These matrices result after solving the following two LMIs (for each *j*) that correspond to (4.1):

$$-\mathbf{X}^{(j)}\mathbf{A}^{(j)} - \mathbf{A}^{(j)}\mathbf{X}^{(j)} + \mathbf{M}^{(j)}\mathbf{X}^{(j)T} + \mathbf{b}^{(j)}\mathbf{M}^{(j)} > 0,$$
$$-\mathbf{X}^{(j)}\mathbf{A}^{(j)} - \mathbf{A}^{(j)}\mathbf{X}^{(j)} - \mathbf{X}^{(j)}\mathbf{A}^{(j)T} - \mathbf{A}^{(j)}\mathbf{X}^{(j)} + \mathbf{M}^{(j)T}\mathbf{b}^{(j)T} \quad (4.33)$$
$$+\mathbf{b}^{(j)}\mathbf{M}^{(j)} + \mathbf{M}^{(j)T}\mathbf{b}^{(j)T} + \mathbf{b}^{(j)}\mathbf{M}^{(j)} \geq 0$$

in order to ensure the asymptotic stabilization of the control system (i.e. the performance specification i.), and the following two LMIs (for each *j*) that correspond to (4.2):

$$\phi^2\mathbf{I} \leq \mathbf{X}^{(j)},$$
$$\begin{pmatrix} \mathbf{X}^{(j)} & \mathbf{M}^{(j)T} \\ \mathbf{M}^{(j)T} & \mu^2\mathbf{I} \end{pmatrix} \geq 0 \quad (4.34)$$

in order to fulfill the constraint imposed to the modulus of the control signal in terms of the control system performance specification ii., where $\mathbf{A}^{(j)}$ and $\mathbf{b}^{(j)}$ result in accordance with Sub-chapter 3.3, and ϕ and μ are the same parameters as the ones chosen in the design of the TP controller.

Finally the state feedback gain matrices are computed for each of the four linear models of PCS derived in Sub-chapter 3.3, as:

$$\mathbf{k}_{SF}^{(j)T} = \mathbf{M}^{(j)}\mathbf{X}^{(j)-1}. \tag{4.35}$$

Considering the same numerical values as in case of the TPCS, i.e. $\phi = 0.01$ and $\mu = 1$, which take into consideration the real operating conditions of the world laboratory equipment, the matrices $\mathbf{X}^{(j)}$ and $\mathbf{M}^{(j)}$ are computed, after solving four LMIs for each linear model of PCS, namely one in (4.33) plus one plus one plus one in (4.34), using the YalmipR2015 solver. The solutions are substituted in (4.35) leading to the values of the state feedback gains in Equation (3) in Appendix 4.

In order to highlight the performance of the five CSs designed for PCS, namely the first one represented by the TPCS, the second one represented by the first SFCS, the third one represented by the second SFCS, the fourth one represented by the third SFCS and the fifth one represented by the fourth SFCS, two testing scenarios (a simulation one plus an experimental one) were considered by employing a staircase change for the reference input ($r_1 = 0.2$ m, $r_2 = 0.4$ m, $r_3 = 0.1$ m) on the time horizon of 20 s. In case of the simulation scenario each controller is tested on its corresponding derived model presented in Sub-chapter 3.4 and in case of the experimental scenario each controller is tested on the PCS laboratory equipment. The initial state vector matching the simulations and experiments is $\mathbf{x}_0 = [0 \quad \pi \quad 0 \quad 0]^T$. The responses of the controlled outputs and the control signals (or control inputs) of the control structures are plotted in Fig. 4.40 and Fig. 4.41 in the simulation scenario and in Fig. 4.42 and Fig. 4.43 in the experimental scenario.

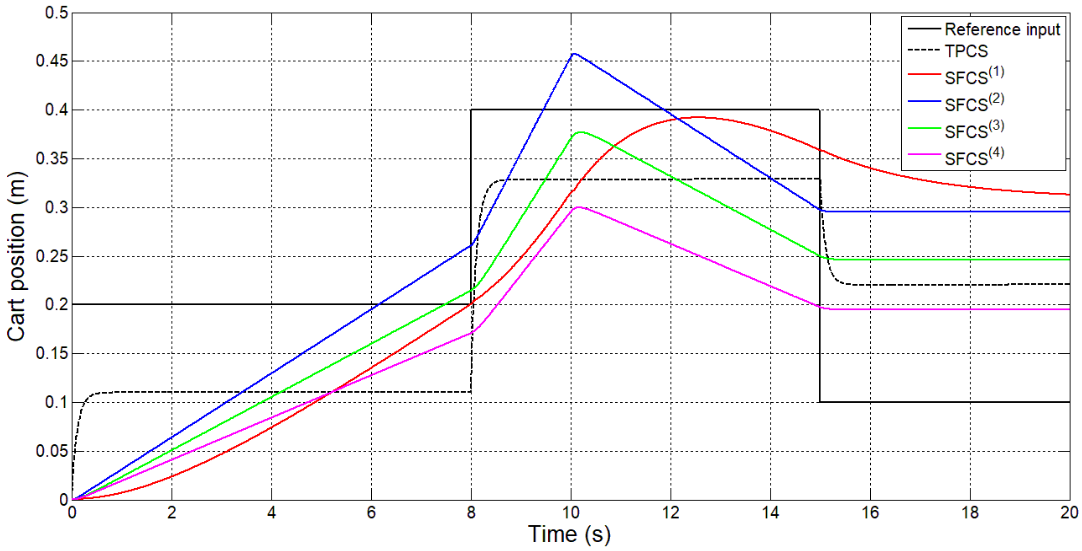

Fig.4.40. Cart position versus time in case of TPCS and the four SFCSs with staircase reference input in the simulation scenario.

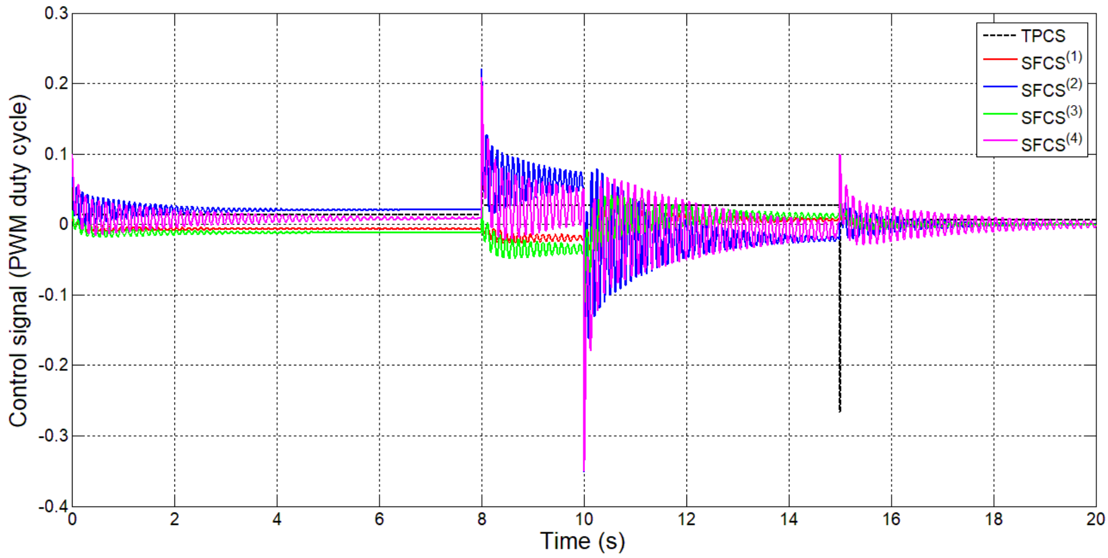

Fig.4.41. Control signal versus time in case of TPCS and the four SFCSs with staircase reference input in the simulation scenario.

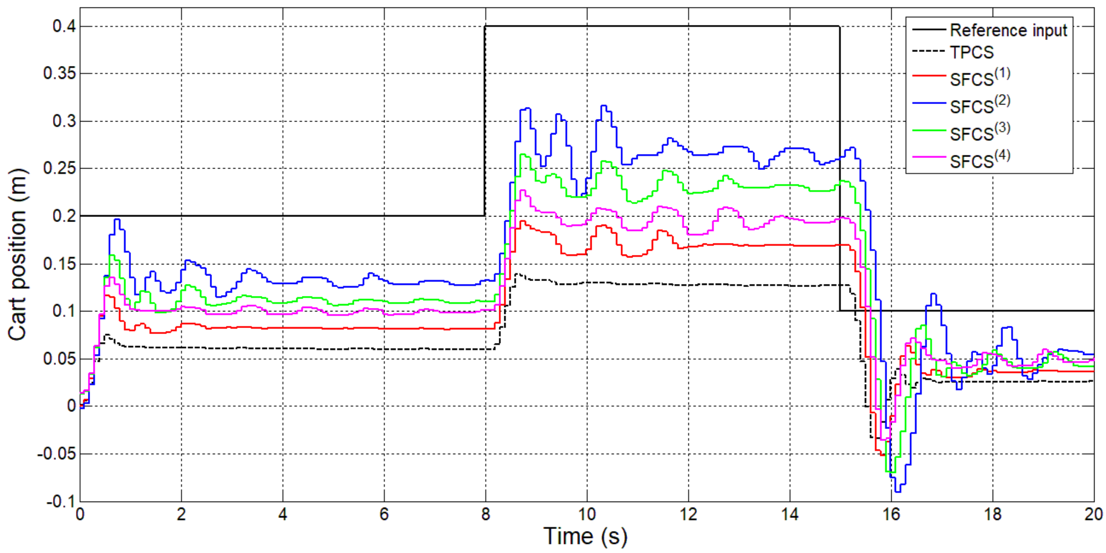

Fig.4.42. Cart position versus time in case of TPCS and the four SFCSs with staircase reference input in the experimental scenario.

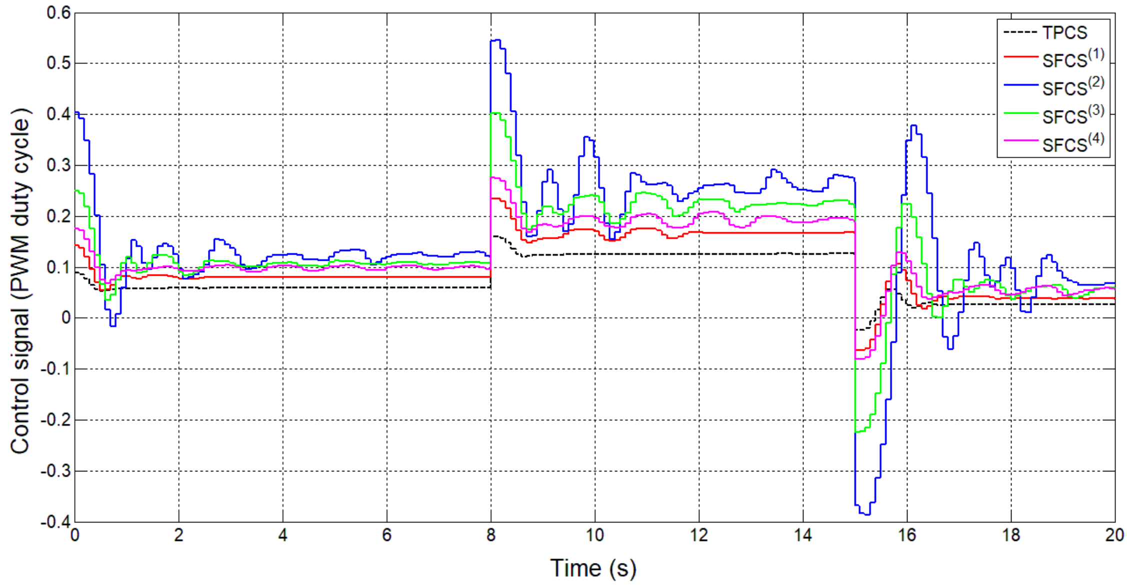

Fig.4.43. Control signal versus time in case of TPCS and the four SFCSs with staircase reference input in the simulation scenario.

The simulation and the experimental results show that all the five CSs designed for PCS fulfill the control system performance specification i., i.e. the stabilization of the CS, and the control system specification ii., i.e. the control signal is constrained. However, they do not ensure zero steady-state control error. Therefore, each of the five CSs is included in a cascade control system structure with a PI controller in the outer control loop.

At first the TPCS, considered as controlled plant, is included in a Single Input Single Output (SISO) cascade control system (PI-TPCS) structure with PI controller in the outer control loop. The state feedback gain matrices given in Equation (3) in Appendix 3 are employed in the computation of the following second-order benchmark type closed-loop t.f.s of the inner control loop, $H_{TPCS}(s)$:

$$H_{TPCS}(s) = k_{TPCS} / [(1 + T_{c1}^{(TPCS)} s)(1 + T_{c2}^{(TPCS)} s)], \quad (4.36)$$

where the numerical values of parameters are obtained by a simple least-squares-based approximation of the inner control loop illustrated in Fig. 4.44. The parameters $k_{TPCS} = 0.001$, $T_{c1}^{(TPCS)} = 1.5$ s and $T_{c1}^{(TPCS)} = 0.004$ s are obtained.

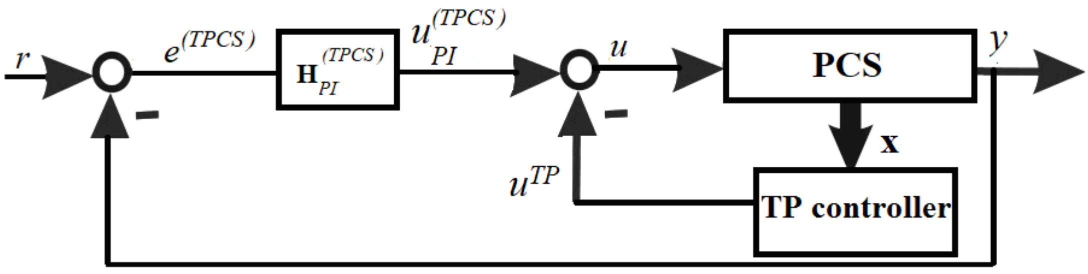

Fig.4.44. Block diagram of the SISO PI-TPCSs designed for PCS.

The PI controllers are designed using Kessler's Modulus Optimum method (MO-m), with the general t.f.s:

$$H_{PI}^{(TPCS)}(s) = k_r^{(TPCS)} (1 + sT_r^{(TPCS)}) / (sT_r^{(TPCS)}), \quad (4.37)$$

where the tuning parameters were computed as [Kes55]:

$$k_r^{(TPCS)} = 1/\left(2k_{TPCS}T_\Sigma^{(TPCS)}\right),$$
$$T_r^{(TPCS)} = T_{c1}^{(TPCS)},\ T_\Sigma^{(TPCS)} = T_{c2}^{(TPCS)}. \quad (4.38)$$

The numerical values of the parameters are $k_r^{(TPCS)} = 125$, $T_r^{(TPCS)} = 1.5$ s.

The control signals applied to PCS are computed by combining the output of the TP-based controller, u_{TP}, and the output of the PI controller, $u_{PI}^{(TPCS)}$.

Next, the four SFCSs designed above, as controlled plants, are also included in four SISO cascade control system (PI-SFCS) structures with PI controllers in the outer control loop. The equivalent state feedback gain matrices given in Equation (3) in Appendix 4 are employed in the computation of the following second-order benchmark type closed-loop t.f.s of the inner control loop, $H_{SFCS}^{(j)}(s)$:

$$k_r^{(TPCS)} = 1/\left(2k_{TPCS}T_\Sigma^{(TPCS)}\right),$$
$$T_r^{(TPCS)} = T_{c1}^{(TPCS)},\ T_\Sigma^{(TPCS)} = T_{c2}^{(TPCS)}, \quad (4.39)$$

where the numerical values of the parameters are given in Table 4.4.1. These parameters are obtained by a simple least-squares-based experimental approximation of the inner control loop illustrated in Fig. 4.45.

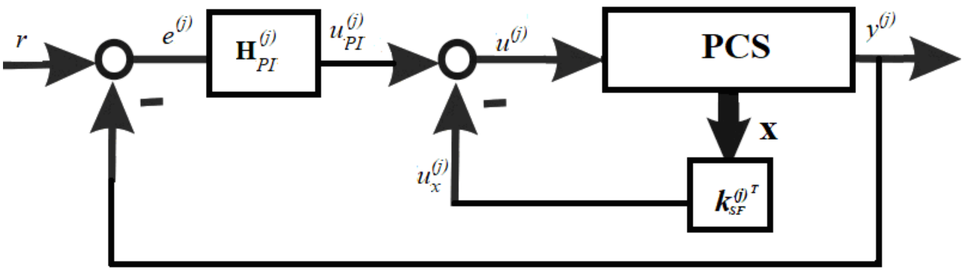

Fig.4.45. Block diagram of the SISO PI-SFCSs designed for PCS.

Table 4.4.1.

Values of parameters of the second order t.f.s. computed for SFCSs.

SFCS$^{(j)}$	$k_{SFCS}^{(j)}$	$T_{c1}^{(j)}$ (s)	$T_{c2}^{(j)}$ (s)
SFCS $^{(1)}$	25.7	197	0.025
SFCS $^{(2)}$	25	212	0.25
SFCS $^{(3)}$	70	200	1.5
SFCS $^{(4)}$	21	78	0.25

The PI controllers are also designed using the MO-m, with the general t.f.:

$$H_{PI}^{(j)}(s) = k_r^{(j)}(1 + sT_r^{(j)})/(sT_r^{(j)}), \quad (4.40)$$

where the tuning parameters were computed as [Kes55]:

$$k_r^{(j)} = 1/\left(2k_{SFCS}T_\Sigma^{(j)}\right),$$
$$T_r^{(j)} = T_{c1}^{(j)},\ T_\Sigma^{(j)} = T_{c2}^{(j)}. \quad (4.41)$$

The numerical values of the parameters are given in Table 4.4.2.

The control signals applied to PCS are computed by combining the output variable of the state feedback controller, $u^{(j)}$, and the output variables of the PI controllers, $u_{PI}^{(j)}$.

Table 4.4.2.
Values of parameters of the PI controllers designed for PCS.

PI-SFCS$^{(j)}$	$k_r^{(j)}$	$T_r^{(j)}$ (s)
PI-SFCS $^{(1)}$	0.77	197
PI-SFCS $^{(2)}$	0.08	212
PI-SFCS $^{(3)}$	0.004	200
PI-SFCS $^{(4)}$	0.095	78

The five control structures, namely PI-TPCS and the four PI-SFCSs, were tested in the same two testing scenario used for TPCS and the four SFCSs, i.e. simulation and experiment. Each PI controller is tested on its corresponding control structure with the t.f.s. given in (4.36) and (4.39) as resulting from the block diagrams in Figs. 4.42 and 4.43. The same values of the parameters of the PI controllers were used both in simulations and experiments. The initial state vector matching the simulations and experiments is $\mathbf{x}_0 = [0 \quad \pi \quad 0 \quad 0]^T$. The responses of the controlled outputs and the control signals of the control structures are plotted in Fig.4.46 and Fig.4.47 in the simulation scenario and in Fig. 4.48 and Fig. 4.49 in the experimental scenario.

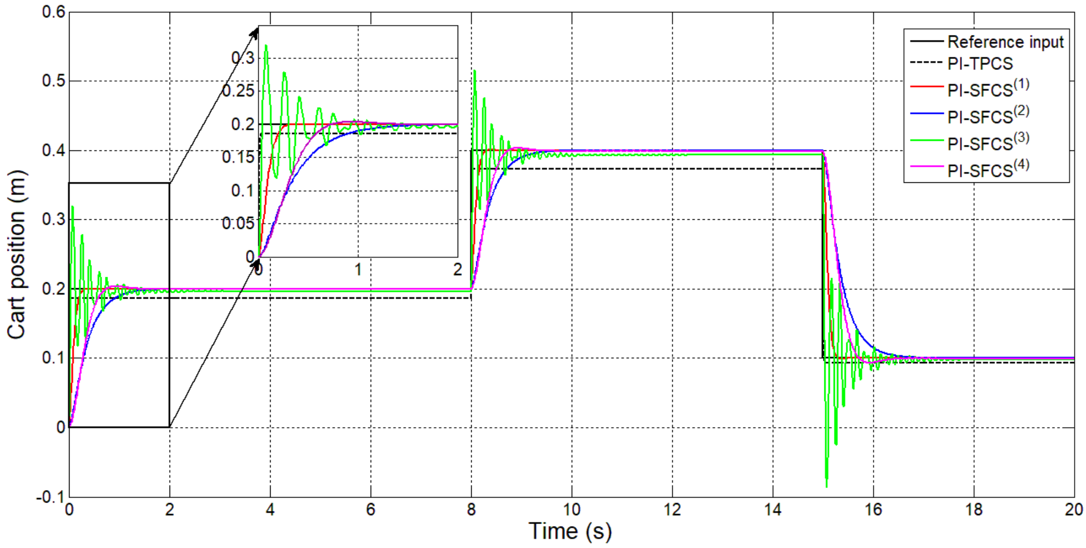

Fig.4.46. Cart position versus time in case of PI-TPCS and the PI-SFCSs designed for the cart position control of PCS in the simulation scenario.

BUPT

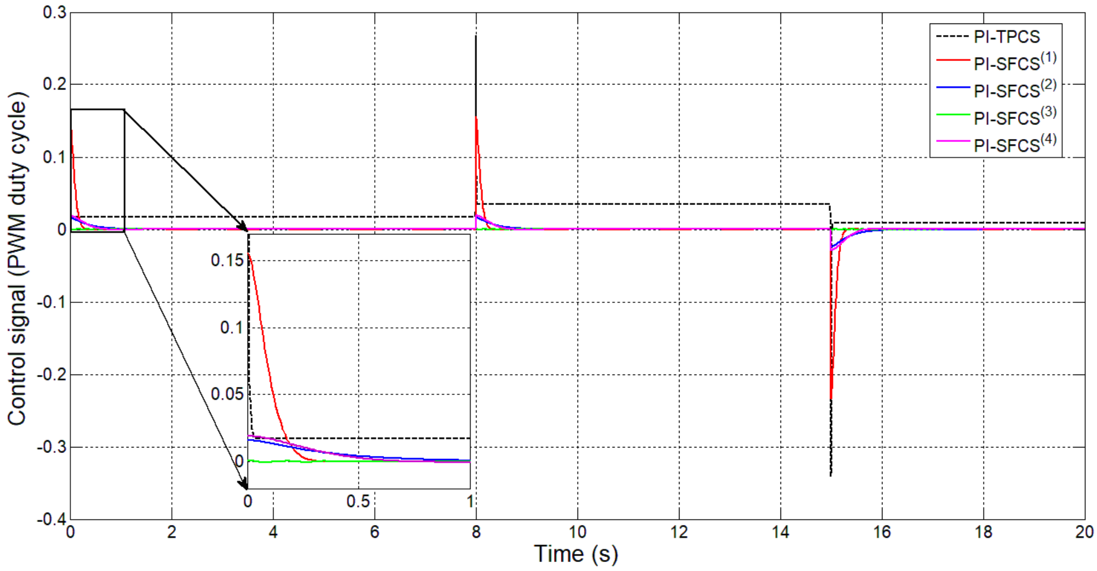

Fig.4.47. Control signal versus time in case of PI-TPCS and the PI-SFCSs designed the cart position control of PCS in the simulation scenario.

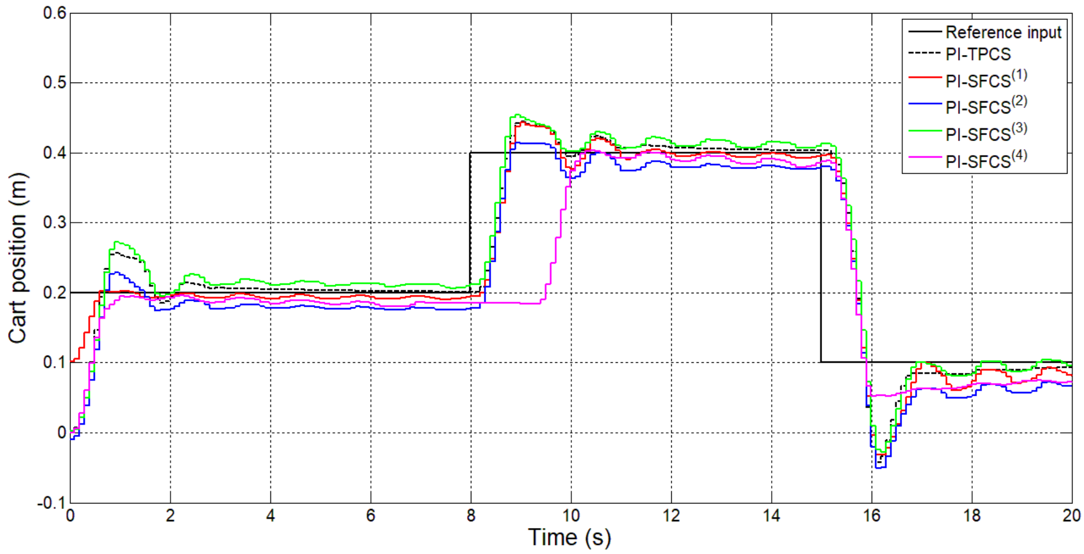

Fig.4.48. Cart position versus time in case of PI-TPCS and the PI-SFCSs designed for the cart position control of PCS in the experimental scenario.

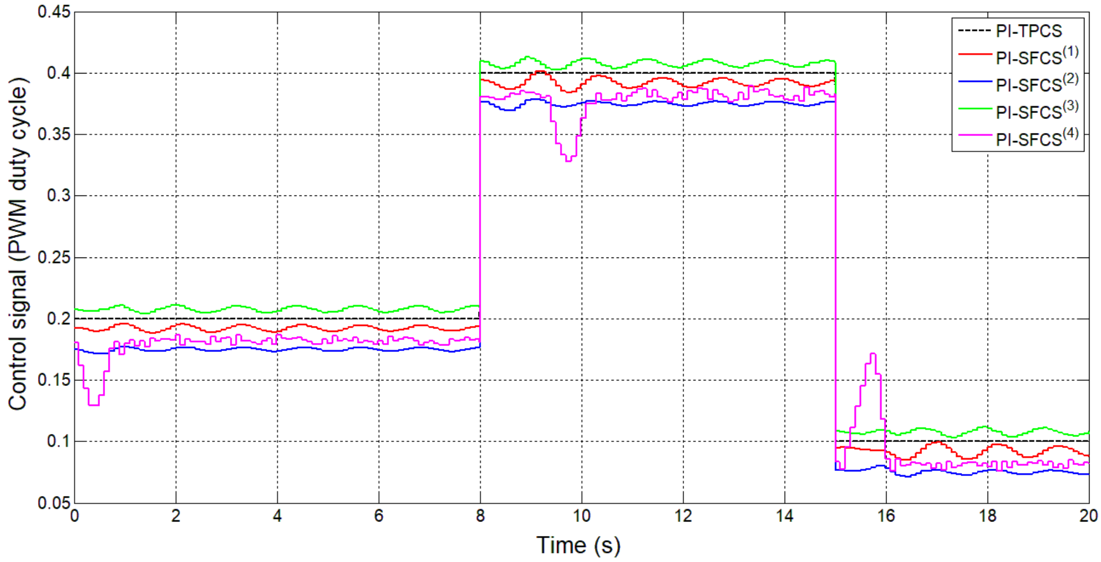

Fig.4.49. Control signal versus time in case of PI-TPCS and the PI-SFCSs designed the cart position control of PCS in the experimental scenario.

The simulation and the experimental results show that all the CSs designed for PCS fulfill both the control system performance specifications i. and ii., i.e. the stabilization of the CS and the constraint applied on the control signal and they also ensure zero steady-state control error.

In order to highlight the performance of the ten derived control structures for psfcMLS, four performance indices, namely the Mean Square Error (MSE), the Mean Square Control Effort (MSU), the settling time and the overshoot are computed.

The MSEs are computed as using (4.16), where e_i^{ψ} represents the control error, which in case of PCS is defined as

$$e^{\psi} = r - y^{\psi}. \qquad (4.42)$$

The MSUs are computed using (4.18) where u^{ψ} represents the control signal applied in case of the control structures designed for PCS.

The superscript $\psi = TPCS$ indicates the TP-based control structure, $\psi = SFCS^{(j)}$ indicates the four state feedback control structures, $\psi = PI - TPCS$ indicates the PI and TP-based control structure, $\psi = PI - SFCS^{(j)}$ indicates the PI and state feedback control structures, y^{ψ} is the first output of the PCS system, i.e. the cart position, r is the reference input, $M = 2001$ is the number of samples and the sampling period $T_s = 0.01$ s.

The values of the four performance indices are given in Table 4.4.3 in the simulation scenario and in Table 4.4.4 in the experimental scenario.

In the simulation scenario, the best performance concerning the MSE is achieved by the PI-TPCS while in the experimental scenario the best performance in terms of MSE is achived by the first PI-SFCS. The best performance in terms of MSU is obtained by the third PI-SFCS in the simulation scenario and by the TPCS in the experimental scenario. The best settling time is achived by the PI-TPCS in both the simulation scenario and the experimental one. The overshoot was present only in case of the third and the fourth PI-SFCS in the simulaton scenario and in case of the PI-TPCS and the four PI-SFCS in the experimental scenario. The first five CSs, namely the TPCS and the SFCSs do not ensure zero steady-state control error in both testing scenarios, i.e. simulation and experiment. Therefore, the implementation of the cascade control system structures is justified. Other numbers of parameters of the TP model derived for PCS would lead to other values of the LTI feedback gains which would lead to other values of the performance indices given in Table 4.4.3 and Table 4.4.4.

Table 4.4.3.
Values of control system performance indices for PCS in the simulation scenario.

Control structures	Performance indices							
	MSE (m^2)	MSU ($\%^2$)	Settling time (s)			Overshoot (%)		
			r_1	r_2	r_3	r_1	r_2	r_3
TPCS	$9.3 \cdot 10^{-3}$	$4.10 \cdot 10^{-4}$	1	1	1	0	0	0
SFCS(1)	$19.3 \cdot 10^{-3}$	$8.18 \cdot 10^{-5}$	-	10	1	0	0	0
SFCS(2)	$15.1 \cdot 10^{-3}$	$12 \cdot 10^{-4}$	-	10	1	0	0	0
SFCS(3)	$14.1 \cdot 10^{-3}$	$2.70 \cdot 10^{-4}$	-	10	1	0	0	0
SFCS(4)	$17.4 \cdot 10^{-3}$	$9.58 \cdot 10^{-4}$	-	10	1	0	0	0
PI-TPCS	$4.32 \cdot 10^{-4}$	$6.75 \cdot 10^{-4}$	0.5	0.5	0.5	0	0	0
PI-SFCS(1)	$5.82 \cdot 10^{-4}$	$3.52 \cdot 10^{-4}$	0.7	0.7	0.7	0	0	0
PI-SFCS(2)	$19 \cdot 10^{-4}$	$1.21 \cdot 10^{-5}$	1.5	1.5	1.5	0	0	0
PI-SFCS(3)	$5.79 \cdot 10^{-4}$	$1.31 \cdot 10^{-8}$	2	2	2	50	50	50
PI-SFCS(4)	$18 \cdot 10^{-4}$	$1.61 \cdot 10^{-5}$	1	1	1	5	5	5

Table 4.4.4.
Values of control system performance indices for PCS in the experimental scenario.

Control structures	Performance indices							
	MSE (m^2)	MSU ($\%^2$)	Settling time (s)			Overshoot (%)		
			r_1	r_2	r_3	r_1	r_2	r_3
TPCS	0.0360	0.0073	2	2	2	0	0	0
SFCS(1)	0.0264	0.0134	3	5	3	0	0	0
SFCS(2)	0.0117	0.0436	6	4	4	0	0	0
SFCS(3)	0.0161	0.0272	4	5	4	0	0	0
SFCS(4)	0.0208	0.0185	2	6	4	0	0	0
PI-TPCS	0.0047	0.0745	2	2	2	25	25	30
PI-SFCS(1)	0.0041	0.0706	2	2	2	0	25	30
PI-SFCS(2)	0.0052	0.0628	2	2	2	10	5	35
PI-SFCS(3)	0.0049	0.0782	2	2	2	25	25	30
PI-SFCS(4)	0.0071	0.0650	1	3	1	0	0	10

4.5. Chapter conclusions

In this chapter, the main steps of the TP-based Model Transformation control algorithm along with the design of TP controllers for three systems, namely Vertical Three Tank System, partial state feedback controlled Magnetic Levitation System and Pendulum Cart System. The TPCSs were compared with state feedback control structures (SFCSs) which were designed aiming the same control design performance as in case of the TPCSs.

In Sub-chapter 4.1, the steps of the TP-based Model Transformation control algorithm were presented in detail.

In Sub-chapter 4.2, the validation through simulation and experiments of the TP controllers designed for Vertical Three Tank System was presented. At first the TP-based control structure (TPCS) was designed. Then the TPCS was compared with four state feedback control structures (SFCSs), which were designed aiming the same control performance as in case of the TPCS, and they were tested in the same scenario. Moreover, in order to improve the control system performance, i.e. to ensure zero steady-state control error, the TPCS and the four SFCS were included into 15 SISO CCSs designed for each of the three tanks. All control structures were tested in the same scenario and four performance indices, namely MSE, MSU, settling time and overshoot were computed and are given in Table 4.2.5 and 4.2.6. The best performance concerning the MSE is achieved by the first PID-SFCS for the first tank in the simulation scenario and by the fourth PID-SFCS for the second tank in the experimental scenario. The best settling time is achived by the third SFCS in case of all three tanks in the simulation scenario and by the four SFCSs for the third tank in the experimental scenario. The best performance in terms of MSU is obtained by the second SFCS in case of all three tanks in the simulation scenario and by the fourth PID-SFCS for the second tank in the experimental scenario. The overshoot is present in case of the PID-TPCS and the second PID-SFCS in the simulation scenario and in case of TPCS and the four SFCSs for the first and second tank and by the PID-TPCS, the seond, the third and the fourth PID-SFCS for the first tank in the experimental scenario. Its smallest value is obtained for the PID-SFCS in case of the first two tanks, by the PID-TPCS in case of the third tank in the simulation scenario and by the TPCS and the four SFCSs for the second tank in the experimental scenario. The first five CSs, namely the TPCS and the SFCSs do not ensure zero steady-state control error. Therefore, the implementation of the cascade control system structures is justified.

In Sub-chapter 4.3, the validation through simulation and experiments of the TP controllers designed for partial state feedback controlled Magnetic Levitation System was presented. At first a TPCS was designed. The TPCS was next compared with four state feedback control structure (SFCS), which were designed aiming the same control performance as in case of the TPCS. In the next step, in order to improve the control performance, i.e. to ensure zero steady state control error, the TPCS and the four SFCS were included into five SISO CCSs with a PI controller in the outer control loop. The ten control structures, namely the TPCS, the four SFCSs, the PI-TPCS and the four PI-TPCS were tested in the same two scenarios (simulation and experiments) and the same performance indices as in case of psfcMLS were computed and are given in Table 4.3.5 and Table 4.3.6. In the simulation scenario the best performance concerning the MSE is achieved by the second PI-SFCS while in the experimental scenario the best performance in terms of MSE is achived by the PI-

TPCS. The best performance in terms of MSU is obtained by the first SFCS in the simulation scenario and by the TPCS in the experimental scenario. The best settling time is achived by all the four SFCSs in the simulation scenario and the settling time was similar for all CSs in the experimental scenario. The overshoot was present only in case of the PI-TPCS and of the first three SFCSs in the experimental scenario. The first five CSs, namely the TPCS and the SFCSs do not ensure zero steady-state control error in both testing scenarios. Therefore, the implementation of the cascade control system structures is again justified.

In Sub-chapter 4.4, the validation through simulations and experiments of the TP controllers designed for Pendulum Cart System in the crane operation mode was presented. At first a TPCS was designed. The TPCS was next compared with four state feedback control structure (SFCS), which were designed aiming the same control performance as in case of the TPCS. In the next step, in order to improve the control performance, i.e. to ensure zero steady state control error, the TPCS and the four SFCS were included into five SISO CCSs with a PI controller in the outer control loop. The ten control structures, namely the TPCS, the four SFCSs, the PI-TPCS and the four PI-TPCS were tested in the same two scenarios (simulation and experiments) and the same performance indices as in case of PCS were computed and are given in Table 4.4.3 and Table 4.4.4. In the simulation scenario, the best performance concerning the MSE is achieved by the PI-TPCS while in the experimental scenario the best performance in terms of MSE is achived by the first PI-SFCS. The best performance in terms of MSU is obtained by the third PI-SFCS in the simulation scenario and by the TPCS in the experimental scenario. The best settling time is achived by the PI-TPCS in both the simulation scenario and the experimental. The overshoot was present only in case of the third and the fourth PI-SFCS in the simulaton scenario and in case of the PI-TPCS and the four PI-SFCS in the experimental scenario. The first five CSs, namely the TPCS and the SFCSs do not ensure zero steady-state control error in both testing scenarios. Therefore, the implementation of the cascade control system structures is once more justified. Other numbers of parameters of the TP model derived for PCS would lead to other values of the LTI feedback gains which would lead to other values of the performance indices given in Table 4.4.3 and Table 4.4.4.

The experimental results have shown that:

- The accuracy and the performance of a TP controller designed for a certain process depend on how good the TP model derived for that process is. The best performance in terms of zero steady state control error was achived by the TP controller designed for PCS.
- The performance of the TP controller can be improved by combining the TP controller with other types of controllers such as PI and PID controllers into cascade control system structures.

The contributions presented in this chapter are:

- The derivation and validation of a TP controller for a Vertical Three Tank system laboratory equipment and a comparative analysis with a state feedback controller designed aiming the same control system performance specifications.
- The derivation and validation of a TP controller for a partial state feedback controlled Magnetic Levitation System and a comparative analysis with a state feedback controller designed aiming the same control system performance specifications.

- The derivation and validation of a TP controller for a Pendulum Cart System laboratory equipment and a comparative analysis with a state feedback controller designed aiming the same control system performance specifications.

These contributions were published in the papers:

1. E.-L. Hedrea, C.-A. Bojan-Dragos, R.-E. Precup and T.-A. Teban, "Tensor product-based model transformation for level control of vertical three tank systems," in Proc. IEEE 21st International Conference on Intelligent Engineering Systems, Larnaca, Cyprus, 2017, pp. 113-118, **indexed in Clarivate Analytics Web of Science, cited in**:

2. L. Kovacs and G. Eigner, "A TP-LPV-LMI based control for tumor growth inhibition," IFAC Papers Online, vol. 51, no. 26, pp. 155-160, 2018, **indexed in Clarivate Analytics Web of Science,**
3. L. Kovacs and G. Eigner, "Tensor product model transformation based parallel distributed control of tumor growth,"Acta Politechnica Hungarica, vol. 15, no. 3, pp. 101-123, 2018, **indexed in Clarivate Analytics Web of Science, impact factor = 1.806 according to Journal Citation Reports (JCR) published by Clarivate Analytics in 2021**.

2. E.-L. Hedrea, R.-E. Precup, C.-A. Bojan-Dragos, C. Hedrea, D. Ples and D. Popovici, "Cascade control solutions for level control of vertical three tank systems," in Proc. IEEE 13th International Symposium on Applied Computational Intelligence and Informatics, Timisoara, Romania, 2019, pp. 353-358, **indexed in Clarivate Analytics Web of Science,**

3. E.-L. Hedrea, C.-A. Bojan-Dragos, R.-E. Precup, R.-C. Roman, E.-M. Petriu and C. Hedrea, "Tensor product-based model transformation for position control of magnetic levitation systems," in Proc. IEEE 26th International Symposium on Industrial Electronics, Edinburgh, Scotland, 2017, pp. 1141-1146, **indexed in Clarivate Analytics Web of Science, cited in:**

1. G.H. Chen and D.X. Yang, "A unified analysis framework of static and dynamic structural reliabilities based on direct probability integral method," Mechanical Systems and Signal Processing, vol. 158, 2021, **indexed in Clarivate Analytics Web of Science, impact factor = 6.823 according to Journal Citation Reports (JCR) published by Clarivate Analytics in 2021,**
2. Y.F. Yang, X.J. Ban, X.L. Huang and C.H. Shan, "A dueling-double-deep Q-network controller for magnetic levitation ball system," in Proc. 39th Chinese Control Conference, Shenyang, China, 2020, pp. 1885-1890, **indexed in Clarivate Analytics Web of Science,**
7. L. Kovacs, G. Eigner, M. Siket and L. Barkai, "Control of diabetes mellitus by advanced robust control solution," IEEE Access, vol. 7, pp. 125609-125622, 2019, **indexed in Clarivate Analytics Web of Science, impact factor = 3.367 according to Journal Citation Reports (JCR) published by Clarivate Analytics in 2021,**
8. L. Kovacs and G. Eigner, "Tensor product model transformation based parallel distributed control of tumor growth,"Acta Politechnica Hungarica, vol. 15, no. 3, pp. 101-123, 2018, **indexed in Clarivate Analytics Web of Science, impact factor = 1.806 according to Journal Citation Reports (JCR) published by Clarivate Analytics in 2021**.

4. **E.-L. Hedrea**, C.-A. Bojan-Dragos, R.-E. Precup and E.-.M. Petriu, "Comparative study of control structures for maglev systems," in Proc. IEEE 18th International Power Electronics and Motion Control Conference, Budapest, Hungary, 2018, pp. 657-662, **indexed in Clarivate Analytics Web of Science,**
5. **E.-L. Hedrea**, R.-E. Precup, C.-A. Bojan-Dragos, R.-C. Roman, O. Tanasoiu and M. Marinescu, "Cascade control solutions for maglev systems," in Proc. 22nd International Conference on System Theory, Control and Computing, Sinaia, Romania, 2018, pp. 20-26, **indexed in Clarivate Analytics Web of Science,**
6. **E.-L. Hedrea**, R.-E. Precup, C.-A. Bojan-Dragos and C. Hedrea, "TP-based fuzzy control solutions for magnetic levitation systems," in Proc. 23rd International Conference on System Theory, Control and Computing, Sinaia, Romania, 2019, pp. 809-814, **indexed in Clarivate Analytics Web of Science,**
7. **E.-L. Hedrea**, R.-E. Precup, E.M. Petriu, C.-A. Bojan-Dragos and C. Hedrea, "Tensor product-based model transformation approach to cart position modeling and control in pendulum-cart systems," Asian Journal of Control, vol. 23, no. 3, pp. 1238-1248, 2021, **indexed in Clarivate Analytics Web of Science, impact factor = 3.452, Journal rank = Q2 according to Journal Citation Reports (JCR) published by Clarivate Analytics in 2021.**

5. Conclusions and personal contributions

5.1. Personal contributions

This thesis was formulated in order to validate the Tensor Product (TP)-based Model Transformation technique by obtaining TP models for various processes, other that the ones already presented in the literature, and also to improve the control performances of the TP-based control structures by combining the TP-based Model Transformation technique with other control techniques in the design of cascade control structures.

As specified in Chapter 1, the first objective of the thesis consisted in the validation of the modeling algorithm of the TP-based Model Transformation technique on many laboratory equipments. The corresponding derived TP models were validated using many testing scenarios and they were compared with other models of the same processes in order to highlight their performance. The first objective was fulfilled by the validation of the TP-based model transformation modeling algorithm on three laboratory equipments namely Vertical Three Tank System (V3TS), the partial state feedback controlled Magnetic Levitation System (psfcMLS) and the Pendulum Cart System (PCS).

As also specified in Chapter 1, the second objective of the thesis consisted in the validation of the control algorithm of the TP-based Model Transformation technique using LMIs and Parallel Distributed Compensation (PDC) framework. Therefore, many conventional and cascade control structures were design for the control of various laboratory equipments. The proposed control structures were tested and compared with other similar ones and their performance was highlighted. The second objective was fulfilled by the validation of the TP-based model transformation control algorithm on three laboratory equipments namely V3TS, psfcMLS and PCS.

The personal contributions included in this thesis are presented as follows and they result from the contributions presented in Chapters 3 and 4:

- The derivation of the TP model for the Vertical Three Tank System (V3TS). This model vas validated and tested in one testing scenario. A comparative analysis was done considering the corresponding outputs of the derived TP model, the nonlinear model and four linear models of the V3TS by computing four performance indices namely Root Mean Square Error (RMSE), Value of Accounted For (VAF), Akaike Information Criterion (AIC) and Bayesian Information Criterion (BIC) for all the derived models of V3TS.
- The derivation of the TP model for the partial state feedback controlled Magnetic Levitation System (psfcMLS). This model vas validated and tested in four testing scenarios. A comparative analysis was done considering the corresponding outputs of the derived TP model, the nonlinear model and four linear models of the psfcMLS by computing four performance indices namely RMSE, VAF, AIC and BIC for all the derived models of psfcMLS.

- The derivation of the TP model for the Pendulum Cart System (PCS). This model vas validated and tested in two testing scenarios. A comparative analysis was done considering the corresponding outputs of the derived TP model, the nonlinear model and four linear models of the PCS by computing four performance indices namely RMSE, VAF, AIC and BIC for all the derived models of PCS.
- The design of a TP-based control structure, namely TPCS, for the liquid level control of the V3TS. This structure was validated and tested in both simulation and experimental scenarios. This structure was compared with four state feedback control structures, namely SFCSs, using LMI control design for the liquid level control of the V3TS and aiming the same control performance as in case of TPCS; four performance indices, namely Mean Square Error (MSE), Mean Square Control Effort (MSU), settlig time and overshoot, were computed and used in the comparison based on simulation and experimental results and the corresponding output responses.
- The design of three cascade control system structures, namely PID-TPCS, with a PID controller in the outer control loop and a TP controller in the inner control loop, for the liquid level control of V3TS. These structures were validated and tested in both simulation and experimental scenarios. These structures were compared with other 12 cascade control system structures, namely PID-SFCS, with a PID controller in the outer control loop and a state feedback controller in the inner control loop for the liquid level control of V3TS; four performance indices, namely MSE, MSU, settlig time and overshoot, were computed and used in the comparison based on simulation and experimental results and the corresponding output responses.
- The design of a TP-based control structure, namely TPCS, for the sphere position control of the psfcMLS. This structure was validated and tested in both simulation and experimental scenarios. This structure was compared with four state feedback control structures, namely SFCSs, using LMI control design for the sphere position control of the psfcMLS and aiming the same control performance as in case of TPCS; four performance indices, namely MSE, MSU, settling time and overshoot, were computed and used in the comparison based on simulation and experimental results and the corresponding output responses.
- The design of a cascade control system structures, namely PID-TPCS, with a PID controller in the outer control loop and a TP controller in the inner control loop for the sphere position control of psfcMLS. This structure was validated and tested in both simulation and experimental scenarios. This structure was compared with another cascade control system structure, namely PI-SFCS, with a PI controller in the outer control loop and a state feedback controller in the inner control loop for the sphere position control of psfcMLS; four performance indices, namely MSE, MSU, settling time and overshoot, were computed and used in the comparison based on simulation and experimental results and the corresponding output responses.
- The design of a TP-based control structure, namely TPCS, for the cart position control of the PCS. This structure was validated and tested in

both simulation and experimental scenarios. This structure was compared with four state feedback control structures, namely SFCSs, using LMI control design for the cart position control of the PCS and aiming the same control performance as in case of TPCS; four performance indices, namely MSE, MSU, settling time and overshoot, were computed and used in the comparison based on simulation and experimental results and the corresponding output responses.

- The design of a cascade control system structure, namely PI-TPCS, with a PI controller in the outer control loop and a TP controller in the inner control loop for the cart position control of PCS. This structure was validated and tested in both simulation and experimental scenarios. This structure was compared with another cascade control system structure, namely PI-SFCS, with a PI controller in the outer control loop and a state feedback controller in the inner control loop for the cart position control of PCS; four performance indices, namely MSE, MSU, settling time and overshoot, were computed and used in the comparison based on simulation and experimental results and the corresponding output responses.

5.2. Dissemination of the results

The results presented in this thesis are published in 14 papers. The author of the thesis is the first author of 12 out of the 14 published papers. The published papers are grouped based on the databases they are indexed in:

- 4 papers in journals with impact factor indexed in Clarivate Analytics Web of Science (with the former name ISI Web of Knowledge), with a **cumulative impact factor = 10.516** according to Journal Citation Reports (JCR) published by Clarivate Analytics in 2021; **2 of these papers are published in journals with Q2 ranks as the first author** and the other 2 ones are published in journals with Q3 ranks (one of them as the first author).
- 10 papers in conference proceedings indexed in Clarivate Analytics Web of Science (with the former name ISI Web of Knowledge).

The published papers received a total number of **49 independent citations** (excluding the selfcitations and the citations of all the co-authors) **with a cumulative impact factor = 150.922**.

The results were published in the following papers:

1. E.-L. Hedrea, R.-E. Precup, R.-C. Roman and E.M. Petriu, "Tensor product-based model transformation approach to tower crane systems modeling," Asian Journal of Control, vol. 23, no. 3, pp. 1313-1323, 2021, **indexed in Clarivate Analytics Web of Science, impact factor = 3.452, Journal rank = Q2 according to Journal Citation Reports (JCR) published by Clarivate Analytics in 2021, cited in:**

1. H. Eivazi, S. Le Clainche, S. Hoyas and R. Vinuesa, "Towards extraction of orthogonal and parsimonious non-linear modes from turbulent flows," Expert Systems with Applications, vol. 202, 2022, **indexed in Google Scholar,**

2. J. Ye, Z. Xu and X. Gou, "An adaptive Grey-Markov model based on parameters Self-optimization with application to passenger flow volume prediction," Expert Systems with Applications, vol. 202, 2022, **indexed in Google Scholar,**
3. J. Wang, Y, Liu, H. Wu, S. Lu and M. Zhou, "Ensemble FARIMA Prediction with stable infinite variance innovations for supermarket energy consumption," Fractal and fractional, vol. 6, no. 5, 2022, **indexed in Google Scholar,**
4. O. Gireesha, A.B. Kamalesh, K. Krithivasan and V.S. Shankar Sriram, "A Fuzzy-multi attribute decision making approach for efficient service selection in cloud environments," Expert Systems with Applications, in Press, 2022, **indexed in Google Scholar,**
5. H. Garg, R. Krishankumar and K.S. Ravichandran, "Decision framework with integrated methods for group decision-making under probabilistic hesitant fuzzy context and unknown weights," Expert Systems with Applications, vol. 200, 2022, **indexed in Google Scholar,**
6. D. Lee, J.W. Jeong and G. Choi, "Short term prediction of PV power output generation using hierarchical probabilistic model," Energies, vol. 14, no. 10, 2021, **indexed in Clarivate Analytics Web of Science, impact factor = 3.004 according to Journal Citation Reports (JCR) published by Clarivate Analytics in 2021,**
7. X.L. Wang and L.Y. Hao, "Event-triggered fault detection for Takagi-Sugeno fuzzy systems via an improved matching membership function approach," Information Sciences, vol. 593, pp. 35-48, 2022, **indexed in Clarivate Analytics Web of Science, impact factor = 6.795 according to Journal Citation Reports (JCR) published by Clarivate Analytics in 2021,**
8. V.M. Nejkovic, M.S. Milicevic, G. Janackovic and M. Grozdanovic, "Application of fuzzy analytic hierarchy process to inductive steel tube welding," Romanian Journal of Information Science and Technology, vol. 25, no. 1, pp. 3-19, 2022, **indexed in Clarivate Analytics Web of Science, impact factor = 0.643 according to Journal Citation Reports (JCR) published by Clarivate Analytics in 2021,**
9. S. Mishra, T. Ahmed, V. Mishra, M. Kaur, T. Martinetz, A.K. Jain and H. Alshazly, "Multivariate and online prediction of closing price using kernel adaptive filtering," Computational Intelligence and Neuroscience, vol. 2021, 2021, **indexed in Clarivate Analytics Web of Science, impact factor = 3.633 according to Journal Citation Reports (JCR) published by Clarivate Analytics in 2021,**
10. M. Siket, K. Novak, H. Redjimi, J. Tar, L. Kovacs and G. Eigner, "Control of type 1 Diabetes Mellitus using Particle Swarm Optimization driven Receding Horizon controller," IFAC Papersonline, vol. 54, no. 15, pp. 293-298, 2021, **indexed in Clarivate Analytics Web of Science,**
11. I. de-Paz-Centeno, M.T. Marcia-Ordas, O. Garcia-Olalla, J. Arenas and H. Alaiz-Moreton, "M-SRPCNN: A fully convolutional neural network approach for handling super resolution reconstruction on monthly energy consumption environments," Energies, vol. 14, no. 16, 2021, **indexed in Clarivate Analytics Web of Science, impact factor = 3.004 according to Journal Citation Reports (JCR) published by Clarivate Analytics in 2021,**

12. H. Zhao, J. Zhang and Y. Ge, "Operation mode selection of NIMBY facility Public Private Partnership projects," Plos One, vol. 16, no. 7, 2021, **indexed in Clarivate Analytics Web of Science, impact factor = 3.24 according to Journal Citation Reports (JCR) published by Clarivate Analytics in 2021,**
13. Q. Shi, S. Yin, K. Wang, L. Teng and H. Li, "Multichannel convolutional neural network-based fuzzy active contour model for medical image segmentation," Evolving Systems, doi: 10.1007/s12530-021-09392-3, 2021, **indexed in Clarivate Analytics Web of Science, impact factor = 1.908 according to Journal Citation Reports (JCR) published by Clarivate Analytics in 2021,**
14. J. Awrejcewicz, G. Sypniewska-Kaminska and O. Mazur, "Analysing regular nonlinear vibrations of nano/micro plates based on the nonlocal theory and combination of reduced order modelling and multiple scale method," Mechanical Systems and Signal Processing, vol. 163, 2021, **indexed in Clarivate Analytics Web of Science, impact factor = 6.823 according to Journal Citation Reports (JCR) published by Clarivate Analytics in 2021,**
15. A.A. AbdullaS. Graovac, V. Papic and B. Kovacevic, "Triple-feature-based particle filter algorithm used in vehicle tracking applications," Advances in Electrical and Computer Engineering, vol. 22, no. 2, pp. 3-14, 2021, **indexed in Clarivate Analytics Web of Science, impact factor = 1.221 according to Journal Citation Reports (JCR) published by Clarivate Analytics in 2021,**
16. A. Volovyk, V. Kychak and D. Havrilov, "Discrete Kalman filter invariant to perturbations," Acta Polytechnica Hungarica, vol. 18, no. 10, 2021, **indexed in Clarivate Analytics Web of Science, impact factor = 1.806 according to Journal Citation Reports (JCR) published by Clarivate Analytics in 2021,**
17. H. Yildiz, E. Uzal and H. Calik, "An analytical solution of a multi-winding coil problem with a magnetic core in spherical coordinates," Acta Polytechnica Hungarica, vol. 18, no. 10, 2021, **indexed in Clarivate Analytics Web of Science, impact factor = 1.806 according to Journal Citation Reports (JCR) published by Clarivate Analytics in 2021,**
18. H.Y. Jiang, S.Y. Yu, C.M. Lin, Y. Chen and S.P. Huang, "Torque prediction of ankle joint from surface electromyographic using recurrent cerebellar model neural network," Acta Polytechnica Hungarica, vol. 18, no. 8, 2021, **indexed in Clarivate Analytics Web of Science, impact factor = 1.806 according to Journal Citation Reports (JCR) published by Clarivate Analytics in 2021,**
19. B. Jaksic, J. Todorovic, D. Bandur, B. Gvozdic and M. Bandur, "Outage performance of macrodiversity reception in the presence rayleigh short-term fading and co-channel interference," Acta Polytechnica Hungarica, vol. 18, no. 7, 2021, **indexed in Clarivate Analytics Web of Science, impact factor = 1.806 according to Journal Citation Reports (JCR) published by Clarivate Analytics in 2021.**

2. **E.-L. Hedrea**, R.-E. Precup, E.M. Petriu, C.-A. Bojan-Dragos and C. Hedrea, "Tensor product-based model transformation approach to cart position modeling and control in pendulum-cart systems," Asian Journal of Control, vol. 23, no. 3, pp. 1238-1248, 2021, **indexed in Clarivate Analytics Web of Science, impact**

factor = 3.452, Journal rank = Q2 according to Journal Citation Reports (JCR) published by Clarivate Analytics in 2021.

3. **E.-L. Hedrea**, R.-E. Precup and C.-A. Bojan-Dragos, "Results on tensor product-based model transformation of magnetic levitation systems," Acta Polytehnica Hungarica, vol. 16, no. 9, pp. 93-111, 2019, **indexed in Clarivate Analytics Web of Science, impact factor = 1.806, Journal rank = Q3 according to Journal Citation Reports (JCR) published by Clarivate Analytics in 2021, cited in:**
   1. X. Liu, N. Wang, D. Molina and F. Herrera, "A least square support vector machine approach based on bvRNA-GA for modeling photovoltaic systems," Applied Soft Computing, vol. 117, doi: 10.1016/j.asoc.2021.108357, **indexed in Clarivate Analytics Web of Science, impact factor = 6.725 according to Journal Citation Reports (JCR) published by Clarivate Analytics in 2021,**
   2. X. Pan, Y. Wang, S. He and K.-S. Chin, "A dynamic programming algorithm based clustering model and its application to interval type-2 fuzzy large-scale group decision-making problem," IEEE Transactions on Fuzzy Systems, vol. 30, no.1, pp. 108-120, 2022, **indexed in Clarivate Analytics Web of Science, impact factor = 12.029 according to Journal Citation Reports (JCR) published by Clarivate Analytics in 2021,**
   3. S. Yan, W. Sun, X, Yu and H. Gao, "Adaptive sensor fault accommodation for vehicle active suspensions via partial measurement information," IEEE Transactions on Cybernetics, doi: 10.1109/TCYB.2021.3072219, 2021, **indexed in Clarivate Analytics Web of Science, impact factor = 11.448 according to Journal Citation Reports (JCR) published by Clarivate Analytics in 2021,**
   4. Y.R. Liu, L. Wang, Z.P. Qiu and X. Chen, "A dynamic force reconstruction method based on modified Kalman filter using acceleration responses under multi-source uncertain samples," Mechanical Systems and Signal Processing, vol. 159, 2021, **indexed in Clarivate Analytics Web of Science, impact factor = 6.823 according to Journal Citation Reports (JCR) published by Clarivate Analytics in 2021,**
   5. E. Nsugbe, O.W. Samuel, M.G. Asogbon and G.L. Li, "Contrast of multi-resolution analysis approach to transhumeral phantom motion decoding," CAAI Transactions on Intelligence Technology, 2021, pp. 1-16, **indexed in Clarivate Analytics Web of Science, without impact factor**,
   6. C.J. Qin, G. Shi, J.F. Tao, H.G. Yu, Y.R. Jin, J.B. Lei and C.L. Liu, "Precise cutterhead torque prediction for shield tunneling machines a novel neural network," Mechanical Systems and Signal Processing, vol. 151, 2021, **indexed in Clarivate Analytics Web of Science, impact factor = 6.823 according to Journal Citation Reports (JCR) published by Clarivate Analytics in 2021**,
   7. Q. Zhang, J.H. Zhou, B. Zhang and E.H. Wu, "DsNet: Dual stack network for detecting diabetes mellitus and chronic kidney disease," Information Sciences, vol. 547, pp. 945-962, 2021, **indexed in Clarivate Analytics Web of Science, impact factor = 6.795 according to Journal Citation Reports (JCR) published by Clarivate Analytics in 2021**,
   8. A.B. Csapo, "Cyclical inverse interpolation: An approach for the inverse interpolation of black-box models using tensor product representations," Asian Journal of Control, vol. 23, pp. 1301-1312, 2021, **indexed in**

Clarivate Analytics Web of Science, impact factor = 3.452 according to Journal Citation Reports (JCR) published by Clarivate Analytics in 2021,

9. K. Kluwak, M. Kulbacki and A. Kolcz, "Applications of Tags in Multimodal Analysis of Motion Ergonomics for Healthcare Environments," Acta Polytechnica Hungarica, vol. 18, no. 10, **indexed in Clarivate Analytics Web of Science, impact factor = 1.806 according to Journal Citation Reports (JCR) published by Clarivate Analytics in 2021**,
10. T.T. Ngoc, L.V. Dai and C.M. Thuyen, "Support vector regression based on grid gearch method of hyperparameters for load forecasting," Acta Polytechnica Hungarica, vol. 18, no. 2, 2021, **indexed in Clarivate Analytics Web of Science, impact factor = 1.806 according to Journal Citation Reports (JCR) published by Clarivate Analytics in 2021**,
11. A. Boonyaprapasorn, S. Kuntanapreeda, P.S. Ngiamsunthorn, E. Pengwang and T. Sangpet, "Tensor product model transformation-based control for fractional-order biological pest control systems," Asian Journal of Control, vol. 23, no. 2, pp. 1340-1351, 2020, **indexed in Clarivate Analytics Web of Science, impact factor = 3.452 according to Journal Citation Reports (JCR) published by Clarivate Analytics in 2021**,
12. Y.Y. He and W.Y. Zhang, "Probability density forecasting of wind power based on multi-core parallel quantile regression neural network," Knowledge-Based Systems, vol. 209, no. 8, 2020, **indexed in Clarivate Analytics Web of Science, impact factor = 8.038 according to Journal Citation Reports (JCR) published by Clarivate Analytics in 2021**,
13. R.C. Suganthe, R.S. Latha, M. Geetha and G.R. Sreekanth, "Diagnosis of Alzheimer's disease from brain magnetic resonance imaging images using deep learning algorithms," Advances in Electrical and Computer Engineering, vol. 20, no. 3, pp. 57-64, 2020, **indexed in Clarivate Analytics Web of Science, impact factor = 1.221 according to Journal Citation Reports (JCR) published by Clarivate Analytics in 2021**,
14. T. Pramanik, G. Muhiuddin, A.M. Alanazi and M. Pal, "An extension of fuzzy competition graph and its uses in manufacturing industries," Mathematics, vol. 8, no. 6, 2020, **indexed in Clarivate Analytics Web of Science, impact factor = 2.258 according to Journal Citation Reports (JCR) published by Clarivate Analytics in 2021**,
15. F. Christudas and A.V. Dhanraj, "System identification using long short term memory recurrent neural networks for real time conical tank system," Romanian Journal of Information Science and Technology, vol. 23, no. T, pp. T57-T77, 2020, **indexed in Clarivate Analytics Web of Science, impact factor = 0.643 according to Journal Citation Reports (JCR) published by Clarivate Analytics in 2021**,
16. M. Turkiewicz, E. Prociow and A. Dziedzic, "Thermovoltaic effect in a multilayer junction structure with an oxide insulation barrier," Acta Polytechnica Hungarica, vol. 17, no. 9, pp. 125-140, 2020, **indexed in Clarivate Analytics Web of Science, impact factor = 1.806 according to Journal Citation Reports (JCR) published by Clarivate Analytics in 2021**,
17. M. Seo, J. Ban, B.Y. Koo and S.W. Kim, "Static model identification for Sendzimir rolling mill using noise corrupted operation data," IEEE Acces, vol. 8, pp. 150685-150695, 2020, **indexed in Clarivate Analytics Web of**

Science, impact factor = 3.367 according to Journal Citation Reports (JCR) published by Clarivate Analytics in 2021.

4. E.-L. Hedrea, R.-E. Precup, C.-A. Bojan-Dragos and C. Hedrea, "TP-based fuzzy control solutions for magnetic levitation systems," in Proc. 23rd International Conference on System Theory Control and Computing, Sinaia, Romania, 2019, pp. 809-814, **indexed in Clarivate Analytics Web of Science.**

5. E.-L. Hedrea, R.-E. Precup, C.-A. Bojan-Dragos and O. Tanasoiu, "Tensor product-based model transformation technique applied to modeling magnetic levitation systems," in Proc. IEEE 23rd International Conference on Intelligent Engineering Systems, Gödöllö, Hungary, 2019, pp. 179-184, **indexed in Clarivate Analytics Web of Science.**

6. E.-L. Hedrea, R.-E. Precup, C.-A. Bojan-Dragos, E.M. Petriu and R.-C. Roman, "Tensor Product-based model transformation and sliding mode control of electromagnetic actuated clutch system," in Proc. 2019 International Conference on Systems, Man and Cybernetics, Bari, Italy, 2019, pp. 1402-1407, **indexed in Clarivate Analytics Web of Science, cited in:**

1. A. Azizi, H. Mobki, H.M. Ouakad and O.R.B. Speily, " Applied mechatronics: on mitigating disturbance effects in MEMS resonators using robust nonsingular terminal sliding mode controllers," Machines, vol. 10, no. 1, 2022, **indexed in Clarivate Analytics Web of Science, impact factor = 2.428 according to Journal Citation Reports (JCR) published by Clarivate Analytics in 2021.**
2. Z. Zhao, X. Zhang and Z. Li, "Tank-level control of liquefied natural gas carrier based on gaussian function nonlinear decoration," Journal of Marine Science and Engineering, vol. 8, no. 9, 2020, **indexed in Clarivate Analytics Web of Science, impact factor = 2.458 according to Journal Citation Reports (JCR) published by Clarivate Analytics in 2021.**

7. E.-L. Hedrea, R.-E. Precup, C.-A. Bojan-Dragos, C. Hedrea, D. Ples and D. Popovici, "Cascade control solutions for level control of vertical three tank systems," in Proc. 13th International Symposium on Applied Computational Intelligence and Informatics, Timisoara, Romania, 2019, pp. 353-358, **indexed in Clarivate Analytics Web of Science.**

8. C.-A. Bojan-Dragos, M.-B. Radac, R.-E. Precup, **E.-L. Hedrea** and O.-M. Tanasoiu, " Gain-Scheduling control solutions for magnetic levitation systems," Acta Polytehnica Hungarica, vol. 15, no. 5, pp. 89-108, 2018, **indexed in Clarivate Analytics Web of Science, impact factor = 1.806, Journal rank = Q3 according to Journal Citation Reports (JCR) published by Clarivate Analytics in 2021, cited in:**

1. J.D. Rubio, E. Lughofer, J. Pieper, P. Cruz, D.I. Martinez, G. Ochoa, M.A. Islas and E. Garcia, "Adapting H-infinity controller for the desired reference tracking of the sphere position in the maglev process," Information Sciences, vol. 569, pp. 669-686, 2021, **indexed in Clarivate Analytics Web of Science, impact factor = 6.795 according to Journal Citation Reports (JCR) published by Clarivate Analytics in 2021,**
2. N. Dalwadi, D. Deb and S.M. Muyeen, "A reference model assisted adaptive control structure for maglev transportation system," Electronics, vol. 10, no. 3, 2021, **indexed in Clarivate Analytics Web of Science, impact factor = 2.397 according to Journal Citation Reports (JCR) published by Clarivate Analytics in 2021,**

3. D. Sain and B.M. Mohan, "Modelling of a nonlinear fuzzy three-input PID controller and its simulation and experimental realization," IETE Technical Review, vol. 28, no. 5, pp. 479-498, 2021, **indexed in Clarivate Analytics Web of Science, impact factor = 2.2 according to Journal Citation Reports (JCR) published by Clarivate Analytics in 2021,**
4. K.M. Deliparaschos, K. Michail and A.C. Zolotas, "Facilitating autonomous systems with AI-based fault tolerance and computational resource economy," Electronics, vol. 9, no. 5, 2020, **indexed in Clarivate Analytics Web of Science, impact factor = 2.397 according to Journal Citation Reports (JCR) published by Clarivate Analytics in 2021.**

9. C.-A. Bojan-Dragos, A.-I. Szedlak-Stinean, R.-E. Precup, L. Gurgui, **E.-L. Hedrea** and I.-C. Mituletu, "Control solutions for vertical three-tank systems," in Proc. 12th International Symposium on Applied Computational Intelligence and Informatics, Timisoara, Romania, 2018, pp. 593-598, **indexed in Clarivate Analytics Web of Science.**

10. E.-L. Hedrea, R.-E. Precup, C.-A. Bojan-Dragos, R.-C. Roman, O. Tanasoiu and M. Marinescu, "Cascade control solutions for maglev systems," in Proc. 22nd International Conference on System Theory, Control and Computing, Sinaia, Romania, 2018, pp. 20-26, **indexed in Clarivate Analytics Web of Science.**

11. E.-L. Hedrea, R.-E. Precup, C.-A. Bojan-Dragos and C. Hedrea, "Tensor product-based model transformation technique applied to modeling vertical three tank systems," in Proc. IEEE 12th International Symposium on Applied Computational Intelligence and Informatics, Timisoara, Romania, 2018, pp. 63-68, **indexed in Clarivate Analytics Web of Science, cited in:**

1. Z.J. Zhao, X.K. Zhang and Z. Li, "Tank-level control of liquefied natural gas carrier based on Gaussian function nonlinear decoration," Journal of Marine Science and Engineering, vol. 8, no. 9, 2020, **indexed in Clarivate Analytics Web of Science, impact factor = 2.458 according to Journal Citation Reports (JCR) published by Clarivate Analytics in 2021**.

12. E.-L. Hedrea, C.-A. Bojan-Dragos, R.-E. Precup and E.M. Petriu, "Comparative study of control structures for maglev systems," in Proc. IEEE 18th International Power Electronics and Motion Control Conference, Budapest, Hungary, 2018, pp. 657-662, **indexed in Clarivate Analytics Web of Science.**

13. E.-L. Hedrea, C.-A. Bojan-Dragos, R.-E. Precup and T.-A. Teban, "Tensor product-based model transformation for level control of vertical three tank systems," in Proc. IEEE 21st International Conference on Intelligent Engineering Systems, Larnaca, Cyprus, 2017, pp. 113-118, **indexed in Clarivate Analytics Web of Science, cited in**:

1. L. Kovacs and G. Eigner, "A TP-LPV-LMI based control for tumor growth inhibition," IFAC Papers Online, vol. 51, no. 26, pp. 155-160, 2018, **indexed in Clarivate Analytics Web of Science,**
2. L. Kovacs and G. Eigner, "Tensor product model transformation based parallel distributed control of tumor growth,"Acta Politechnica Hungarica, vol. 15, no. 3, pp. 101-123, 2018, **indexed in Clarivate Analytics Web of Science, impact factor = 1.806 according to Journal Citation Reports (JCR) published by Clarivate Analytics in 2021**.

14. E.-L. Hedrea, C.-A. Bojan-Dragos, R.-E. Precup, R.-C. Roman, E.-M. Petriu and C. Hedrea, "Tensor product-based model transformation for position control of magnetic levitation systems," in Proc. IEEE 26th International Symposium on Industrial Electronics, Edinburgh, Scotland, 2017, pp. 1141-1146, **indexed in Clarivate Analytics Web of Science, cited in:**

1. G.H. Chen and D.X. Yang, "A unified analysis framework of static and dynamic structural reliabilities based on direct probability integral method," Mechanical Systems and Signal Processing, vol. 158, 2021, **indexed in Clarivate Analytics Web of Science, impact factor = 6.823 according to Journal Citation Reports (JCR) published by Clarivate Analytics in 2021,**
2. Y.F. Yang, X.J. Ban, X.L. Huang and C.H. Shan, "A dueling-double-deep Q-network controller for magnetic levitation ball system," in Proc. 39th Chinese Control Conference, Shenyang, China, 2020, pp. 1885-1890, **indexed in Clarivate Analytics Web of Science,**
3. L. Kovacs, G. Eigner, M. Siket and L. Barkai, "Control of diabetes mellitus by advanced robust control solution," IEEE Access, vol. 7, pp. 125609-125622, 2019, **indexed in Clarivate Analytics Web of Science, impact factor = 3.367 according to Journal Citation Reports (JCR) published by Clarivate Analytics in 2021,**
4. L. Kovacs and G. Eigner, "Tensor product model transformation based parallel distributed control of tumor growth,"Acta Politechnica Hungarica, vol. 15, no. 3, pp. 101-123, 2018, **indexed in Clarivate Analytics Web of Science, impact factor = 1.806 according to Journal Citation Reports (JCR) published by Clarivate Analytics in 2021**.

5.3. Future research

The author proposes the following future research directions which are meant to improve the results obtained and presented in this thesis:

- the improvement of the TP-based Model Transformation modeling algorithm by using input-output data of the process in the derivation of the TP model;
- the design of a modeling software and interface in order to ease the acces of various types of users to the TP-based Model Transformation modeling algorithm;
- the comparative analysis between the derived TP model and the TP controller with similar nonlinear models and controllers, such as fuzzy models and controllers, LPV models, with controller design using such that to fulfil the same performance specifications (for a fair comparison) and design approach based on LMIs;
- the development of hybrid control techniques with focus on the TP-based model transformation but using fresh results transferred from fuzzy control.

Bibliography

[Aka73] H. Akaike, "Information theory and an extension of the maximum likelihood principle," in Proc. 2nd International Symposium on Information Theory, Budapest, Hungary, 1973, pp. 267-281.

[Apk95] P. Apkarian and P. Gahinet, "A convex characterization of gain scheduled controllers," IEEE Transactions in Automatic Control, vol. 40, no. 5, pp. 853-864, 1995.

[Bar03a] P. Baranyi and R.J. Patton, "A numerical control design method for prototypical aeroelastic wing section with structural non-linearity," in Proc. 2003 European Control Conference, Cambridge, UK, 2003, pp. 2095-2100.

[Bar03b] P. Baranyi and A.R. Várkonyi-Kóczy, "Asymptotic stabilization of aeroelastic systems via TP transformation," in Proc. 2003 IEEE International Symposium on Intelligent Signal Processing, Budapest, Hungary, 2003, pp. 143-148.

[Bar04a] P. Baranyi and P. Michelberger, "Global asymptotic stabilization of the aeroelastic wing section: a TP model transformation based approach," in Proc. 2004 IEEE International Conference on Fuzzy Systems, Budapest, Hungary, 2004, pp. 1063-1068.

[Bar04b] P. Baranyi, "TP model transformation as a way to LMI-based controller design," IEEE Transactions on Industrial Electronics, vol. 51, no. 2, pp. 387-400, 2004.

[Bar05a] P. Baranyi, K. Tanaka, and P. Korondi, "TP model transformation based stabilization of a 3-DOF RC Helicopter," in Proc. 2005 International Conference on Control and Automation, Budapest, Hungary, 2005, pp. 443-448.

[Bar05b] P. Baranyi and A.R. Várkonyi-Kóczy, "TP Transformation Based Dynamic System Modeling for Nonlinear Control," IEEE Transactions on Instrumentation and Management, vol. 54, no. 6, pp. 2191-2203, 2005.

[Bar06a] P. Baranyi, L. Szeidl, and P. Várlaki, "Numerical reconstruction of the HOSVD based canonical form of polytopic dynamic models," in Proc. 2006 International Conference on Intelligent Engineering Systems, London, UK, 2006, pp. 196-201.

[Bar06b] P. Baranyi, P. Várlaki, L. Szeidl, and Y. Yam, "Definition of the HOSVD based canonical form of polytopic dynamic models," in Proc. IEEE International Conference on Mechatronics, Budapest, Hungary, 2006, pp. 660-665.

[Bar06c] P. Baranyi and Y. Yam, "Case study of the TP-model transformation in the control of a complex dynamic model with structural nonlinearity," IEEE Transactions on Industrial Electronics, vol. 53, no.3, pp. 895-904, 2006.

[Bar06d] P. Baranyi, "Tensor-product model-based control of two-dimensional aeroelastic system," Journal of Guidance, Control, And Dynamics, vol. 29, no. 2, pp. 391-400, 2006.

[Bar13] P. Baranyi, Y. Yam, and P. Varlaki, TP Model Transformation in Polytopic Model-Based Control. Boca Raton, FL: Taylor & Francis, 2013.

[Bar14] P. Baranyi, "The generalized TP model transformation for T-S fuzzy model manipulation and generalized stability verification," IEEE Transactions on Fuzzy Systems, vol. 22, no. 4, pp. 934-948, 2014.

[Bar15] P. Baranyi, "TP model transformation as a manipulation tool for QLPV analysis and design," Asian Journal of Control, vol. 17, no. 2, pp. 497-507, 2015.
[Bar16] P. Baranyi, TP-Model Transformation-Based-Control Design Frameworks. Cham, Switzerland: Springer International Publishing, 2016.
[Bar18] P. Barayi, "Extension of the multi-TP model transformation to functions with different numbers of variables," Complexity, vol. 2018, no. 3, pp. 1-9, 2018.
[Bar22a] P. Baranyi, "Extracting LPV and qLPV structures from state-space functions: a TP model transformation based framework," IEEE Transactions on Fuzzy Systems, vol. 28, no. 3, pp. 499-509, 2022.
[Bar22b] P. Baranyi, "How to vary the input space of a TS fuzzy model: a TP model transformation based approach," IEEE Transactions on Fuzzy Systems, vol. 30, no. 2, pp. 345-356, 2022.
[Boj16] C.-A. Bojan-Dragos, S. Preitl, R.-E. Precup, S. Hergane, E. G. Hughiet, and A.-I. Szedlak-Stinean, "State feedback and proportional-integral-derivative control of a magnetic levitation system," in Proc. IEEE 14th International Symposium on Intelligent Systems and Informatics, Subotica, Serbia, 2016, pp. 111-116.
[Boj18a] C.-A. Bojan-Dragos, M.-B. Radac, R.-E. Precup, E.-L. Hedrea, and O.-M. Tanasoiu, "Gain-scheduling control solutions for magnetic levitation systems," Acta Polytechnica Hungarica, vol. 15, no. 5, pp. 89-108, 2018.
[Boj18b] C.-A. Bojan-Dragos, A.-I. Szedlak-Stinean, R.-E. Precup, L. Gurgui, E.-L. Hedrea and I.-C. Mituletu, "Control solutions for vertical three-tank systems," in Proc. 12th International Symposium on Applied Computational Intelligence and Informatics, Timisoara, Romania, 2018, pp. 593-598.
[Boj19] C.-A. Bojan-Dragos, E.-L. Hedrea, R.-E. Precup, A.-I. Szedlak-Stinean and R.-C. Roman, " MIMO fuzzy control solutions for the level control of vertical two tank systems," in Proc. 16th International Conference on Informatics in Control, Automation and Robotics, Prague, Czech Republic, 2019.
[Bok05] J. Bokor, P. Baranyi, P. Michelberger, and P. Várlaki, "TP model transformation in non-linear system control," in Proc. IEEE 3rd International Conference on Computational Cybernetics, Mauritius, 2005, pp.111-120.
[Boo20] A. Boonyaprapasorn, S. Kuntanapreeda, P.S. Ngiamsunthorn, E. Pengwang, and T. Sangpet, "Tensor product model transformation-based control for fractional-order biological pest control systems," Asian Journal of Control, vol. 23, no. 2, pp. 1340-1351, 2020.
[Cha20] F. Chang and G. Zhao, "Receding horizon H_∞ control for nonlinear systems with tensor product model transformation," in Proc 39th Chinese Control Conference, Shenyang, China, 2020, pp. 2150-2157.
[Che14] J. Chen, R. Li, and C. Cao, "Convex polytopic modeling for flexible joints industrial robot using TP-model transformation," in Proc. IEEE International Conference on Information and Automation, Hailar, China, 2014, pp. 1046-1050.
[Che17] Z. Chen, S. Chen, X. Xin, Z. Li, Z. Song, and X. Liu, "H_∞ control using tensor product model transformation," in Proc 36th Chinese Control Conference, Dalian, China, 2017, pp. 1385-1390.
[Csa21] A.B. Csapo, "Cyclical inverse interpolation: An approach for the inverse interpolation of black-box models using tensor product representations," Asian Journal of Control, vol. 23, pp. 1301-1312, 2021.

[Eig16a] G. Eigner, I.J. Rudas, and L. Kovács, "Investigation of the TP-based modeling possibility of a nonlinear ICU diabetes model," in Proc. 2016 IEEE International Conference on Systems, Man, and Cybernetics, Budapest, Hungary, 2016, pp.3405-3410.

[Eig16b] G. Eigner, P. Pausits, and L. Kovács, "Control of T1DM via tensor product-based framework," in Proc. 17th IEEE International Symposium on Computational Intelligence and Informatics, Budapest, Hungary, 2016, pp. 55-60.

[Eig17a] G. Eigner, I. Böjthe, P. Pausits, and L. Kovács, "Investigation of the TP modeling possibilities of the Hovorka T1DM model," in Proc. 17th IEEE International Symposium on Applied Machine Intelligence and Informatics," Herl'any, Slovakia, 2017, pp. 259-264.

[Eig17b] G. Eigner, I. Rudas, A. Szakál, and L. Kovács, "Tensor product based modeling of tumor growth," in Proc. IEEE International Conference on Systems, Man, and Cybernetics, Banff, Canada, 2017, pp. 900-905.

[Fee98] Feedback, Digital Pendulum System, Teaching Manual, Feedback Instruments Ltd., Crowborough, UK, 1998.

[Gal13] P. Galambos, J. Kuti, and P. Baranyi, "On the tensor product based qLPV modeling of bio-inspired dynamic processes," in Proc. IEEE 17th International Conference on Intelligent Engineering Systems, Costa Rica, 2013, pp. 79-84.

[Gal15a] P. Galambos, J. Kuti, P. Baranyi, G. Szögi, and I.J. Rudas, "Tensor Product based convex polytopic modeling of nonlinear insulin-glucose dynamics," in Proc. 2015 IEEE International Conference on Systems, Man, and Cybernetics, Kowloon, China, 2015, pp.2597-2602.

[Gal15b] P. Galambos and P. Baranyi, "TP Model transformation: a system modeling framework to handle internal time delays in control systems," Asian Journal of Control, vol. 17, no. 2, pp. 1-11, 2015.

[Gon20] H. Gong, Y. Yu, L. Zheng, B. Wang, Z. Li, T. Fernando, H.H.C. Iu, X. Liao, and X. Liu, "Nonlinear H_∞ filtering based on tensor product model transformation," IEEE Transactions on Circuits and Systems, vol. 67, no. 6, pp. 1074-1078, 2020.

[Gro10] P. Gróf, B. Takarics, Z. Peters, and P. Korondi, "Tensor product model type polytopic decomposition of a pneumatic system with friction phenomena taken into account," in Proc. 8th IEEE International Symposium on Applied Machine Intelligence and Informatics, Herl'any, Slovakia, 2010, pp. 153-158.

[Gro12] P. Gróf, P. Galambos, and P. Baranyi, "Convex hull manipulation based control performance optimization: case study of impedance model with feedback delay," in Proc. 10th IEEE Jubilee International Symposium on Applied Machine Intelligence and Informatics, Herl'any, Slovakia, 2012, pp. 495-499.

[Gro15] P. Gróf and Y. Yam, "Furuta pendulum-a tensor product model-based design approach case study," in Proc. 2015 IEEE International Conference on Systems, Man, and Cybernetics, Kowloon, China, 2015, pp. 2620-2625.

[Han17] X. Han, T. Wang, and S. Yu, "Predictive control of mobile robot based on Tensor Product model transformation," in Proc. 29th Chinese Control And Decision Conference, Chongqing, China, 2017, pp.7872-7876.

[He16] Z. He, M. Yin, and Y. Lu, "Tensor product model-based control of morphing aircraft in transition process," Journal Aerospace Engineering, vol. 230, no. 2, pp. 378-391, 2016.

[Hed17a] L.-E. Hedrea, C.-A. Bojan-Dragos, R.-E. Precup, R.-C. Roman, E.M. Petriu, and C. Hedrea, "Tensor product-based model transformation for position control of magnetic levitation systems," in Proc. IEEE 26th International Symposium on Industrial Electronics, Edinburgh, UK, 2017, pp. 1141-1146.

[Hed17b] E.-L. Hedrea, C.-A. Bojan-Dragos, R.-E. Precup, and T.-A. Teban, "Tensor product-based model transformation for level control of vertical three tank systems," in Proc. IEEE 21st International Conference on Intelligent Engineering Systems, Larnaca, Cyprus, 2017, pp. 113-118.

[Hed18a] E.-L. Hedrea, R.-E. Precup, C.-A. Bojan-Dragos, and C. Hedrea, "Tensor product-based model transformation technique applied to modeling vertical three tank systems," in Proc. IEEE 12th International Symposium on Applied Computational Intelligence and Informatics, Timisoara, Romania, 2018, pp. 63-68.

[Hed18b] E.-L. Hedrea, C.-A. Bojan-Dragos, R.-E. Precup, and E.M. Petriu, "Comparative study of control structures for Maglev systems," in Proc. IEEE 18th International Power Electronics and Motion Control Conference, Budapest, Hungary, 2018, pp. 657-662.

[Hed18c] E.-L. Hedrea, R.-E. Precup, C.-A. Bojan-Dragos, R.-C. Roman, O. Tanasoiu, and M. Marinescu, "Cascade control solutions for Maglev systems," in Proc. 22nd International Conference on System Theory, Control and Computing, Sinaia, Romania, 2018, pp. 20-26.

[Hed19a] E.-L. Hedrea, R.-E. Precup, C.-A. Bojan-Dragos, C. Hedrea, D. Ples, and D. Popovici, "Cascade control solutions for level control of vertical three tank systems," in Proc. IEEE 13th International Symposium on Applied Computational Intelligence and Informatics, Timisoara, Romania, 2019, pp. 352-357.

[Hed19b] E.-L. Hedrea, R.-E. Precup, C.-A. Bojan-Dragos, and O. Tanasoiu, "Tensor product-based model transformation technique applied to modeling magnetic levitation systems," in Proc. IEEE 23rd International Conference on Intelligent Engineering Systems, Gödöllö, Hungary, 2019, pp. 179-184.

[Hed19c] E.-L. Hedrea, R.-E. Precup, C.-A. Bojan-Dragos, and C. Hedrea, "TP-based fuzzy control solutions for magnetic levitation systems," in Proc. 23rd International Conference on System Theory, Control and Computing, Sinaia, Romania, 2019, pp. 809-814.

[Hed19d] E.-L. Hedrea, R.-E. Precup, C.-A. Bojan-Dragos, E.M. Petriu, and R.-C. Roman, "Tensor product-based model transformation and sliding mode control of electromagnetic actuated clutch system," in Proc. 2019 IEEE International Conference on Systems, Man and Cybernetics, Bari, Italy, 2019, pp. 1402-1407.

[Hed19e] E.-L. Hedrea, R.-E. Precup, and C.-A. Bojan-Dragos, "Results on tensor product-based model transformation of magnetic levitation systems," Acta Polytehnica Hungarica, vol. 16, no. 9, pp. 93-111, 2019.

[Hed21a] E.-L. Hedrea, R.-E. Precup, E.M. Petriu, C.-A. Bojan-Dragos, and C. Hedrea, "Tensor product-based model transformation approach to cart position modeling and control in pendulum-cart systems," Asian Journal of Control, vol. 23, pp. 1238-1248, 2021.

[Hed21b] E.-L. Hedrea, R.-E. Precup, R.-C. Roman, and E.M. Petriu, "Tensor product-based model transformation approach to tower crane systems modeling," Asian Journal of Control, vol. 23, pp. 1313-1323, 2021.

[Hed21c] E.-L. Hedrea, R.-E. Precup, R.-C. Roman, E.M. Petriu, C.-A. Bojan-Dragos, and C. Hedrea, "Tensor product-based model transformation technique

applied to servo systems modeling," in Proc. IEEE 30th International Symposium on Industrial Electronics, Miyako Messe, Kyoto, Japan, 2021, pp. 1-6.
[Hua12] Y. Huang, C. Sun, C. Qian, R. Zhang, and J. Zhang, "Polytopic LPV gain-scheduled control for a flexible air-breathing hypersonic vehicle," in Proc. 31st Chinese Control Conference, Hefei, China, 2012, pp. 329-334.
[Hua15] S. Huang, G. Zhao, Y, Yuan, Q. Ren, and Y. Liu, "Intelligent tensor product mode transformation-based three-sliding-surface sliding mode controller design," in Proc 34th Chinese Control Conference, Hangzhou, China, 2015, pp. 3258-3263.
[Ile11] Š. Ileš, J. Matuško, and F. Kolonić, "TP transformation based control of rotary pendulum," in Proc. 34th International Convention MIPRO, Opatija, Croatia, 2011, pp. 833-839.
[Ile14] Š. Ileš, J. Matuško, and F. Kolonić, "Real-time predictive control of 3D tower crane," in Proc. IEEE 23rd International Symposium on Industrial Electronics, Istanbul, Turkey, 2014, pp. 224-230.
[Ile21] Š. Ileš, J. Matuško, and M. Lazar, "Piece-wise ellipsoidal set-based model predictive control of linear parameter varying systems with application to a tower crane," Asian Journal of Control, vol. 23, no. 3, pp. 1324-1339, 2021.
[Int07] Inteco, Multitank System, User's Manual. Krakow, Poland: Inteco Ltd., 2007.
[Int08] Inteco Ltd., Magnetic Levitation System 2EM (MLS2EM), User's Manual (Laboratory Set). Krakow, Poland: Inteco Ltd., 2008.
[Kes55] C. Kessler, "Über die Vorausberechnung optimal abgestimmter Regelkreise Teil III. Die optimale Einstellung des Reglers nach dem Betragsoptimum," Regelungstechnik, vol. 3, no. 1-12, pp. 40-49, 1955.
[Kol06] F. Kolonic and A. Poljugan, "Experimental control design by TP model transformation," in Proc. 2006 IEEE International Conference on Mechatronics, Budapest, Hungary, 2006, pp. 666-671.
[Kor06] P. Korondi and Z. Peters, "Sliding mode control based on tensor product model transformation," in Proc. 2006 IEEE International Conference on Mechatronics, Budapest, Hungary, 2006, pp. 672-677.
[Kov16] L. Kovács and G. Eigner, "Convex polytopic modeling of diabetes mellitus: a Tensor Product based approach," in Proc. 2016 IEEE International Conference on Systems, Man, and Cybernetics, Budapest, Hungary, 2016, pp. 3393-3398.
[Kuc19] M. Kuczmann, "TP-based control of the crane model," in Proc. 1st IEEE International Conference on Gridding and Polytope Based Modeling and Control, Győr, Hungary, 2019, pp. 9-12.
[Kuc21] M. Kuczmann, "Study of tensor product model alternatives," Asian Journal of Control, vol. 23, no. 3, pp. 1249-1261, 2021.
[Kun07] Y. Kunii, B. Solvang, G. Sziebig, and P. Korondi, "Tensor product transformation based friction model," in Proc. 11th International Conference on Intelligent Engineering Systems, Budapest, Hungary, 2007, pp. 259-264.
[Kut16] J. Kuti, P. Galambos, and P. Baranyi, "Non-simplex enclosing polytope generation concept for tensor product model transformation based controller design," in Proc 2016 IEEE International Conference on Systems, Man, and Cybernetics, Budapest, Hungary, 2016, pp. 3368-3373.
[Kut17a] J. Kuti, P. Galambos, and P. Baranyi, "Minimal Volume Simplex (MVS) polytopic model generation and manipulation methodology for TP model transformation," Asian Journal of Control, vol. 19, no. 1, pp. 1-13, 2017.

[Kut17b] J. Kuti and P. Galambos, "Computational relaxations for affine tensor product model transformation," in Proc. IEEE 15th International Symposium on Intelligent Systems and Informatics, Subotica, Serbia, 2017, pp. 333-338.
[Lat00] L. Lathauwer, B. De Moor, and J. Vandewalle, "A multilinear singular value decomposition," SIAM Journal on Matrix Analysis and Applications, vol. 21, no. 4, pp. 1253-1278, 2000.
[Liu17a] X. Liu, Y. Yu, Z. Li, H.H.C. Iu and T. Fernando, "An efficient algorithm for optimally reshaping the TP model transformation," IEEE Transactions on Circuits and Systems-II: Express Briefs, vol. 64, no. 10, pp. 1187-1191, 2017.
[Liu17b] X. Liu, X. Xin, Z. Li, and Z. Chen, "Near optimal control based on the Tensor-Product technique," IEEE Transactions on Circuits and Systems-II: Express Briefs, vol. 64, no. 5, pp. 560-564, 2017.
[Mah15] A. S. A. Mahmoud, M. Khan, and A. S. Siddique, "Discrete-time control of Maglev system using switched fuzzy controller," in Proc. 2015 Annual IEEE India Conference, New Delhi, India, 2015, pp. 1-6.
[Mat11] J. Matuško, V. Lešić, F. Kolonić, and S. Ileš, "Tensor product based control of the single pendulum gantry process with stable neural network based friction compensation," in Proc. 2011 IEEE/ASME International Conference on Advanced Intelligent Mechatronics, Budapest, Hungary, 2011, pp. 1010-1015.
[Mil17] M. B. Milovanovic, D. S. Antic, S. S. Nikolic, S. L. Peric, M. T. Milojkovic, and M. D. Spasic, "Neural network based on orthogonal polynomials applied in magnetic levitation system control," Elektronika ir Elektrotechnika., vol. 23, no. 2, pp. 24-29, 2017.
[Nag07a] S. Nagy, Z. Peters, P. Baranyi, L. Szeidl, and P. Michelberger, "Polytopic decomposition of the linear parameter-varying model of the parallel-type double inverted pendulum," in Proc. 11th International Conference on Intelligent Engineering Systems, Budapest, Hungary, 2007, pp. 271-275.
[Nag07b] S. Nagy, Z. Peters, P. Baranyi, and H. Hashimoto, "Computational relaxed TP model transformation by restriction of the computation to subspaces of the dynamic model," in Proc. 2007 International Symposium on Computational Intelligence and Intelligent Informatics, Agadir, Marocco, 2007, pp. 99-104.
[Nag07c] S. Nagy, Z. Petres, and P. Baranyi, "TP tool - a Matlab toolbox for TP model transformation," in Proc. 8th International Symposium of Hungarian Researchers on Computational Intelligence and Informatics, Budapest, Hungary, 2007, pp. 483-495.
[Nag08] S. Nagy, Z. Peters, and P. Baranyi, "TP model transformation based controller design for the parallel-type double inverted pendulum," in Proc. 2008 IEEE International Conference on Fuzzy Systems, Hong Kong, China, 2008, pp. 1374-1380.
[Nem19] Z. Németh and M. Kuczmann, "Tensor Product transformation based modelling of induction machine," in Proc. 1st IEEE International Conference on Gridding and Polytope Based Modeling and Control, Győr, Hungary, 2019, pp. 31-36.
[Nem21] Z. Németh and M. Kuczmann, "Tensor product transformation-based modeling of an induction machine," Asian Journal of Control, vol. 23, no. 3, pp. 1280-1289, 2021.
[Pet04] Z. Peters, B. Reskó, and P. Baranyi, "Reference signal control of the TORA system: a TP model transformation based approach," in Proc. 2004 IEEE International Conference on Fuzzy Systems, Budapest, Hungary, 2004, pp. 1081-1086.

[Pet06] Z. Peters, P. Baranyi, and H. Hashimoto, "Decrease of the computational load of TP model transformation," in Proc. 2006 IEEE International Conference on Mechatronics, Budapest, Hungary, 2006, pp. 655-659.

[Pet07] Z. Peters, P. Baranyi, P. Korondi, and H. Hashimoto, "Trajectory tracking by TP model transformation: case study of a benchmark problem," IEEE Transactions on Industrial Electronics, vol. 54, no. 3, pp. 1654-1663, 2007.

[Pet08] Z. Peters, S. Nagy, P. Gáspar, and P. Baranyi, "H_∞ gain-scheduling based control of the heavy vehicle model, a TP model transformation based control," in Proc. 2008 IEEE International Conference on Fuzzy Systems, Hong Kong, China, 2008, pp. 1542-1547.

[Pre08] R.-E. Precup, S. Preitl, B.-I. Ursache, P.A. Clep, P. Baranyi, and J.K. Tar, "On the combination of tensor product and fuzzy models," in Proc. 2008 IEEE International Conference on Automation, Quality and Testing, Robotics, Cluj-Napoca, Romania, 2008, pp. 48-53.

[Pre10a] R.-E. Precup, L.-T. Dioanca, E.M. Petriu, M.-B. Radac, S. Preitl, and C.-A. Dragos, "Tensor Product-based real-time control of the liquid levels in a three tank system," in Proc. IEEE/ASME International Conference on Advanced Intelligent Mechatronics, Montréal, Canada, 2010, pp. 768-773.

[Pre10b] R.-E. Precup, C.-A. Dragos, S. Preitl, M.-B. Radac, and E.M. Petriu, "Tensor Product models for automotive applications," in Proc. 14th International Conference on System Theory and Control, Sinaia, Romania, 2010, pp. 405-410.

[Pre12] R.-E. Precup, C.-A. Dragos, S. Preitl, M.-B. Radac, and E.M. Petriu, "Novel Tensor Product models for automatic transmission system control," IEEE Systems Journal, vol. 6, no. 3, pp. 488-498, 2012.

[Pre15] R.-E. Precup, E.M. Petriu, M.-B. Radac, S. Preitl, L.-O. Fedorovici, and C.-A. Dragos, "Cascade control cystem-based cost effective combination of tensor product model transformation and fuzzy control," Asian Journal of Control, vol. 17, no. 2, pp. 381-391, 2015.

[Sch78] G. Schwartz, "Estimating the dimension of a model," The Annals of Statististics, vol. 6, no. 2, pp. 461-464, 1978.

[Sub12] A. Subiantoro, F. Yusivar, B. Budiardjo, and M.I. Al-Hamid, "Identification and control design of fuzzy Takagi-Sugeno model for pressure process rig," Advances Materials Research, vol. 605-607, pp. 1810-1818, 2012.

[Sun18] K. Sunil and J. Jacob, "LMI Based design approach for the stabilization and tracking of a 3-DOF remote controlled helicopter, modeled in TP form," in Proc. International Conference on Advances in Computing, Communications and Informatics, Bangalore, India, 2018, pp. 1267-1272.

[Sza09] Z. Szabó, P. Gáspár, S. Nagy, and P. Baranyi, "Control-oriented qLPV modeling using TP transformation," in Proc. 2009 European Control Conference, Budapest, Hungary, 2009, pp. 2640-2645.

[Sza10] Z. Szabó, P. Gáspár, and J. Bokor, "A novel control-oriented multi-affine qLPV modeling framework," in Proc. 18th Mediterranean Conference on Control & Automation, Marrakech, Morocco, 2010, pp. 1019-1024.

[Sze07] L. Szeidl, P. Baranyi, Z. Petres, and P. Várlaki, "Numerical reconstruction of the HOSVD based canonical form of polytopic dynamic models," in Proc. International Symposium on Computational Intelligence and Intelligent Informatics, Agadir, Marocco, 2007, pp. 111-116.

[Szo14a] A. Szöllősi and P. Baranyi, "The tensor product model transformation as the link connecting biological and cognitive systems with control theory," in

Proc. 5th IEEE International Conference on Cognitive Infocommunications, Vietri sul Mare, Italy, 2014, pp. 569-574.

[Szo14b] A. Szöllősi, P. Baranyi, and P. Várlaki, "Example for convex hull tightening increasing the feasible parameter region at linear matrix inequality based control design," in Proc. IEEE 18th International Conference on Intelligent Engineering Systems, Tihany, Hungary, 2014, pp. 175-180.

[Szo14c] A. Szöllősi and P. Baranyi, "Influence of complexity relaxation and convex hull manipulation on LMI based control design," in Proc. 9th IEEE International Symposium on Applied Computational Intelligence and Informatics, Timisoara, Romania, 2014, pp. 145-151.

[Szo15] A. Szöllősi, P. Baranyi and P. Várlaki, "Influence of the manipulation of the polytopic Tensor Product model representation on the control performance of LMI based design," in Proc. IEEE International Conference on Systems, Man, and Cybernetics, Kowloon, China, 2015, pp. 2603-2608.

[Szo18] A. Szöllősi, TP Model Transformation Based Control Theory Optimization of Nonlinear Models, PhD Dissertation, Budapest University of Technology and Economics, Budapest, Hungary, 2017.

[Tak10a] B. Takarics, P. Korondi, and P. Baranyi, "TP model transformation based sliding mode control design for nonlinear systems," in Proc. 14th International Power Electronics and Motion Control Conference, Ohrid, Macedonia, 2010, pp. 61-68.

[Tak10b] B. Takarics, P. Korondi, and P. Baranyi, "Tensor product model transformation based friction compensation of a mechatronic system," in Proc. IEEE 14th International Conference on Intelligent Engineering Systems, Las Palmas, Spain, 2010, pp. 259-264.

[Tak10c] B. Takarics, P. Gróf, P. Baranyi, and P. Korondi, "Friction compensation of an aeroelastic wing - A TP model transformation based approach," in Proc. IEEE 8th International Symposium on Intelligent Systems and Informatics, Subotica, Serbia, 2010, pp. 527-533.

[Tak13] B. Takarics and P. Baranyi, "TP type polytopic modelling of the bergman minimal model of the diabetes mellitus," in Proc. IEEE 17th International Conference on Intelligent Engineering Systems, Costa Rica, 2013, pp. 73-78.

[Tak15] B. Takarics and P. Baranyi, "Friction compensation in TP model form - aeroelastic wing as an example system," Acta Polytehnica Hungarica, vol. 12, no. 4, pp. 127-145, 2015.

[Tak16] Á. Takács, J. Kuti, T. Haidegger, P. Galambos, and I.J. Rudas, "Polytopic model based interaction control for soft tissue manipulation," in Proc. IEEE International Conference on Systems, Man, and Cybernetics, Budapest, Hungary, 2016, pp. 3899-3905.

[Tak18] B. Takarics, A. Szöllősi, and B. Vanek, "Tensor Product type polytopic LPV modeling of aeroelastic aircraft," in Proc. IEEE Aerospace Conference, Big Sky, MT, USA, 2018, pp. 1-10.

[Tak21] B. Takarics and B. Vanek, "Robust control design for the FLEXOP demonstrator aircraft via tensor product models," Asian Journal of Control, vol. 23, no. 3, pp. 1290-1300, 2021.

[Tik04] D. Tikk, P. Baranyi, and R.J. Patton, "On the approximation properties of TP model forms," in Proc. 2004 IEEE International Conference on Fuzzy Systems, Budapest, Hungary, 2004, pp. 1069-1074.

[Var21] P. Várlaki, L. Palkovics, and A. Rövid, "On modeling and identification of empirical partially intelligible white noise processes," Asian Journal of Control, vol. 23, no. 3, pp. 1262-1279, 2021.
[Wan18] B. Wang, H. Gong, F. Zhang, Y. Yu, N. Dong, Z. Li, and X. Liu, "Nonlinear H_2 filtering based on tensor product model transformation for nonlinear discrete system," in Proc. 37th Chinese Control Conference, Wuhan, China, 2018, pp. 1776-1781.
[Wib13] W. Wiboonjaroen and S. Sujitjorn, "Stabilization of a magnetic levitation control system via state-PI feedback," International Journal of Mathematical Models and Methods in Applied Sciences, vol. 7, no. 7, pp. 717-727, 2013.
[Wu13] K.K. Wu and Y. Yam, "Control Stability of TP Model Transformation Design via Probabilistic Error Bound of Plant Model," in Proc. IEEE International Conference on Systems, Man, and Cybernetics, Manchester, UK, 2013, pp. 1259-1264.
[Yu19] Y. Yu, Z. Li, X. Liu, K. Hirota, X. Chen, T. Fernando, and H.H.C. Iu, "A nested tensor product model transformation," IEEE Transactions on Fuzzy Systems, vol. 27, no. 1, pp. 1-15, 2019.
[Zha14] G. Zhao, C. Zhao, and D. Wang, "Tensor product model transformation based integral sliding mode control with reinforcement learning strategy," in Proc. 33rd Chinese Control Conference, Nanjung, China, 2014, pp. 77-82.
[Zha18] G. Zhao, W. Wu, and D. Wang, "Enhancement of the variable universe of discourse control by Hammersley sequence-based TP model transformation," in Proc. 8th International Conference on Information Science and Technology, Granada, Cordoba, and Seville, Spain, 2018, pp. 401-408.
[Zho18] H. Zhou, H. Deng, and J. Duan, "Hybrid fuzzy decoupling control for a precision maglev motion system," IEEE/ASME Transactions on Mechatronics, vol. 32, no. 1, pp. 389-401, 2018.

Appendices

Appendix 1. The state-space system matrices of three linearized processes

The state-space system matrices obtained after the linearization of V3TS at the two o.p.s are given as follows:

$$\begin{aligned}
\mathbf{A}^{(1)} &= \begin{bmatrix} -0.0199 & 0 & 0 \\ 0.0250 & -0.0250 & 0 \\ 0 & -0.0198 & -0.0198 \end{bmatrix}, \quad \mathbf{b}^{(1)} = \begin{bmatrix} 0.005 \\ 0 \\ 0 \end{bmatrix}, \\
\mathbf{A}^{(2)} &= \begin{bmatrix} -0.0137 & 0 & 0 \\ 0.0112 & -0.0112 & 0 \\ 0 & -0.0104 & -0.0104 \end{bmatrix}, \quad \mathbf{b}^{(2)} = \begin{bmatrix} 0.005 \\ 0 \\ 0 \end{bmatrix}.
\end{aligned} \tag{1}$$

The state-space system matrices obtained after the linearization of psfcMLS at the two o.p.s are given as follows:

$$\begin{aligned}
\mathbf{A}^{(1)} &= \begin{bmatrix} 0 & 1 & 0 \\ 4022 & 0 & -41 \\ 2150 & 523 & -117 \end{bmatrix}, \quad \mathbf{b}^{(1)} = \begin{bmatrix} 0 \\ 0 \\ 322 \end{bmatrix}, \\
\mathbf{A}^{(2)} &= \begin{bmatrix} 0 & 1 & 0 \\ 3886 & 0 & -40 \\ 2275 & 523 & -191 \end{bmatrix}, \quad \mathbf{b}^{(2)} = \begin{bmatrix} 0 \\ 0 \\ 337 \end{bmatrix}.
\end{aligned} \tag{2}$$

The state-space system matrices obtained after the linearization of PCS at one o.p. are given as follows:

$$\mathbf{A}^{(1)} = \begin{bmatrix} 0 & 0 & 1 & 0 \\ 0 & 0 & 0 & 1 \\ 0 & 547.8 & -25.6 & 0.0026 \\ & -1521.6 & 69.9 & -0.0074 \end{bmatrix}, \quad \mathbf{b}^{(1)} = \begin{bmatrix} 0 \\ 0 \\ 439.7 \\ -1200 \end{bmatrix}. \tag{3}$$

Appendix 2. The LTI system matrices of three processes

The LTI system matrices obtained after the derivation of the TP model for V3TS are given as follows:

$$\mathbf{A}^{(1)} = \begin{bmatrix} 0 & 0 & 1 & 0 \\ 0 & 0 & 0 & 1 \\ 0 & 547.8 & -25.6 & 0.0026 \\ & -1521.6 & 69.9 & -0.0074 \end{bmatrix}, \quad \mathbf{b}^{(1)} = \begin{bmatrix} 0 \\ 0 \\ 439.7 \\ -1200 \end{bmatrix}. \tag{3}$$

$$\mathbf{S}_1 = \left[\begin{array}{ccc|c} 0.0922 & 0 & 0 & -0.0198 \\ -0.0922 & 0.0794 & 0 & 0 \\ 0 & -0.0794 & 0.0788 & 0 \end{array}\right],$$

$$\mathbf{S}_2 = \left[\begin{array}{ccc|c} 0.0288 & 0 & 0 & 0.0055 \\ -0.0288 & -0.0220 & 0 & 0 \\ 0 & 0.0220 & -0.0218 & 0 \end{array}\right]. \tag{1}$$

The LTI system matrices obtained after the derivation of the TP model for the psfcMLS are given as follows:

$$\mathrm{S}_1 = \left[\begin{array}{ccc|c} 0 & 1 & 0 & 0 \\ 11864 & 0 & -60.7 & 0 \\ 5385 & 131.51 & -44.43 & 81.18 \end{array}\right], \ \mathrm{S}_2 = \left[\begin{array}{ccc|c} 0 & 1 & 0 & 0 \\ 5440 & 0 & -55.32 & 0 \\ 9388 & 229.24 & -77.46 & 141.51 \end{array}\right], \tag{2}$$

$$\mathrm{S}_3 = \left[\begin{array}{ccc|c} 0 & 1 & 0 & 0 \\ 3566 & 0 & -36.26 & 0 \\ 25001 & 609.98 & -206.10 & 376.53 \end{array}\right].$$

The LTI system matrices obtained after the derivation of the TP model for the PCS are given as follows:

$$\mathbf{S}_1 = \left[\begin{array}{cccc|c} 0 & 0 & 1 & 0 & 0 \\ 0 & 0 & 0 & 1 & 0 \\ 0 & 33.85 & -1427 & -0.0031 & 590.9 \\ 0 & 2864.7 & 81 & -0.0010 & 1381 \end{array}\right], \ \mathbf{S}_2 = \left[\begin{array}{cccc|c} 0 & 0 & 1 & 0 & 0 \\ 0 & 0 & 0 & 1 & 0 \\ 0 & 34.65 & -6018 & 0.0022 & 329 \\ 0 & -1507.3 & 57 & -0.0056 & -974 \end{array}\right],$$

$$\mathbf{S}_3 = \left[\begin{array}{cccc|c} 0 & 0 & 1 & 0 & 0 \\ 0 & 0 & 0 & 1 & 0 \\ 0 & -35.73 & 6745 & -0.0010 & -317.4 \\ 0 & 611.9 & -26 & -0.0054 & 451.4 \end{array}\right], \ \mathbf{S}_4 = \left[\begin{array}{cccc|c} 0 & 0 & 1 & 0 & 0 \\ 0 & 0 & 0 & 1 & 0 \\ 0 & 1073.2 & -6024 & 0.0022 & 422.6 \\ 0 & 541.6 & 57 & -0.0072 & -977 \end{array}\right], \tag{3}$$

$$\mathbf{S}_5 = \left[\begin{array}{cccc|c} 0 & 0 & 1 & 0 & 0 \\ 0 & 0 & 0 & 1 & 0 \\ 0 & 978.9 & 1659 & -0.0018 & 144.7 \\ 0 & -1265.9 & -48 & -0.0025 & 824.2 \end{array}\right].$$

Appendix 3. The LTI state feedback gain matrices of three processes

The LTI state feedback gain matrices obtained for the V3TS are given as follows:

$$\begin{aligned}\mathbf{K}_1 &= [-5.7919 \quad 1.9751 \quad -0.7096],\\ \mathbf{K}_2 &= [-6.6004 \quad 3.3668 \quad -1.4166].\end{aligned} \tag{1}$$

The LTI state feedback gain matrices obtained for the psfcMLS are given as follows:

$$\begin{aligned}\mathbf{K}_1 &= [-213.62 \ -2.80 \ 1.86],\\ \mathbf{K}_2 &= [-156.72 \ -2.07 \ 1.38],\\ \mathbf{K}_3 &= [-117.35 \ -1.33 \ 1.02].\end{aligned} \tag{2}$$

The LTI state feedback gain matrices obtained for the PCS are given as follows:

$$\begin{aligned}\mathbf{K}_1 &= [0 \quad 9.1676 \quad 26.9510 \quad 0.0103],\\ \mathbf{K}_2 &= [0 \quad 2.8438 \quad 8.6331 \quad 0.0025],\\ \mathbf{K}_3 &= [0 \quad 1.3043 \quad 2.7203 \quad 0.0022],\\ \mathbf{K}_4 &= [0 \quad 3.7069 \quad 9.8204 \quad 0.0030],\\ \mathbf{K}_5 &= [0 \quad -0.0829 \quad -2.7517 \quad -0.0004].\end{aligned} \tag{3}$$

Appendix 4. The state feedback gain matrices of three processes

The state feedback gain matrices obtained for the four linear models of V3TS are given as follows:

$$\begin{aligned}
\mathbf{k}_{SF}^{(1)\,T} &= [0.5225 \quad 0.3251 \quad 0.2064], \\
\mathbf{k}_{SF}^{(2)\,T} &= [0.6101 \quad 0.3141 \quad 0.2013], \\
\mathbf{k}_{SF}^{(3)\,T} &= [0.5841 \quad 0.33857 \quad 0.2030], \\
\mathbf{k}_{SF}^{(4)\,T} &= [0.5378 \quad 0.3282 \quad 0.2031].
\end{aligned} \tag{1}$$

The state feedback gain matrices obtained for the four linear models of psfcMLS are given as follows:

$$\begin{aligned}
\mathbf{k}_{SF}^{(1)\,T} &= [34.19 \quad 0.77 \quad -0.24], \\
\mathbf{k}_{SF}^{(2)\,T} &= [17.01 \quad 0.50 \quad -0.11], \\
\mathbf{k}_{SF}^{(3)\,T} &= [50.05 \quad 0.49 \quad -0.36], \\
\mathbf{k}_{SF}^{(4)\,T} &= [31.60 \quad 0.54 \quad -0.21].
\end{aligned} \tag{2}$$

The state feedback gain matrices obtained for the four linear models of PCS are given as follows:

$$\begin{aligned}
\mathbf{k}_{SF}^{(1)\,T} &= [3.9 \cdot 10^{-7} \quad 1.24 \quad 0.0172 \quad 2.7 \cdot 10^{-7}], \\
\mathbf{k}_{SF}^{(2)\,T} &= [2.7 \cdot 10^{-5} \quad 0.62 \quad 0.0048 \quad 6.1 \cdot 10^{-4}], \\
\mathbf{k}_{SF}^{(3)\,T} &= [8.5 \cdot 10^{-5} \quad 1.21 \quad -0.0012 \quad 1.5 \cdot 10^{-3}], \\
\mathbf{k}_{SF}^{(4)\,T} &= [2.5 \cdot 10^{-4} \quad 1.33 \quad 0.0029 \quad 2.4 \cdot 10^{-3}].
\end{aligned} \tag{3}$$